2017

The Effects of Chemical Reagents and Physical Environment on the In Vitro and In Vivo Properties of Adipose-Derived Multipotent Stromal Cells Isolated from Different Species

Wei Duan
Louisiana State University and Agricultural and Mechanical College

THE EFFECTS OF CHEMICAL REAGENTS AND PHYSICAL ENVIRONMENT ON THE IN VITRO AND IN VIVO PROPERTIES OF ADIPOSE-DERIVED MULTIPOTENT STROMAL CELLS ISOLATED FROM DIFFERENT SPECIES

A Dissertation

Submitted to the Graduate Faculty of the
Louisiana State University and
Agricultural and Mechanical College
in partial fulfillment of the
requirements for the degree of
Doctor of Philosophy

in

Biomedical and Veterinary Medical Sciences
through the
Department of Veterinary Clinical Sciences

by
Wei Duan
M.S., Shanghai Institute of Ceramics, Chinese Academy of Sciences, 2012
B.S., Huazhong University of Science & Technology, 2009
August 2017

This dissertation is dedicated to my family for all their love and support. I am particularly grateful for my parents and my girlfriend, for their unconditional love, care and support. They have provided me with all a son could ever ask for, inspired me in all aspects, supported my interests, and urged me on every step of the way. I would like to thank my lovely girlfriend, for loving, inspiring and encouraging me to purchase what I want. I would like to give my back to her. I would like to thank my grandparents, uncles and aunts for being my models in life and work. Thank you for all the love, education and company for all these years for encouraging and facilitating my pursuit of a Ph.D. in the U.S.

ACKNOWLEDGEMENTS

This dissertation would not have been possible without the help from my colleagues in the Laboratory of Equine and Comparative Orthopedic Research. I would like to express my deepest appreciation to my major professor, Dr. Mandi J. Lopez, for all her support, knowledge and advice. She has instilled in me to many qualities of being a professional scientist. She provided me with a wonderful environment to work in with excellent management, resources, personnel and teamwork. Dr. Lopez continually provides me with opportunities to communicate and collaborate with people from diverse backgrounds.

I would like to express my appreciation to all of my committee members. Dr. Frank M. Andrews has always supported me and has never hesitated to provide me with wonderful chances to further my education. I would like to thank Dr. Shaomian Yao and Dr. Kenneth R. Bondioli for their help and support.

I would like to acknowledge and extend my gratitude to my co-workers in the laboratory: Dr. Nan Zhang, Carmel Fargason, Holly Attuso, Corrine Plough, Javier Jarazo, Catherine Takawira, Heather A. Richbourg, Aimee M Soileau, Robert A Walton, Dr. Carmen B Arsuaga, Evan T Boatwright, Dr. Raphael A Malbrue, and Dominique Angibeau. I could not have accomplished my work without their endless help. I have been very blessed to work in an environment with such a supportive team. I would like to show my appreciation to Marilyn Dietrich, Dr. Xiaochu Wu, Dr. Julia Sokolova, Dr. Newcomer, and Thaya Stoufflet for their expertise. I would also thank Dr. Dale L. Paccamonti, Lindsey S Saunders, Jackie Bourgeois and everyone in Department of Biomedical and Veterinary Medical Sciences and the Equine Health Studies Program for their kind help.

TABLE OF CONTENTS

LIST OF TABLES

LIST OF FIGURES

ABSTRACT

Adult adipose derived mesenchymal stromal cells (ASCs) have been characterized in various species. Many factors may affect ASC fate and ASCs from different species may have different response to these factors. The first study was to identify the differences of the canine ASCs isolated from subcutaneous and infrapatellar adipose tissues, and evaluate the impact of cryopreservation on the cells. Based on paired comparisons of fresh and cryopreserved ASCs, cryopreserved ASCs had lower CD29 and CD44 protein expression and lower proliferation rates. The cryopreserved ASCs had relative lower mitochondria in the cytoplasm compared to the fresh ASCs regardless of tissue sources. The second study was to apply human ASCs for bone regeneration. The spinner flask bioreactor system was employed to load human ASCs onto three commercial scaffolds and the cell-scaffold constructs were cultured in stromal, osteogenic, or osteogenic for 48 hours followed by stromal medium for up to 28 days. The distinct scaffold up-regulated different osteogenic signaling pathways, suggesting distinct osteogenic cell signaling pathways were selectively upregulated by scaffold composition. The third study was designed to quantify in vivo equine multipotent stromal cell (MSC) osteogenesis on synthetic polymer scaffolds with distinct mineral combinations 9 weeks after implantation in a murine model. Addition of mineral to polymer scaffolds enhanced equine MSC osteogenesis over polymer alone, and contributions by both exo- and endogenous MSCs were confirmed. The fourth study was designed to evaluate the effects of collagenase digestion and cryopreservation on equine ASCs. Higher collagenase concentration yielded more nucleated cells, and the percentages of MHCII-, CD44+, CD105+ cells in freshly isolated and cryopreserved cells were similar. The embryonic gene expression was enhanced and the essential gene expression decreased after cryopreservation. The fifth study was to demonstrate the endodermal transdifferentiation capability in feline ASCs.

Feline-specific pancreatic β cell induction medium was developed in the study, and islet-like cell clusters that secrete insulin in response to glucose stimulation were created. Overall, the investigations in this dissertation provide critical information for canine, feline, equine and human MSC based tissue engineering therapies and may contribute to better efficiency and efficacy of cell preservation techniques.

CHAPTER 1. THE EFFECTS OF CRYOPRESERVATION, CHEMICAL REAGENTS, AND PHYSICAL ENVIRONMENT ON ADULT MULTIPOTENT STROMAL CELLS

1.1. Adult Multipotent Stromal Cell Cryopreservation: Pluses and Pitfalls

1.1.1. Introduction

Adult multipotent stromal cells (MSCs) are increasing as standard therapy for a multitude of pathologic conditions as diverse as cancer, renal disease and musculoskeletal and cardiac tissue injury [1-5]. Isolation of adequate cell numbers for several therapeutic doses with minimally invasive tissue harvest is a perpetual struggle [6]. Based on current knowledge, distinct MSC immunophenotype subpopulations are most effective for specific clinical applications [7]. Extensive in vitro culture expansion of low frequency MSC immunophenotypes is necessary to achieve sufficient cell numbers, and potential for genetic alterations and contamination increases with culture time [8-11]. In addition to immunogenicity concerns of allogeneic donors,[12] MSC quality varies with age and health status [13]. Thermally dependent metabolic processes do not occur below -120^{o}C, so MSCs are in metabolic stasis at liquid nitrogen temperature, around -196^{o}C [14]. Multiple cell aliquots collected over time from an individual or set of donors can be maintained for later administration immediately upon revitalization or after short-term expansion of pooled or individual isolates [15, 16]. Cryopreservation also increases MSC availability since frozen cells can be delivered to patients over long distances using standard transportation [17]. Despite prevalent MSC cryopreservation, relatively little focus has been directed toward the effects cryopreservation on cell morphology and behavior.

There is a growing awareness of differences between fresh and cryopreserved MSCs [6, 18-22], though cryopreservation effects on retention of MSC characteristics vary widely [18-21, 23, 24]. Most veterinary MSC cryopreservation techniques are derived from human and murine

protocols[18, 25] for cell aliquots of 1-4 × 10^6 cells in cryopreservation medium that contains cryoprotectants (CP) and exogenous serum (Fig. 1) [26]. A cooling process is used to reduce the temperature to about -80ºC prior to transfer to liquid nitrogen [25-27]. For revitalization, cells are thawed and then washed with buffer or medium to remove cryopreservation medium ingredients [14]. Each step, as well as cryopreservation duration can impact MSC survival and attributes [14].

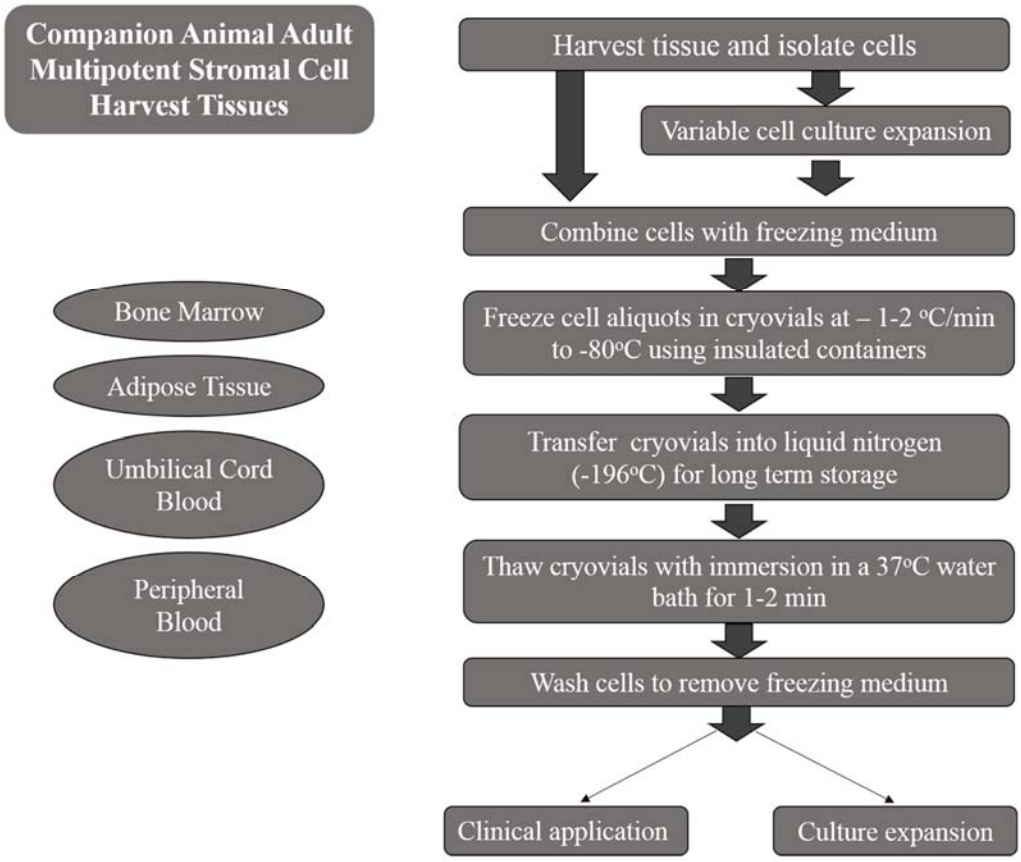

Figure 1. Schematic of domestic animals (cat, dog and horse) adult multipotent stromal cell (MSC) cryopreservation process

1.1.2. Cooling Process

Cryopreservation maintains unfrozen cells at a supercool temperature within frozen medium [28]. The freezing point of the medium surrounding the cells is reduced by CPs to around -5 to -15ºC. During the cooling process, fluid moves from the lower solute concentrations in the

unfrozen cells into partially frozen medium while the plasma membrane prevents extracellular ice crystals from entering them. Slow cooling permits fluid loss from the cells at a rate that results in a balanced osmotic pressure between cells and medium by the time the medium freezes. If the cooling rate is too slow, cells are fatally dehydrated or the plasma membranes irreversibly damaged before solutes crystallize at the eutectic temperature [14]. Excessively rapid cooling results in insufficient extracellular fluid migration to maintain the high solute concentration to prevent fatal cell freezing [29].

As described above, cell cooling rate is a delicate balance of fast enough to avoid solute and electrolyte imbalances that result in cell dehydration and uneven sample freezing and slow enough to prevent lethal extra- and intracellular ice crystal formation [14]. Unique membrane permeability among cell types influences fluid movement rate as well [14]. Conventional slow freezing at a rate of -1^{o}C/min [30] with microprocessor-controlled freezers or freezing containers with a heat transfer interface (isopropyl alcohol or insulation) between the samples and an ultra-low temperature environment [31, 32] reportedly has minimal effect on MSC immunophenotype, proliferation or lineage differentiation [31, 32]. Slow freezing of sterile specimens within sealed vials also minimizes contamination risk [33]. Limitations of this cooling mechanism include cell dehydration and membrane damage, intracellular ice formation (IIF) and exposure to CPs [14].

Another form of cooling used for MSC cryopreservation, vitrification, involves extremely rapid cooling (>-1,000^{o}C/s) of cells immersed in CPs within open storage vessels [34, 35]. While the process prevents fluid crystallization, potentially cytotoxic concentrations of CPs are necessary to facilitate the freezing process and protect the cells [34]. Additionally, samples must be maintained at cryogenic temperatures, and open containers are a potential source of contamination

[36, 37]. Largely due to technical challenges, vitrification is not used as frequently as slow freezing for veterinary MSC cryopreservation, so the focus of this review is on the latter.

1.1.3. Thawing Process

Cells pass through the critical temperature range for ice crystal formation, -15 to -60ºC, during the freezing and thawing processes [14]. Rapid thawing, 90-100ºC/min, is often employed to prevent fluid crystallization by immersing samples in a 37ºC water bath until all ice melts [38]. When murine hematopoietic progenitor cells are cooled at -1.5ºC/min, survival is higher when they are thawed rapidly at 900ºC/min versus slowly at 2ºC/min [39]. Recovery rates of human erythroid progenitor cells are reported to be the same when they are thawed rapidly at 37ºC versus more slowly at 20ºC [40]. It is likely that the best thawing mechanism varies between both cells and CPs with the ideal rate a balance of preventing ice formation versus prolonged exposure to CPs at temperatures when cells are metabolically active. Both freezing and thawing processes should be customized and then consistently utilized for a given species and MSC harvest tissue.

1.1.4. Cryoprotectants

The primary function of CPs is to prevent cell damage during freezing and thawing [37, 41-43]. Cryoprotectant formulation and concentration varies among species, MSC type, and cooling technique, among other considerations [30, 37, 43]. Even relatively low concentrations of CPs used for slow freezing, 1-2M, are associated with toxicity that differs among cell types and increases with time, temperature, concentration and metabolic activity [37, 43]. There are two major CP categories based cell membrane permeability, permeable and impermeable [37, 43]. Those with high permeability tend to be the most cytotoxic [14]. Combinations of permeable CPs like dimethyl sulfoxide (DMSO), ethylene glycol, methanol, propylene glycol, dimethylacetamide, and less permeable CPs like polyvinypyrrolidone, hydroxyethylstarch, polyethylene glycol and

dexamethasonetran, reduces permeable CP concentrations and associated problems [14, 37, 43]. Dimethyl sulfoxide and fetal bovine serum (FBS) are among the most common CPs used for companion animal MSC cryopreservation [1, 25]. The carcinogenic properties of DMSO [4] and xenogeneic proteins in FBS may alter the cells and impact post implantation behavior [18, 44]. Some of the functions and limitations of these as well as alternative CPs follow.

Dimethyl Sulfoxide

One of the most popular CPs, DMSO, stabilizes cell proteins [45], and penetrates cells to displace fluid and equilibrate electrolyte concentrations between the intra- and extracellular fluid to maintain cell volume [46, 47]. Protein stabilization is mediated via hydrophobic interactions between DMSO and positively charged proteins, including those in the cell membrane phospholipid bilayer [45]. Additionally, DMSO forms high energy hydrogen bonds with water molecules, interfering with interactions among them to prevent ice formation [48, 49].

Dimethyl sulfoxide can cause MSC chemical toxicity and osmotic shock [44, 46, 47]. The same hydrophobic interactions that protect vital proteins during cryopreservation can also denature and deactivate them [50]. Increasing DMSO concentrations (5 – 20%) in the freezing medium is associated with lower survival and increased apoptotic gene expression (Bak and Bcl2) in porcine bone marrow derived stromal cells (BMSCs) [19-21, 51-53]. In vivo, neurotoxicity can occur from 10% DMSO solutions, a typical concentration in cryopreservation medium [54]. Sedation, headache, nausea, vomiting, hypertension, bradycardia, hypotension, central nervous system depression, and anaphylactic shock have been attributed to DMSO in cell suspensions administered intravenously to humans [54]. Washing cells to reduce DMSO concentration after thawing results in cell loss and lower colony forming units [55], and complete DMSO removal can

be complex and time consuming [56, 57]. These points, among others, support continued efforts to identify replacements for DMSO in cryopreservation medium [37, 43].

Fetal Bovine Serum

Fetal bovine serum collected at different gestational stages [58] is a common culture medium ingredient that provides growth factors, nutrients and hormones for cell proliferation and adhesion [46, 47]. It is also thought to act as a CP through protection of cell proteins and stabilization of osmotic pressure, though the mechanisms have not been completely defined [46, 47, 59]. In addition to ethical, zoonosis, and xenogeneic protein concerns, compositional variation of FBS lots contributes to inconsistent cell culture performance [58]. A recent finding that cryopreserved canine ASCs have increased CD44 expression compared to fresh cells was attributed to FBS in the freezing medium [18]. The US Food and Drug Administration (FDA) does not permit use of FBS in products intended for humans or animals owing to potential immunogenicity [60]. Autologous and allogeneic serum in MSC freezing media reportedly compare favorably to FBS in terms of MSC viability, morphology, and plasticity [41, 42, 61]. A study to assess different media effects on equine BMSCs included two freezing media composed of 20% serum, 10% DMSO, 70% DMEM or 95% serum and 5% DMSO, both with autologous serum, commercial pooled equine serum or FBS added [61]. There was no difference in post-thaw cell viability, morphology or growth kinetics among different freezing media, and 95% autologous serum with 5% DMSO was recommended for short-term (2-3 days) cryopreservation [61]. Serum free MSC cryopreservation medium has been shown to have similar or superior post-cryopreservation outcomes compared to FBS-containing media [59, 62]. Increasing availability of FBS-free freezing media may be important to improving consistency in MSC pre- and post-cryopreservation characteristics.

Impermeable Cryoprotectants

Methylcellulose (MC) is a high-molecular weight polymer in MSC freezing medium, including serum-free [30, 62]. Human ASC post-thaw cell viability with freezing medium containing MC in Dulbecco's Modified Eagle's medium (DMEM) is greater than DMEM alone, but lower than that containing 80% serum, 10% DMSO and 10% DMEM [41, 42]. Another nontoxic, impermeable, high molecular weight polymer, polyvinylpyrrolidone (PVP), is also a fairly popular MSC CP [56, 57, 63]. As extracellular fluid ice forms at -10 to -20^{o}C, the concentration of dissolved PVP in the unfrozen fluid increases and creates an osmotic gradient that drives fluid out of cells to prevent IIF [64]. Despite lower intracellular fluid, IFF may occur at low PVP levels, and high concentrations of 20-40% can cause excessive cellular dehydration, cell necrosis and membrane damage [56, 57, 63]. Human ASC viability and plasticity appears to be maintained with 10% PVP as the CP [56, 57]. Carboxylated ε-poly-L-lysine polyampholytes are effective CPs in MSC freezing medium without exogenous protein, but it has had little use in companion animals [65]. Hydroxyethyl starch (HES) is a synthetic polymer CP that absorbs water molecules (0.5g water per 1g HES) and maintains them in a glassy state, solid without crystallization, during the cooling process [66, 67]. The polymer, widely used as a plasma volume substitute, is metabolized by glycolytic enzymes in vivo, so it does not have to be removed from thawed cells [66, 67]. A "6&5 solution" composed of physiologic saline, 6% HES, 5% DMSO and 4% human serum albumin appears to maintain better cell viability, recovery rates and plasticity of human peripheral blood progenitors, cord blood stem cells, peripheral blood cells and BMSCs compared to 10% DMSO in Roswell Park Memorial Institute (RPMI) 1640 medium [66, 67]. Similar findings are reported for canine CD34+ BMSCs cryopreserved in the same "6&5" solution [68-72]. Novel cryopreservation solutions that support cell stasis without impacting inherent

characteristics will continue to promote availability and standardization of cell therapies across species.

1.1.5. Cryopreservation of Mesenchymal Stem Cells from different species (Fig. 2, 3, & 4)

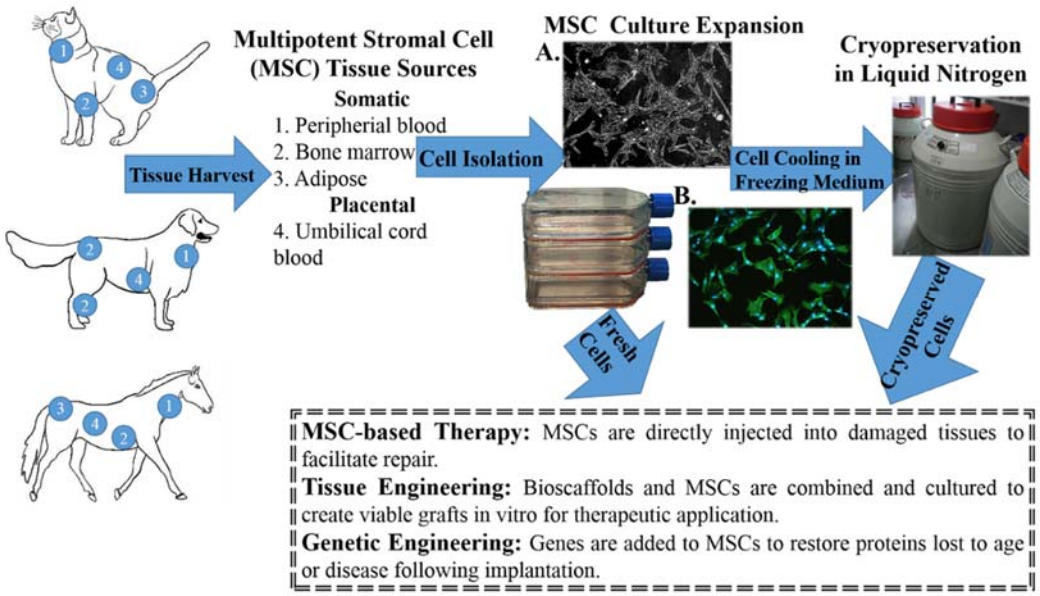

Figure 2. Schematic diagram of domestic animals (cat, dog and horse) adult multipotent stromal cell (MSC) processing for clinical applications. A. Photomicrographs of MSCs culture in stromal medium, 5×; B. Fluorescent photomicrographs of MSCs with cytoskeleton (actin, green) and nuclear (DNA, blue) staining.

Some of the earliest descriptions of cryopreservation were for spermatozoa, ova, and embryos in the field of theriogenology [73, 74]. Cell cryopreservation has vastly expanded with the rapidly evolving field of cell-based regenerative medicine [75]. It is increasingly apparent that cryopreservation should be customized for species and cell type, especially with established differences among immunophenotypes in primary cell isolates [18-21, 26]. Despite numerous variables, conflicting outcomes and inconsistent cryopreservation effects across and within species, consistent findings have emerged and are summarized below.

Comparisons among fresh and cryopreserved cells provide important information about storage and behavior to guide therapeutic and research applications and assessments, respectively.

Much of the existing literature documents similar, though not identical changes in cell plasticity and expansion potential across species. Canine ASCs from subcutaneous and intra-articular adipose tissues have lower sex determining region Y-box2 (SOX2) protein expression and distinct ultrastructure and immunophenotype compared to fresh ASCs following 30 days of cryopreservation in 80% FBS, 10% DMSO and 10% DMEM [18]. Two reports indicate that while canine ASCs and BMSCs maintain their fibroblast-like morphology, alkaline phosphatase (ALP) activity and plasticity following cryopreservation, there are significant differences from fresh cells [26, 82]. Specifically, after 12 months of cryopreservation in freezing medium composed of 90% FBS and 10% DMSO, canine MSCs have lower proliferation and telomerase activity than fresh cells [26], and, separately, canine BMSCS have lower viability and proliferative capacity following seven days of cryopreservation in freezing medium with 10% DMSO and 10% FBS [82]. In contrast to these studies, another found lower ALP activity and plastic adhesion in canine BSMCs cryopreserved for one month [68, 83]. Equine peripheral blood MSCs cryopreserved in 90% FBS and 10% DMSO have faster proliferation but lower telomerase activity and myogenic plasticity compared to unfrozen cells [25]. The in vitro osteogenic differentiation of fresh and cryopreserved rat, lapin and porcine ASCs are reportedly similar on direct comparison [84]. Human ASCs have lower proliferation and adipocytic and osteoblastic plasticity following cryopreservation in 90% FBS and 10% DMSO, and cryopreserved cells less effectively enhance calvarial healing in an athymic mouse model compared to fresh [23, 24]. These findings support the need to definitively characterize cell isolates before and after cryopreservation and to establish and maintain cryopreservation procedures for consistent cell characteristics.

Another common finding among species is more rapid loss of progenitor cell expansion and multipotentiality with passage following cryopreservation. Canine BMSCs cryopreserved in

80% FBS, 10% DMSO and 10% DMEM for one month had lower fibroblastic and osteoblastic colony forming unit frequencies than fresh cells with increasing passage [77]. Feline ASCs cryopreserved in identical freezing medium for one month had lower CD9 and CD105 expression compared to fresh cells, and the proliferation rate and osteoblastic capability decreased to a greater extent with increasing passage in cryopreserved versus fresh cells [6, 22, 85]. The cell proliferation rate of equine ASCs frozen in 20% FBS, 70% DMEM-high glucose and 10% DMSO significantly declined at P12 while fresh cells did not show a similar decline until P15 [86]. The potential aging effects of cryopreservation on MSCs that contribute to more rapid waning of cell expansion and plasticity compared to fresh cells is an important area of continued discovery to anticipate both in vitro and in vivo cell potential.

Harvest Tissue	Passage	Cell Aliquot (cells/ml)	Freezing Medium	Freezing Rate	Cooling Process	Thawing Process	Effects	Ref
Adipose	0	~ 2×10^6	DMEM, 10% FBS, 10% DMSO	-1°C/min	Cryovials were in an insulated container for 24 hours at -80°C and then moved to liquid nitrogen	N/A	N/A	[76]
	0	1×10^6	Serum-free medium, 80% FBS, 10% DMSO	-1°C/min	Cryovials were in an insulated container at -80°C overnight and then moved to liquid nitrogen	Cryovials removed from liquid nitrogen and immersed in a 37°C water bath for 2-3 min	None	[77-79]
	0	N/A	Low glucose DMEM, 30% FBS, 5% DMSO	N/A	N/A	N/A	N/A	[80, 81]
	1	3×10^6	90% FBS,10% DMSO	-1°C/min	Cryovials were placed in an insulated container at -80°C for 1 week and then moved to liquid nitrogen	Cryovials removed from liquid nitrogen and immersed in a 37°C water bath for 1-2 min followed by wash with 10% FBS, 90% DMEM	Lower proliferation ratio and telomerase activity	[26]
Bone Marrow	0	1.0×10^6	10% DMSO, 10% FBS, α-MEM	-1°C/min	Cryovials were placed in an insulated container and kept at -80°C for 7 days	Cryovials removed from liquid nitrogen and immersed in a 37°C for 1 min	Lower cell viability and proliferative capacity	[82]

Figure 3. Adult Canine MSC Freezing Medium Components, Cryopreservation Conditions and Behaviors

1.1.6. Cell Passage Number and Cryopreservation Duration

The amount of cell expansion prior to and duration of cryopreservation is an established factor in post-cryopreservation cell characteristics [30, 87, 88]. There is a direct relationship between equine umbilical cord blood MSC viability and pre-cryopreservation passage number following cryopreservation in 20% DMEM, 70% FBS and 10% DMSO for 8 weeks. Specifically, cell viability decreases from about 80.4% for P1 to 51.2% for P10 [87, 88]. Similarly, a comprehensive study of human ASCs to assess cooling rate, end temperature, hold time and thawing rate on cell membrane integrity showed that a significant effect of thawing rate was limited to P3 and P4 cells while the interaction between cooling rate and end temperature was significant for cell passages P0-P4 [30]. The impact of cryopreservation duration may be most detectable following short term storage. Human BMSCs reportedly maintain tri-lineage differentiation capacity after 7 years of cryopreservation [38]. However, total cell recovery is reportedly significantly lower after 5 (80%) versus 1 (90%) months of cryopreservation in 10% fetal calf serum, 10% DMSO and 30% bovine serum albumin [89]. These findings convey the importance of consistent cell expansion and consideration of the length of cryopreservation when preparing MSCs for potential clinical application.

1.1.7. Cell Transportation

Cell delivery from current Good Manufacturing Processes (cGMP) facilities to patient administration sites requires maintenance of frozen cells for variable time periods despite external temperature fluctuations [17, 35, 90]. Vitrified cells are transported at cryogenic temperatures in dry shippers with liquid nitrogen in absorbent materials to avoid sample contact with liquid [56, 57]. Slow cooled samples can be shipped frozen in approved, polystyrene containers without the need for dry shippers [35, 90]. Cryovials are often wrapped with precooled, absorbent material

and placed in a leak-proof, biohazard grade container to prevent direct contact of samples with dry ice placed on top of the container within the polystyrene shipping box. Sample transportation responsibilities extend beyond sample preparation and packaging, however. A detailed inventory should be included with the shipment, all samples permanently labeled, signage applied to shipping containers and all necessary shipping manifests filed. Shipping should be tracked and clear guidelines provided to the recipient surrounding sample handling and administration [56, 57]. Contemporary travel mechanisms makes it possible to transport cryopreserved samples globally. It is imperative, however, that national and international laws and regulations are observed.

Harvest Tissue	Passage	Cell Aliquot (cells/ml)	Freezing Medium	Freezing Rate	Cooling Process	Thawing Process	Effects	Ref
Adipose	N/A	~ 5×10^5	20% FBS, 10% DMSO, DMEM	-1°C/min	Cryovials were kept at -80°C before moved to liquid nitrogen.	Cryovials were placed in a 37°C water bath for 2 min and followed by wash twice with 20% FBS, 70% DMEM	Decreased proliferation rate	[85]
Bone Marrow	N/A	~1×10^6	10% FBS, 10% DMSO, DMEM	-1°C/min	Cryovials were in an insulated container for 24 hours at -80°C then moved to liquid nitrogen	N/A	N/A	[27]
		~ 10×10^6	20% serum, 10% DMSO, α-MEM or 95% serum, 5% DMSO	-1°C/min	Cryovials were in an isopropyl alcohol freeze container at -80°C for 24 h before moved to liquid nitrogen for 2-5 days	Cryovials were thawed at 35°C in a water bath until ice was no longer present.	Lower MSC numbers	[61]
Peripheral Blood	2-3	2×10^6	90% FBS, 10% DMSO	-1°C/min	Cryovials were in an insulated contained at -80° for one week and then moved to liquid nitrogen	Cryovials were placed in a 37°C water bath for 1-2 min followed by wash with 10% FBS, 90% DMEM	Lower proliferation rate	[25]
Umbilical cord blood	N/A	1×10^6	10% DMSO, 70% FBS, DMEM	N/A	Cryovials were stored at -20°C for 1 h and then transferred to -80°C overnight before moved to liquid nitrogen	Cryovials were placed in a 37°C water bath for 3 min followed by wash with 60% FBS, 40% DMEM	Lower cell viability that decreased more rapidly with passage than fresh	[86, 87]

Figure 4. Adult Equine MSC Freezing Medium Components, Cryopreservation Conditions and Behaviors

1.1.8. Regulation of Cryopreserved Regenerative Cells for Veterinary Use

Regulation of veterinary medicine in the United States has a complicated history with some products regulated by the United States Department of Agriculture (USDA) and others by the Food and Drug Administration Center for Veterinary Medicine (CVM). The Federal Food, Drug, and Cosmetic (FDC) Act of 1938 established federal government's responsibility to regulate animal health products. Since then, a number of additional laws surrounding veterinary medicine product approval and use have gone into effect. In the mid-1990's, Congress passed two major Animal Health Acts. The Animal Medicinal Drug Use Clarification Act of 1994 allowed veterinarians to prescribe human drugs and extra-label use of veterinary drugs for animals under specific circumstances. The Animal Drug Availability Act of 1996 added moderation to the animal drug approval process, including flexible labelling and more direct communication between drug sponsors and the FDA. During the infancy of adult stem cell therapy discovery and development in 2002, the FDA announced a current good manufacturing practice (cGMP) initiative to enhance and update regulation of manufacturing processes and end-product quality of animal and human drugs and biological medicines**.** The goals of the initiative were to drive focus on the greatest to public health risks of manufacturing procedures and ensure that process and product quality standards did not impede innovation. In 2004, passage of the Minor Use and Minor Species Animal Health Act encouraged development of treatments for species that may otherwise attract little interest. Collectively, these laws provided veterinarians reasonable discretion and freedom to use emergent drugs and medical devices within their practices. There was no specific guidance surrounding development and use of regenerative cell therapies for industry or practicing veterinarians prior to 2015.

The Guidance for Industry Publication #218 – Cell-Based Products for Animal Use was published by the CVM in June of 2015, to clarify Agency regulation of cell therapies. Non-primary cells that are culture expanded and intended to treat patients other than the donor are considered to be "drugs" and must go through FDA drug licensing and approval processes [91]. Autologous cryopreserved cells to treat injury or disease in the donor are classified as either type I or type II cell based products (Table 1). Both are regulated as drugs and must undergo all indicated safety and efficacy testing and receive CVM authorization for use similar to allogeneic cell therapies. For type II classification, autologous cells must be: 1) minimally manipulated, 2) for homologous use and 3) for non-food-producing animals. They cannot be combined with anything other than water, crystalloids or a sterilizing, preserving or storage agent that do not raise additional safety concerns. Additionally, cells may not be combined with or modified by adding them with a drug or a device. Prior to the advent of stem cell based products, the term "type II autologous cells" was generally understood to mean whole or fractionated peripheral[2, 92], umbilical cord [93-96] or marrow-derived blood cells [97] intended for transplantation, cells within cryopreserved mesenchymal tissues like fat, bone, ligament and tendon, cartilage grafts [1, 3, 15, 16, 98], or β cell pancreatic islets for diabetes therapy [99].

Improved methods of cell preservation with ingredients beyond serum and DMSO complicate cell classification since commercial cryopreservation solution components may be considered drugs in some circumstances. Use of cryopreserved cells in combination with popular blood derivatives like platelet rich plasma occupies a nebulous area in the classification scheme that requires further clarification. The speed of discovery in the stem cell arena exceeds development of regulations governing their use. Similarly, definitions of "homologous use" and "minimally manipulated" do not entirely capture current knowledge of stem cell functionality.

Academic and industrial scientists continue to work with the regulatory authorities to achieve and maintain contemporary language that is consistent with intended and practical use.

In summary, CMV consultation should be sought prior to manufacture and use of cryopreserved cells as a commercial treatment, especially since cells transported across state lines are automatically within federal regulatory jurisdiction. Additionally, state requirements for reporting and licensing GTP Cell Bank facility must be abided by. Use of cell processing and banking services provided by veterinary regenerative medicine companies appears to be acceptable as the long the provider has implemented appropriate quality and safety standards.

Table 1. Autologous Cell-based Therapy Classification

Autologous Type I Cell Therapy Criteria (One must be true)	Autologous Type II Cell Therapy Criteria (All must be true)
More than minimally manipulated (Example: Cells cultured in vitro for an extended period of time)	Minimally manipulated (Example: Cells are only centrifuged)
For non-homologous use	For homologous use
For use in a food-producing animal	For use in nonfood-producing animals
Effects are dependent on metabolic activity of living cells	No statement regarding metabolic activity
Manufacture of the ASCP involves combination of the cells with another article (Except water, crystalloids, or a sterilizing, preserving, or storage agent that does not raise new product safety concerns)	Manufacture does not involve combination of cells with another article (Except water, crystalloids, or a sterilizing, preserving, or storage agent, provided that the addition of water, crystalloids, or the sterilizing, preserving, or storage agent that does not raise new product safety concerns)

1.1.9. Conclusion

Cryopreservation of adult MSCs is central to their development, availability and use. The practice is relatively new in veterinary medical disciplines compared to human counterparts, and its importance and use will only continue to grow in concert with regenerative medicine [41, 42, 63]. It is readily clear that fresh and frozen MSCs are not identical. However, mechanisms, extent and full implication of distinctions between them is uncharted and complicated by numerous variables before, during and after cryopreservation. Efforts to discover and standardize cryopreservation protocols based on species, tissue and, potentially, cryostasis duration will continue to advance therapeutic efficacy and safety of cryopreserved cells.

Table 2. Differentiation media components and β cell induction of MSCs from different tissue sources[123]

Species	Cell Type	Differentiation Factors	References
Mouse	BMSC	Activin-A, conophyline, nicotinamide, L-glutamine, betacellulin-delta4; fibronectin (FN), laminin (LAM), hepatocyte growth factor (HGF), extendin-4,	[100]
Human	ASC	Glucose, nicotinamide, activin-A, exendin-4, HGF, pentagastrin, betacellulin	[103]
Human	Umbilical cord blood derived MSCs	Glucose, retinoic acid, nicotinamide, exendin-4, epidermal growth factor, B27	[102]

1.2. Transdifferentiation of Multipotent Stromal Cells into Insulin Producing Clusters

A series of transition steps are required to induce the differentiation of MSCs to β cells in vitro. Currently numerous studies reported that several stem cell types have the capability to form insulin producing β cells [100-103] and different factors are used for specific cell type (Table 2).

Currently, there is no standard protocol for pancreatic differentiation. However, most reports use B27 and N2 rather than FBS to support prolonged self-renewal of MSCs [104, 105]. Nicotinamide is another additive that is widely used to induce human BMSCs [105], human ASCs [104], and other MSC types [106-112]. In previous studies, nicotinamide has been shown to have the ability to promote the islet-like cell cluster formation and increase the rate of proinsulin biosynthesis [70, 113-121]. Pentagastrin is an artificially synthesized polypeptide that can stimulate β cell neogenesis and increase the β cell mass [122]. Besides these supplements, there are several growth factors and extrinsic proteins used to promote β cell proliferation and differentiation (Table 3).

1.3. The Effects of the Physical Environment on Multipotent Stromal Cell Osteogenesis

1.3.1. Bioreactor Systems for Bone Tissue Engineering

The general definition of bioreactor is a device that can closely monitor and tightly control environmental conditions (e.g. pH, oxygen concentration, pressure, nutrient supply, flow rate, and waste removal) to achieve desired biological and/or biochemical results [124]. Since the reliability, reproducibility, control and automation introduced by bioreactors for specific tissue engineering approaches have been established, they are widely used in many fields, such as bone [125], cartilage [126], vascular tissue [127], cardiac tissue [128], liver [129], and so on [124]. In this section, several common bioreactor systems, including spinner flasks, rotating wall and perfusion

bioreactors as well as the effects of hydrodynamic shear stress on osteoblastic differentiation will also be discussed.

Table 3. Extrinsic growth factors for β cell proliferation and/or differentiation [123]

Extrinsic growth factors	Function	Ref
Glucagon like peptide	Enhance the effect of insulin secretion from β cells; increase the β-cell mass; enhance fetal pig β-cell differentiation and initiate their functional maturation	[130-133]
Betacellulin	Promote the differentiation, regeneration and proliferation of pancreatic β cells	[70, 113-115]
Activin-A	Regulate neogenesis of β cells	[134]
Hepatocyte growth factor	Promote β cell proliferation and regeneration of islets; Increase insulin content and islet cell growth	[109, 135, 136]
Endothelial growth factor	Enhance the nestin-positive cell growth	[137]
Basic fibroblast growth factor	Enhance the nestin-positive cell growth	[137]
Laminin	Enhance differentiation of MSCs into insulin producing cells and insulin secretion	[101]
Fibronectin	Enhance differentiation of MSCs into insulin producing cells and insulin secretion	[101]
Extendin-4	Promote β-cell proliferation and maturation	[36]

Spinner flask bioreactor

A spinner flask is a simple and inexpensive bioreactor [125]. Normally a spinner flask is composed of a glass media reservoir with side arms, a stir bar or another stirring mechanism [125]. Scaffolds can be attached to a needle connected to the lid of the flask and the side arms fitted with porous covers to allow oxygen and CO_2 exchange [125]. Numerous studies demonstrate that the spinner flask can enhance the early osteogenic marker alkaline phosphatase (ALP), late osteoblastic marker osteocalcin (OCN), calcium deposition, and cell proliferation in various cell types compared to static controls (Table 6) [138-143]. Besides the advantages of cellular proliferation and differentiation from the transportation of nutrients and oxygen throughout the scaffold, another advantage is its low cost [144]. In static culture, because of nutrient and oxygen concentration gradients, cells in the center of the scaffold do not receive the same nutrition and oxygenation as cells on the periphery [144]. In a spinner flask bioreactor system, nutrients and oxygen are delivered throughout the scaffold [145]. However, there are several drawbacks of the system that should be considered. The possible formation of a dense superficial cell layer can hamper nutrient and oxygen supply, leading to cell death in the center of the scaffolds [140]. The spinner flask bioreactor system may not adequately transport nutrients and oxygen in large scaffolds [125]. Additionally, the shear stress from medium flow around the cell-scaffold constructs is not applied homogenously throughout the scaffold as the highest shear forces occur on the construct surfaces closest to the stirring mechanism [125].

Rotating bioreactor systems

The rotating wall bioreactor contains two concentric cylinders with culture media and cell-scaffold constructs in the space between them [144]. The inner cylinder is stationary and provides gas exchange [144]. Typically the outer cylinder one of two designs: 1) a free-fall design where

scaffolds freely moving in the space; or 2) rotating bed bioreactor (RBB) design where scaffolds are fixed to the outer cylinder rather. Using the first bioreactor system design, the expression of osteogenic genes (ALP, OCN, and OPN) was upregulated while the proliferation was not affected in rat calvarial osteoblastic cells on poly (lactide-co-glycolide) (PLGA) scaffolds [146]. However, in another study the ALP activity decreased and the OCN activity did not change in osteoblastic cells [147]. Meanwhile, the rotating wall bioreactor cannot enhance ALP activity and OCN secretion in rat BMSCs [138]. In this design, scaffolds may collide with the bioreactor wall and damage scaffolds and disrupt attached cells [144]. The RBB system was developed to avoid this problem [148-151]. Using this system, affixed human bio-derived bone scaffolds had enhanced cell proliferation, ALP expression, mineralized nodule formation compared to the spinner flask and static culture [148]. Other studies demonstrated that the RBB system has positive effects on cell proliferation, extracellular matrix (ECM) deposition, and osteogenic differentiation in various cell types (human MSCs and MC3T3-E1 cells) [149-151]. One major potential disadvantage of the rotating wall bioreactor systems is that nutrients, oxygen transportation, mineralization and cell distribution are limited to the outside of the scaffolds [138, 144].

Perfusion-based bioreactor systems

Many different perfusion bioreactor systems have been developed to meet distinct requirements, but most systems consist of a media reservoir, a pump, a tubing circuit, and a chamber or cassette [152]. In a flow perfusion bioreactor system, medium is pumped through cell-scaffold constructs at a controlled rate [152]. Perfusion bioreactor are divided into indirect and direct perfusion bioreactors based on the cassette where the cell-scaffold constructs maintained during perfusion [144, 152]. In an indirect perfusion system, medium flows through the space between the constructs and the cassette. Therefore, the medium flow can follow the path of least

resistance around the constructs and flow-derived shear stress may not reach the cells in the center of the constructs [144]. The ALP activity and OCN secretion were increased in rat osteoblasts on β-tricalcium phosphate (β-TCP) scaffolds using this system compared to static culture [153]. Bone formation was also enhanced by perfusion bioreactor constructs were implanted into rats.

Cell Type	Scaffold material	Pore size (μm)	Shape and dimensions	Effect	Reference
Human MSC-TERT cell	Coralline hydroxyapatite	200 ~ 500	Diameter: 10mm Thickness: 2mm	Proliferation ↑, ALP ↑, cellular distribution ↑	[138]
Human BMSCs	PLGA	150 ~ 600	Cubic, 8×8×5mm	Proliferation ↑, ALP ↑, calcium content ↑, early osteogenesis gene (Col1α1, BMP2, RUNX2) ↑	[139]
Rat BMSCs	PLGA	900 ~ 1000	Diameter: 12.7mm Thickness: 50mm	Proliferation ↑, ALP ↑, calcium content ↑, OCN secretion ↑	[137]
Human BMSCs	Aqueous-derived Silk	900 ~ 1000	Diameter: 15mm Thickness: 5mm	Proliferation ↑, ALP ↑, mineralization ↑, osteogenesis gene (Col1α1 and OPN) expression ↑	[142]
Rat calvarial osteoblast cells	PLG		Diameter: 4mm Thickness: 2.5mm	ALP ↑, OCN and OPN secretion ↑	[145]
Human BMSC	Collagen	N/A	Diameter: 13.3mm Thickness: 3mm	ALP ↑, calcium deposition ↑	[141]

Figure 5. Studies utilizing spinner flask bioreactor for bone tissue engineering. ALP: alkaline phosphatase; PLGA: Poly (D, L-lactic-co-glycolic acid); PLG: poly (lactide-co-glycolide); BSP: bone sialoprotein; Col1α1: collagen 1α1; OCN: osteocalcin; TERT: telomerase reverse transcriptase; OPN: osteopontin; RUNX2: Runt-related transcription factor-2; ↑: positive effect

In a direct perfusion system, the scaffolds are fixedin cassettes in a press-fit manner so that the medium cannot flow around the scaffold [144]. Because of this characteristic, this system enhances biophysical forces and medium delivery to the cells throughout the scaffold [152]. This

system design has been used with numerous scaffold materials including titanium, starch-based, and calcium phosphate ceramics [154-160]. In this system, the center cell distribution in the scaffold center is improved and cell proliferation and osteogenesis, and mineralized ECM deposition are enhanced compared to static culture [156, 161, 162].

Table 4. Comparison among spinner flask, rotating wall, and direct perfusion bioreactor systems for bone tissue engineering

Bioreactor	Advantage	Disadvantage	Shear Stress	Reference
Spinner flask	Low cost; Enhance cell proliferation and expression of osteogenic marker genes; Benefit mineralization	Internal nutrient and oxygen transport limitations; Shear stress distribution is not homogenous.	The degree of shear stress depends on the stirring speed	[144]
Rotating wall vessel	Low cost; Enhance the expression of osteogenic marker	Internal nutrient and oxygen transport limitations; Limitations of mineralization and culturing benefits; Scaffolds may be damaged and cell attachment may be disrupted.	The degree of shear stress depends on the centrifugal forces of the cylinder balance with the force of gravity	[138, 144]
Direct perfusion bioreactor	Enhance cell proliferation, distribution, differentiation, and viability in the interior of scaffolds;	Need more devices to build the system	In vivo studies to prove the effectiveness of the systems are necessary; The maintenance of the system is time-consuming; The difficulty of perfusing media directly through a scaffold	[125]

In a rat cranial defect model, rat BMSCs were seeded onto the titanium scaffolds overnight and then followed cultured in the flow perfusion bioreactor system at a flow rate of 1 ml/min for 8 days before implanted into the cranial defects sites in rats [163]. After 30 days implantation, there were no significant differences between the groups of perfusion versus static culture [163]. Currently, there are few in vivo studies that prove the effectiveness of the flow perfusion systems. Additionally, to develop a successful flow perfusion bioreactor, it is necessary to customize the cassette to direct the medium flow through a scaffold design. The maintenance of these systems can be time-consuming [125].

1.3.2. Effect of Shear Stress and Mass Transfer on Proliferation and Osteoblastic Differentiation

Table 5. Comparison of shear stresses reported in different perfusion bioreactor systems [125]

Shear stress (dyn/cm^2)	Cell Type	Effects	Ref
0.007 ~ 0.1	Human BMSC	Increasing perfusion rate improved proliferation rate, cell distributions and the osteogenic specific protein and mineralization.	[170]
<0.05	Human BMSC	More calcium content and higher ALP activity	[142]
0.05	Rat BMSC	Higher amounts of calcified matrix deposition; More homogeneous ECM distribution; Enhanced cellular proliferation and differentiation.	[171]
0.05 ~ 0.15	Human BMSC	Increasing shear stress accelerated the osteogenic differentiation and enhanced the ECM mineralization	[168]

(Table 5 Continued)

Shear stress (dyn/cm^2)	Cell Type	Effects	Ref
0.1	Human ASC	Improve the cell distribution and bone matrix deposition	[172]
0.1 ~ 0.3	Rat BMSC	Enhance the expression of the osteoblastic phenotype and the mineralized ECM production and distribution	[169]
0.2 ~ 0.3	Rat BMSC	Increase calcium deposition	[159]
< 1.0	Rat BMSC	Increasing shear stress increase mineralized matrix production	[154]
1.6	Rat BMSC	Repeated application of shear stress stimulate late osteogenic marker expression	[166]

The positive effects of fluid shear on osteogenic signal expression and osteoblastic differentiation of MSCs have been reported numerous times [164-167]. Most long-term, three dimensional bioreactor studies use continuous flow at a set rate [125]. In a bioreactor system, the shear forces from fluid flow in scaffold pores are determined by flow rate and difficult to calculate correctly for long term culture because cell growth and ECM deposition can alter local velocity and shear stress[125]. As discussed above, bioreactor systems improve mass transport which can be expressed by flow rate and the increasing mass transport could result in the change in cell proliferation [125, 142, 168]. When the mass transport is sufficient for the cell proliferation, the shear stress would be the main effectors on the osteogenic signal expression and cell osteogenesis

[168]. Shear stresses are reported to range from 0.05 to 1.0 dyn/cm^2 (Table 5) in different perfusion bioreactor systems. One report indicates that calcium deposition increased with increasing viscosity [169]. All bioreactor systems require a fluid rate necessary for optimal nutrient and gas transport that does not generate shear forces that interfere with cell attachment and function [168].

CHAPTER 2. EFFECTS OF CRYOPRESERVATION ON CANINE MULTIPOTENT STROMAL CELLS FROM SUBCUTANEOUS AND INFRAPATELLAR ADIPOSE TISSUE *

2.1. Introduction

Tissue engineering with adult multipotent stromal cells (MSCs) harvested from adipose tissue, adipose derived multipotent stromal cells (ASCs), is rapidly emerging as a therapeutic reality in human and veterinary medicine [75, 173]. Higher MSC tissue density and comparable cell plasticity to bone marrow derived multipotent stromal cells are some of the characteristics that establish adipose tissue as a viable MSC source [77]. Existing knowledge supports potential differences in ASC behavior among adipose depots in numerous species [174, 175]. One rationale for observed differences is varying proportions of brown and white adipose tissue among harvest sites [176]. Intra-articular and visceral adipose tissue are predominantly white while subcutaneous adipose tissues are mostly brown [177]. Distinctions between cells isolated from brown versus white adipose tissue like lower plasticity of brown adipose tissue cells, have been attributed to epigenetic factors and functional differences, endocrine versus thermogenic of white and brown, respectively [178, 179]. Distinct features of cells isolated from brown and white adipose tissues contribute to efforts to optimize isolation procedures and culture conditions for cells from each [180].

Canine infrapatellar adipose tissue ASCs reportedly have similar in vitro properties as bone marrow derived multipotent stromal cells and higher expansion capacity and plasticity than undifferentiated cells from joint capsular and cranial cruciate ligament synovium [181]. This makes them appealing for intra-articular tissue regeneration. Subcutaneous adipose tissue harvest

*This chapter previously appeared as [Wei Duan, and Mandi Lopez. "Effects of Cryopreservation on Canine Multipotent Stromal Cells from Subcutaneous and Infrapatellar Adipose Tissue." Stem Cells Reviews and Report 12 (2016): 257-268]. It is reprinted by permission of [Springer and BioMed Center]

is less invasive and more abundant than intra-articular [96, 182]. Hence, use of subcutaneous adipose tissue ASCs may reduce morbidity and augment tissue resources for generation of intra-articular structures.

A recent study highlighted differences between ASCs from intraarticular and subcutaneous adipose tissues in and around the human knee [182]. Published reports of canine subcutaneous and infrapatellar ASCs suggest similarities between cells from the two harvest sites [180, 183], but a side by side in vitro characterization is necessary to anticipate the ability of each cell type to support complex tissue generation. This study was designed to determine in vitro expansion capabilities and plasticity of paired canine ASCs harvested from subcutaneous (SUB) and infrapatellar (IFP) adipose tissues before and after cryopreservation to test the hypothesis that IFP ASCs have the highest in vitro expansion rates, plasticity and MSC immunophenotypes that are sustained over multiple cell passages.

2.2. Materials and Methods

2.2.1. Ethics Statement

All animal procedures were approved by the Institutional Animal Care and Use Committee.

2.2.2. Study Design

Subcutaneous and infrapatellar IFP adipose tissues were collected from 6 adult, mixed-breed dogs (3.5 ± 0.8 years of age, mean ± standard error of the mean (SEM)). Adipocyte and ASC ultrastructure were evaluated with transmission electron microscopy (TEM). Cell doublings (CDs) and doubling time (DT) were determined for fresh and cryopreserved ASC passages (fresh, P; cryopreserved, tP) 0-3 from both tissues of each dog. For P0, 1, 3 and tP1 and 3, CD29+, CD34+, CD44+, and CD90+ cell percentages were quantified. Fibroblastic (CFU-F), osteoblastic (CFU-Ob), and adipocytic (CFU-Ad) colony-forming unit frequency percentages and lineage-specific

target gene mRNA expression levels were determined (peroxisome proliferator-activated receptor γ (PPAR-γ) and leptin - adipogenesis; osteoprotegerin (OPG) and collagen type 1α1 (Col1α1) - osteogenesis) after culture in lineage-specific induction or stromal media. Similarly, P3 and tP3 chondrogenic pellet alcian blue (proteoglycan) staining, CD29, CD34, CD44 and CD90 protein expression and target protein expression (PPAR-γ - adipogenesis; osteopontin (OPN) - osteogenesis; sex determining region Y-box 2 (SOX2) – progenitor) were also quantified following standard induction procedures. A seeding density of 5×10^3 cells/cm^2 and humidified culture conditions (37ºC, 5% CO_2) were used for all cell culture experiments. Materials were from Sigma-Aldrich, St. Louis, MO unless otherwise noted.

2.2.3. Cell Isolation

Cells from SUB and IFP adipose tissues were isolated according to published procedures with minor modifications [181]. Briefly, tissue was rinsed with phosphate buffered saline (PBS, Hyclone, Logan, UT) and minced, followed by digestion in an equal volume of Dulbecco's modified Eagle's medium: F-12 (DMEM/F-12, Hyclone, Logan, UT), 0.1% collagenase type I (Worthington Biochemical Corporation, Lakewood, NJ) and 1% bovine serum albumin (BSA) for 90 minutes with agitation. The tissue suspension was then filtered (100 μm, BD Falcon, Bedford, MA). Subsequently, the digest was centrifuged (260×g, 5 minutes), and the pellet was suspended in stromal medium (DMEM/F-12 medium, 10% (v/v) fetal bovine serum (FBS, Hyclone), 1% (v/v) antibiotic/antimycotic solution). An equal volume of red cell lysis buffer (0.16 mol/L NH_4Cl, 0.01 mol/L $KHCO_3$, 0.01% ethylenediaminetetraacetic acid (EDTA)) was added, and the mixture was maintained at room temperature for 30 minutes. The solution was centrifuged, and the resulting stromal vascular fraction (SVF) pellet resuspended in stromal medium followed by culture in T75 flasks (CellStar, Greiner, NC). Medium was refreshed after 24 hours to remove unattached cells,

and then every 3 days [181]. Subsequent passages were performed at 80-90% cell confluence. For purposes of this study, the primary cell isolate was the SVF and the first cell passage of primary cells was P0. Aliquots of each SVF were suspended in freezing medium (10% DMEM/F-12, 10% dimethyl sulfoxide (DMSO, Fisher Scientific, Fair Lawn, NJ), 80% FBS) during the first cell passage and cryopreserved in the cryopreserved medium composed of 10% DMSO and 80% FBS in DMEM in CoolCell® (BioCision, LLC) overnight. The cryopreserved cells were then moved in liquid nitrogen for a minimum of 30 days. Cells were revitalized and seeded in T75 flasks as tP0 after the cryopreservation period.

2.2.4. Adipocyte and ASC Ultrastructure (adipocytes, P1, tP1) - Transmission Electron Microscopy

Harvested SUB and IFP adipose tissues, P1 and tP1 ASCs were rinsed with PBS and then fixed in 2% paraformaldehyde and 1.25% glutaraldehyde in 0.1 M sodium cacodylate (CAC) buffer (pH 7.4). Samples were rinsed in 0.1M CAC buffer with 5% sucrose and incubated with 1% osmium tetroxide in 0.1M CAC buffer. The tissues were dehydrated in a series of ethanol-distilled water solutions and embedded in Epon (Plano, Marburg, FRG). Ultrathin sections were evaluated with a transmission electron microscope (JEM-1011, JEOL, Japan).

2.2.5. Cell Expansion (P0-3, tP1- 3)

Cells were cultured in 12-well plates (Thermal Fischer Scientific, Denmark) to calculate CD and DT after 2, 4 and 6 days of culture using standard formulae (CD= ln(Nf/Ni)/ln(2) and DT=CT/CD; Ni: initial cell number; Nf: final cell number; CT: culture time) [184]. Cell counts were performed with a hemocytometer. Day 2 and 4 cell numbers were used as the Ni for days 4 and 6, respectively.

2.2.6. Multipotentiality (P0, 1, 3, tP1, 3) - Limiting Dilution Assays and Pellet Chondrogenesis

Limiting dilution assays were used to determine fibroblastic (CFU-F), adipocytic (CFU-Ad), and osteoblastic (CFU-Ob) colony-forming unit frequencies [77]. A total of 5000, 2500, 1250, 625,

312 or 156 cells were seeded in each well of one row in a 96-well plate for 8 replicates of each cell number/well. Fibroblastic (CFU-F) colonies were fixed with 2% formalin (Anapath, Mckinney, TX) and stained with 0.1% toluidine blue after 7 days of culture in stromal medium. For CFU-Ob, cells were cultured in stromal medium for 7 days followed by culture in osteogenic medium (DMEM/F-12, 10% FBS, 10 mmol/L β-glycerophosphate, 10 nmol/L dexamethasone, 50 μg/ml sodium 2-phosphate ascorbate) for 21 additional days. Cells were fixed in ice cold 70% ethanol and then alkaline phosphatase (ALP) was stained with 5-bromo-4chloro-3indolyl phosphate/nitro blue tetrazolium (BCIP/NBT, 0.15mg/ml BCIP, 0.30 mg/ml NBT). To determine CFU-Ad, cells were cultured in stromal medium for 7 days followed by culture in adipogenic medium (DMEM/F12, 3% FBS, 1% antibiotic/antimycotic solution, 33 μmol/L biotin, 17 μmol/L pantothenate, 1 μmol/L dexamethasone, 100 μmol/L indomethacin, 1 μmol/L insulin, 0.5 mmol/L isobutylmethylxanthine (IBMX), 5 μmol/L rosiglitazone (TZD, AK Scientific, Union City, CA)) for 21 additional days. Cells were fixed in 4% formalin and stained with 0.3% oil red O. Wells with 10 or more toluidine blue-stained, oil red O-stained, or BCIP/NBT-stained colonies were considered positive for fibroblastic, adipocytic or osteoblastic colonies, respectively. The ratio of negative to total wells per row was used to estimate the CFU frequencies according to Poisson's ratio ($F=e^{-x}$; F: ratio of negative to total wells; e: natural logarithm constant 2.71; x: CFU) [77, 181, 184]. CFU frequency was expressed as a percentage percentage (1/CFU frequency × 100).

For chondrogenesis, 2.5×10^5 cells were centrifuged (200×g, 5 minutes) to form a pellet after 7 days of culture in stromal medium. Pellets were cultured in stromal or chondrogenic medium (DMEM/F-12, 3% FBS, 1% antibiotic/antimycotic solution, 50 μg/ml ascorbate phosphate, 100nmol/L dexamethasone, 40 μg/mL proline, 2 mmol/L sodium pyruvate (Invitrogen, Carlsbad, CA), 1% insulin-transferrin-selenium (ITS, Invitrogen), 10 ng/mL recombinant human

transforming growth factor-β3 (rTGF-β3, R&D systems, Minneapolis, MN)) for 21 days. They were then fixed with 10% neutral buffered formalin, embedded in paraffin, sectioned (5 μm) and stained with 1% alcian blue (Acros Organics, Belgium) and 3% nuclear fast red.

2.2.7. Immunophenotype - Flow Cytometry (P0, 1, 3, tP1, 3)

Cell aliquots (10^5 cells) were suspended in 200 μl PBS containing 0.1 μl (200 μg/ml) of labeled or unlabeled antibody (CD34-PE, CD44-FITC, CD90-PE, CD29) specific for canine antigens or validated for canine cross reactivity for 30 minutes at room temperature **(**Table 6**)**. Cells were then washed with PBS and fixed with 4% neutral buffered formalin. For CD29, cells were incubated with labeled anti-immunoglobulin (IgG-FITC) for 30 minutes at room temperature, washed with PBS and then fixed with 4% neutral buffer formalin. For the autoflourescence control, cells were not incubated with antibodies. Cell fluorescence was quantified by flow cytometry using a FACSCalibur flow cytometer and Cell Quest Pro software (BD Biosciences, San Jose, CA).

2.2.8. Gene Expression – RT-PCR (P0, 1, 3, tP1, 3)

Total RNA was isolated from cells (RNeasy Plus Mini Kit, Qiagen) and the concentration determined spectrophotometrically (NanoDrop ND-1000; NanoDrop Technologies, Montchanin, DE, USA). A QuantiTect Reverse Transcription Kit (Qiagen, GmbH, Germany) was used to generate cDNA. Target gene levels, glyceraldehyde 3-phosphate dehydrogenase (GAPDH), PPAR-γ, leptin, Col1α1 and OPG (Table 7) were quantified with real-time RT-PCR using SYBR Green (Qiagen) technology and an MJ Research Chromo 4 Detector (Bio-Rad Laboratories, Hercules, CA). The $2^{-\Delta\Delta Ct}$ values were determined relative to the reference gene GAPDH and target gene expression in cells cultured in stromal medium.

2.2.9. Protein Expression – Immunocytochemistry, western blot (P3, tP3)

Immunocytochemistry. Cells were cultured in stromal medium in 4-well chamber slides for 3 days and then fixed with 10% neutral buffered formalin for 24 hours. Antigen retrieval was performed with SDS/TBS antigen retrieval buffer (1% SDS, 100 mM Tris, 138 mM NaCl, 27 mM KCl, pH=7.4) for 5 minutes at room temperature. Cell preparations were blocked with goat serum (1:10 in TBS) overnight at 4ºC and then incubated with antibodies against CD34-PE (1:200), CD44-FITC (1:500) or CD90-PE (1:500**) (**Table 6**)** for 2 hours at room temperature. Cells were washed with TBS buffer and nuclei were stained with DAPI (1μg/ml). For CD29 labeling, cells were incubated with antibodies against CD29 (1:500) for 2 hours at 37ºC followed by IgG-FITC (1:800) and DAPI nuclear stain. Photomicrographs were obtained for all labeled cells (Leica DM 4500b).

Western blot. Total protein was extracted from cells cultured in stromal and induction medium using RIPA buffer (150 mM NaCl, 1.0% Triton X-100 (Thermo Scientific, Rockford, IL), 0.5% sodium deoxycholate, 0.1% SDS, 50 mM Tris (pH=8.0), protease inhibitor (Thermo Scientific)). Protein concentrations were determined with the Bicinchoninic Acid (BCA) Protein Assay Kit (Thermo Scientific). Protein aliquots (20 μg) were denatured for 10 minutes at 95ºC in an equal volume of 1x SDS loading buffer. Proteins were separated on a 12% SDS-PAGE gel and transferred (300 mA, 90 minutes) to nitrocellulose membranes (Bio-Rad Laboratories, Hercules, CA). Membranes were blocked (4% BSA, 0.05% sodium azide) for 1 hour at room temperature and then incubated with primary antibodies directed against OPN (1:300), PPAR-γ (1:500) or SOX2 (1:500) at 4º C overnight (Table 6). Tris buffer saline with Tween-20 (TBST, 0.1% Tween-20, 0.24% Tris, 0.8% NaCl) washes were followed by incubation with horseradish-peroxidase-conjugated (HRP) IgG (1:3000) at room temperature for 2 hours. Labeled bands were imaged by exposure to light sensitive film (GE Healthcare, Chalfont St. Giles, Buckinghamshire, UK)

following color development with Amersham ECL prime western blotting detection reagents (GE Healthcare). Target protein bands were to β-actin standards.

Table 6. Antibodies for flow cytometry and immunocytochemistry

Antibody	Label	Marker Expression	Manufacturer	Cat No.	Species	Target Species	Diluent
CD29	N/A	β1 integrin	BD Biosciences	610468	Mouse	Human	PBS
CD34	PE	Hematopoietic progenitor (HSC)	BD Biosciences	559369	Mouse	Dog	PBS
CD44	FITC	Hyaluronic acid receptor	eBiosciences	115440	Mouse	Dog	PBS
CD90	PE	Thy-1, fibroblasts, MSC, HSC	eBiosciences	125900	Mouse	Dog	PBS
Goat anti-mouse IgG	FITC	Secondary antibody	Sigma-Aldrich	F9006	Goat	Mouse	PBS
β-actin	N/A	Cytoskeletal protein	Thermo Scientific	RB-9421-P0	Rabbit	Dog	TBS
Sox-2	N/A	Transcription factor	LifeSpan BioSciences	LS-B4562	Rabbit	Dog	5% Skim milk/PBS
PPAR-γ	N/A	NHR/NR1 Thyroid homone-like	LifeSpan BioSciences	LS-B651	Rabbit	Dog	5% BSA/TBS
OPN	N/A	Secreted Phosphoprotein 1	LifeSpan BioSciences	LS-B425	Rabbit	Dog	5% BSA/TBS
CD29	N/A	β1 integrin	BD Biosciences	610468	Mouse	Human	TBS
CD44	N/A	Hyaluronic acid receptor	Monoclonal Antibody Center	DG-BOV2037	Mouse	Dog	TBS
Goat anti-rabbit IgG	HRP	Secondary antibody	Santa Cruz Biotechnology	sc-2004	Goat	Rabbit	TBS
Goat anti-mouse IgG	HRP	Secondary antibody	Santa Cruz Biotechnology	sc-2005	Goat	Mouse	TBS

Table 7. Primer sequences

Lineage	Primer	Sequence	Accession No.
Housekeeping	GAPDH	F: TGGCAAAGTGGATATTGTCG R: AGATGGACTTCCCGTTGATG	XM_003435649.2
Adipogenic	PPAR-γ	F: TTCTCCAGCATTTCCACTCC R: AGGCTCCACTTTGATTGCAC	XM_005632014.1
	Leptin	F: TGTGTTGAAGCTGTGCCAAT R: CCCTCTGTTTGGAGGAGACA	XM_005628342.1
Osteogenic	Col1α1	F: GGTGGTGGCTATGACTTTGG R: CAGTTCTTGGCTGGGATGTT	XM_005628344.1
	OPG	F: TGTCTATACTGCAGGCCGGTG R: TCAGGCAGAACTCAAGCTCCA	XM_003639448.2

For evaluation of surface marker protein expression, total protein was extracted with NP-40 buffer (150 mM sodium chloride, 1.0% Triton X-100, 50 mM Tris, pH=8.0) from fresh and cryopreserved P3 cells cultured in stromal media. Protein concentration determination and western blot procedures were identical to above with the exception of incubation with primary antibodies directed against CD29 (1:200) and CD44 (1:2000) at room temperature for 1 hour (Table 1) followed by IgG-HRP (1:2000). Protein bands were quantified using ImageJ software (Rasband, WS, ImageJ; National Institutes of Health, Bethesda, MD, http://rsb.info.nih.gov/ij).

2.2.10. Statistical Analysis

Statistical analyses were performed with commercially available software (SAS 9.2, Institute, Cary, NC). Analysis of variance (ANOVA) models were used to evaluate cell surface marker precentages, CD, DT, CFU frequency percentages and gene expression among tissue sources within passages and among passages within tissue sources. Tukey's post hoc tests were applied

for multiple group comparisons ($p<0.05$). Normality and homogeneity of variance were assessed with Shapiro-Wilk tests and residual plots.

2.3. Results

2.3.1. Adipocyte and ASC Ultrastructure (adipocytes, P1, tP1) - Transmission Electron Microscopy

Adipocytes and ASCs had different morphologies from each other and between tissue sources. There were large, unilocular lipid vacuoles that peripherally displaced cytoplasm and organelles in adipocytes from both tissue sources. However, SUB adipocytes had numerous mitochondria concentrated near the cell membrane compared to mitochondria distributed throughout the cytoplasm in IFP adipocytes. Further, IFP adipocytes had abundant small lipid vacuoles (in addition to the central vacuole) among mitochondria whereas SUB had fewer (Fig. 6). Cultured ASCs were smaller than adipocytes, and they did not have central, large lipid vacuoles. Fresh IFP and SUB ASCs had mitochondria clustered around the nucleus and small, cytoplasmic lipid vacuoles, though IFP ASCs tended to have more vacuoles and fewer mitochondria. After cryopreservation, IFP ASCs had many small lipid vacuoles and few mitochondria in the cytoplasm compared to few lipid vacuoles in the cytoplasm and mitochondria clustered around the nucleus in SUB ASCs (Fig. 6). Additionally, the relative number of mitochondria in cryopreserved SUB ASCs appeared to be lower than in fresh ASCs based on subjective assessment.

2.3.2. Cell Expansion (P0-3, tP1-3)

The CDs of fresh and revitalized IFP and SUB ASCs decreased with passage, while the corresponding DTs increased (Fig. 7). Significant differences were less incremental in fresh versus cryopreserved cells with P0 and 1 tending to expand more quickly than P2 and 3. The CDs were significantly lower for P0 SUB ASCs versus IFP ASCs. The CDs and DT were significantly lower and higher, respectively, for cryopreserved P3 versus fresh ASCs from the same tissue source.

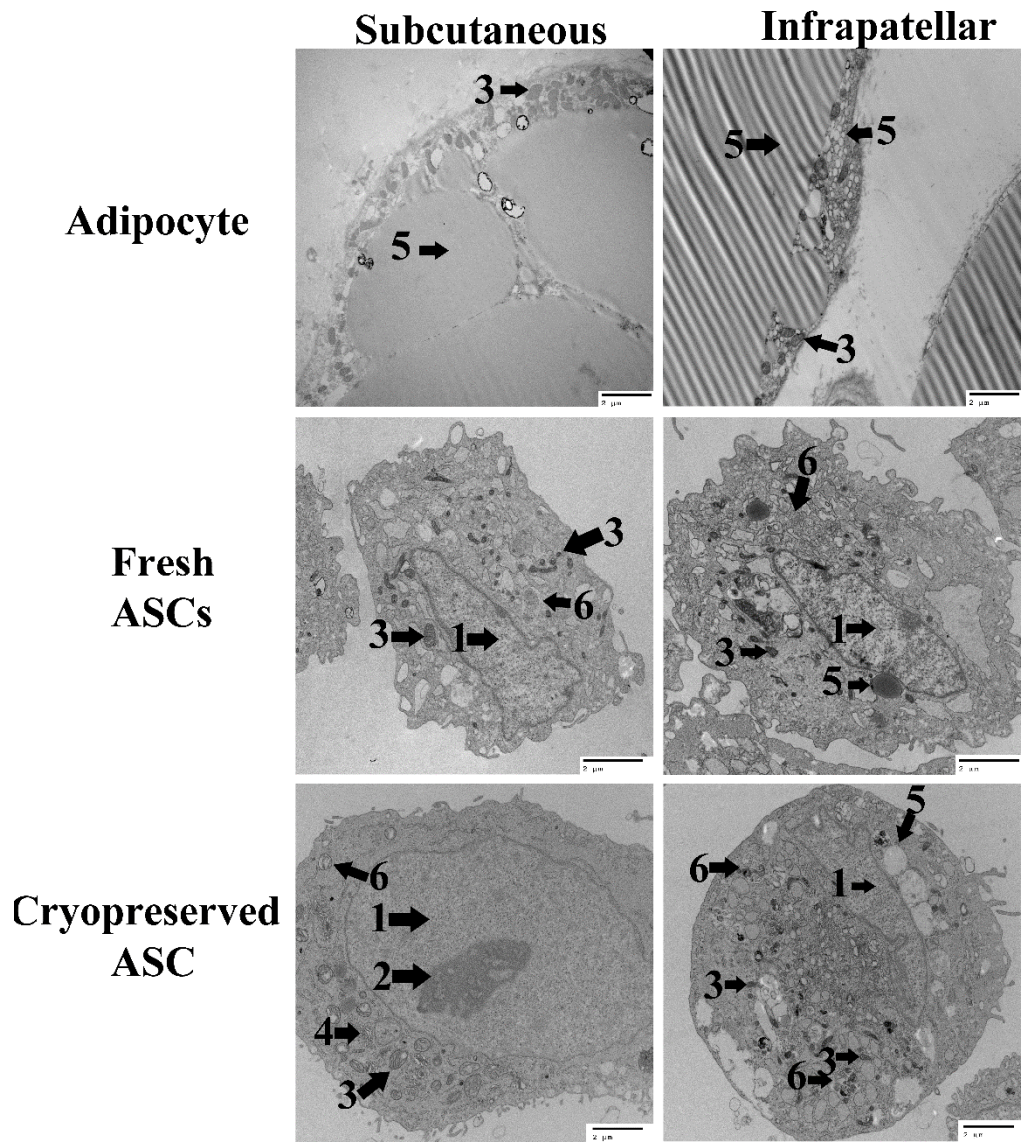

Figure 6 Transmission electron microscopy (TEM) image of adipocytes and adipose derived multipotent stromal cells (ASCs) from canine subcutaneous (SUB) and infrapatellar (IFP) adipose tissues. Legend: 1 – nucleus, 2 – euchromatin, 3 – mitochondria, 4 – Golgi apparatus, 5 – lipid droplet, 6 – lysosome. Scale bar = 2 μm.

2.3.3. Multipotentiality (P0, 1, 3, tP1, 3) – Limiting Dilution Assays and Pellet Chondrogenesis

Based in histochemical staining, fresh and revitalized IFP and SUB ASCs showed robust adipogenesis and osteogenesis for all passages evaluated. The CFU frequency percentage indicates the percentage of cells capable of forming a colony of fibroblastic (CFU-F), osteoblastic (CFU-Ob) or adipogenic (CFU-Ad) lineage. Before and after cryopreservation, SUB and IFP ASCs

showed similar CFU frequency percentages, and, though values tended decrease after cryopreservation, they were not significantly different among fresh and cryopreserved cells from the same tissues within passages (Fig. 8). In fresh and cryopreserved cells, the frequencies decreased with passage and were significantly lower in P3 versus P0. For CFU-F, P0 and 1 were significantly higher than P3, and for CFU-Ob, P0 was significantly higher than P1 which was significantly higher than P3. The only difference in behavior between cell sources was that P1 SUB ASC CFU-Ad was significantly lower than P0 while IFP ASC CFU-Ad was significantly higher in P0 and 1 than P3 in fresh cells. Fresh and cryopreserved SUB and IFP ASCs displayed characteristic chondrogenic differentiation including glycosaminoglycan (GAG) deposition and tissue organization, both of which were absent in the control group (Fig. 9).

2.2.4. Immunophenotype -Flow Cytometry (P0, 1, 3, tP1, 3)

The majority of fresh cells from both adipose tissue depots were CD29+, CD44+, CD90+ and CD34- for all passages evaluated (Fig. 10). The percentage of CD29+ ASCs was significantly higher in P0 compared to 1 and 3 for fresh SUB and IFP ASCs (Fig. 10a). There were significantly higher percentages of CD29+ and CD44+ ASCs in cryopreserved P1 versus P3 for both tissue sources (Fig. 10a, c). Fresh P1 SUB and P3 ASCS from both tissue sources had significantly higher percentages of CD29+ cells than the same passages after cryopreservation (Fig. 10a). There were significantly higher percentages in of CD44+ P1 ASCs after cryopreservation compared to fresh cells within tissue source (Fig. 10c). However, cryopreserved P3 ASCs had significantly lower percentages of CD44+ than fresh. There were significantly fewer fresh CD90+ P3 SUB ASCs compared to cryopreserved (Fig. 10d).

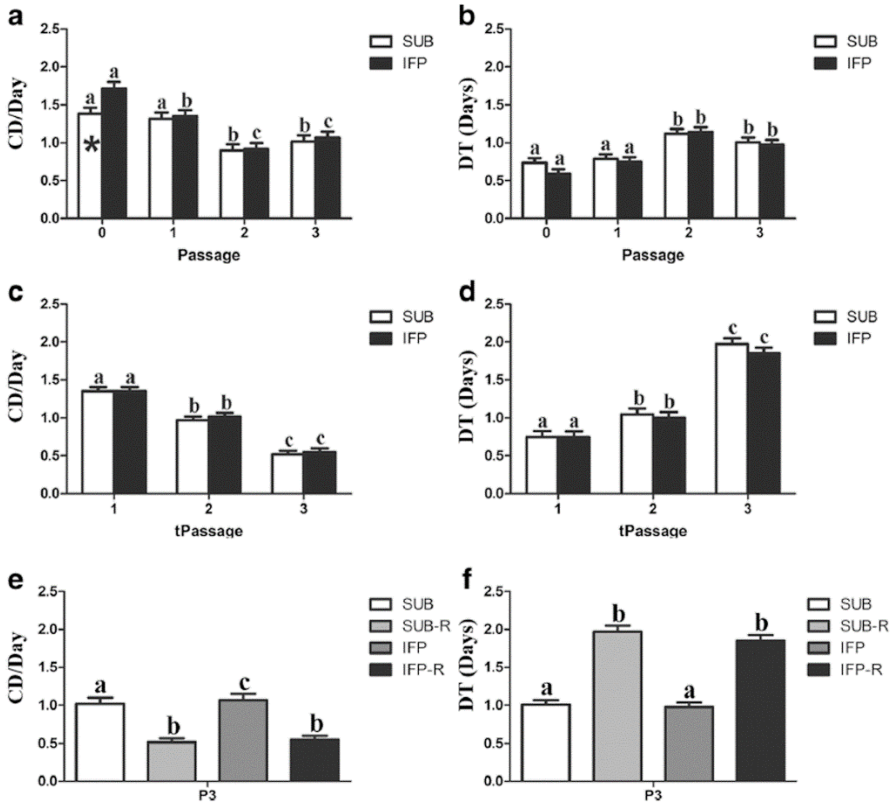

Figure 7. Cell doublings (CD) and doubling time (DT) (mean ± SEM) for fresh (a, b), revitalized (c, d) and both fresh and revitalized canine ASCs (e, f) from SUB and IFP adipose tissues. Columns with asterisks within passages are significantly different between cell tissue source (a), columns with distinct superscripts within cell tissue source (a-d), and columns with distinct superscripts within passage (e, f) are significantly different ($P < .05$).

2.2.5. Gene Expression - RT-PCR (P0, 1, 3 tP1, tP3)

With increasing passage, adipocytic and osteoblastic target gene expression decreased significantly in both fresh and cryopreserved cells (Fig. 11). Both P1 and tP1 SUB and IFP ASCs had significantly higher levels of PPAR-γ and leptin after adipogenic induction as well as OPG and Col I after osteogenic induction compared to P3 and tP3 (Fig. 11a, b). Additionally, PPAR-γ expression was significantly lower in P3 ASCs following induction after cryopreservation in cells from both tissue sources.

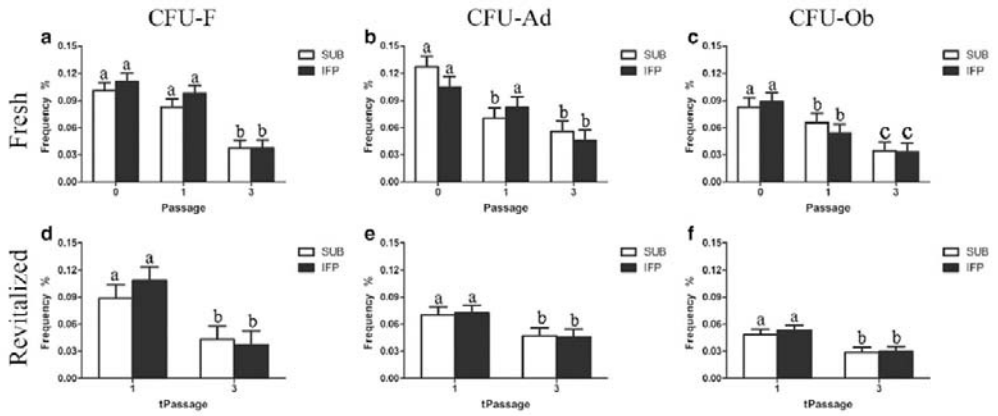

Figure 8. Colony forming unit (CFU) frequencies (mean ± SEM) for fresh (a, b, c) and revitalized (d, e, f) canine ASCs from subcutaneous (SUB) or infrapatellar (IFP) adipose tissue after culture in stromal (CFU-F), osteogenic (CFU-Ob), or adipogenic (CFU-Ad) medium. Columns with different superscripts within cell source are significantly different among passages ($P < .05$).

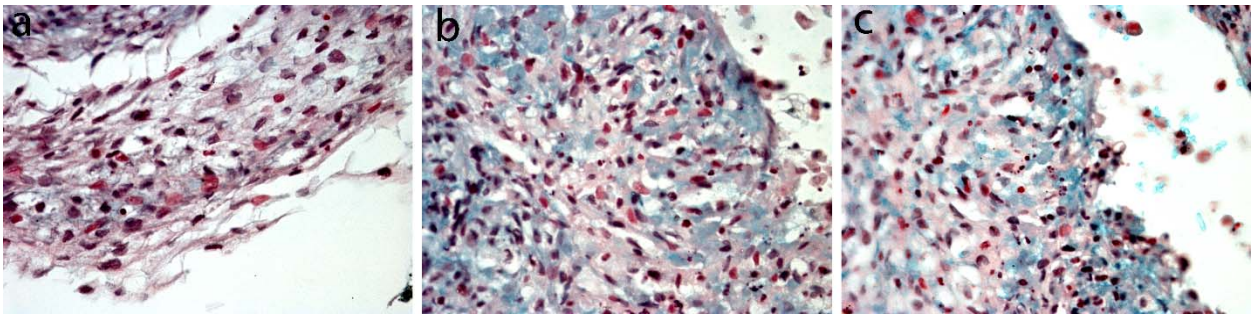

Figure 9. Light photomicrographs of fresh P3 canine ASCs from SUB (a, b) and IFP (c) after pellet culture in stromal (a) or chondrogenic (b, c) medium. Alcian blue staining of proteoglycans with nuclear fast red counter stain. 63× magnification. Scale bar = 20 μm.

2.2.6. Protein Expression – Immunocytochemistry, western Blot (P3, tP3)

Immunocytochemistry. Cell surface marker expression (CD29+, CD44+, CD90+, and CD34-) was confirmed with immunocytochemistry in all ASCs before and after cryopreservation (Fig. 12).

Western blot. The mean gray value for each band was measured to quantify protein bands. The measured values for band increased with increasing protein expression. The PPAR-γ and OPN protein expression increased in P3 and tP3 ASCs cultured in adipogenic or osteogenic induction medium, respectively, while SOX2 decreased (Fig. 13b, c, e and f). Additionally, SOX2 protein expression decreased after cryopreservation in cells from both tissues cultured in stromal medium

(Fig. 13d). Cryopreserved P3 SUB and IFP ASCs had significantly lower protein expression of CD29 and CD44 compared to fresh P3 ASCs (Fig. 14).

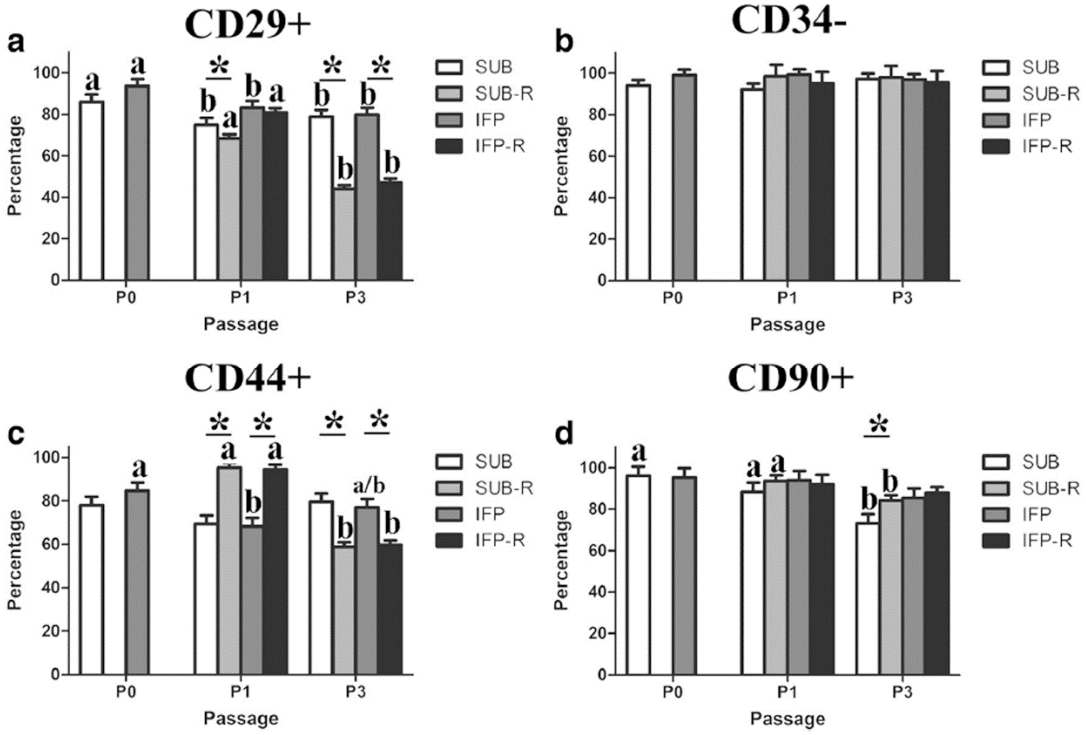

Figure 10 Percentages (mean ± SEM) of CD29+ (a), CD34- (b), CD44+ (c), and CD90+ (d) fresh and revitalized (-R) ASCs from canine SUB and IFP adipose. Columns connected by lines with asterisks are significantly different within passage and columns with distinct superscripts within cell tissue source and treatment (fresh or cryopreserved) are significantly different among passages ($p<.05$).

2.5. Discussion

Paired comparisons of fresh and cryopreserved ASCs from canine SUB and IFP adipose tissue in this study showed comparable in vitro expansion and multipotentiality up to passage 3. Fresh and cryopreserved canine ASC expansion metrics, CD and DT, and CFU frequency percentages had similar values and cell passage changes to previous reports using the same techniques [77, 181]. However, detectable effects of cryopreservation on ultrastructure, immunophenotype, and both surface marker and transcription factor expression indicates that cryopreserved canine ASCs may not be directly interchangeable with fresh. In spite of the potential impact of cryopreservation on

ASC potential, study results suggest that ASCs from either tissue source are promising candidates for future studies to optimize cell isolation, cryopreservation, tissue regeneration strategies and therapeutic applications.

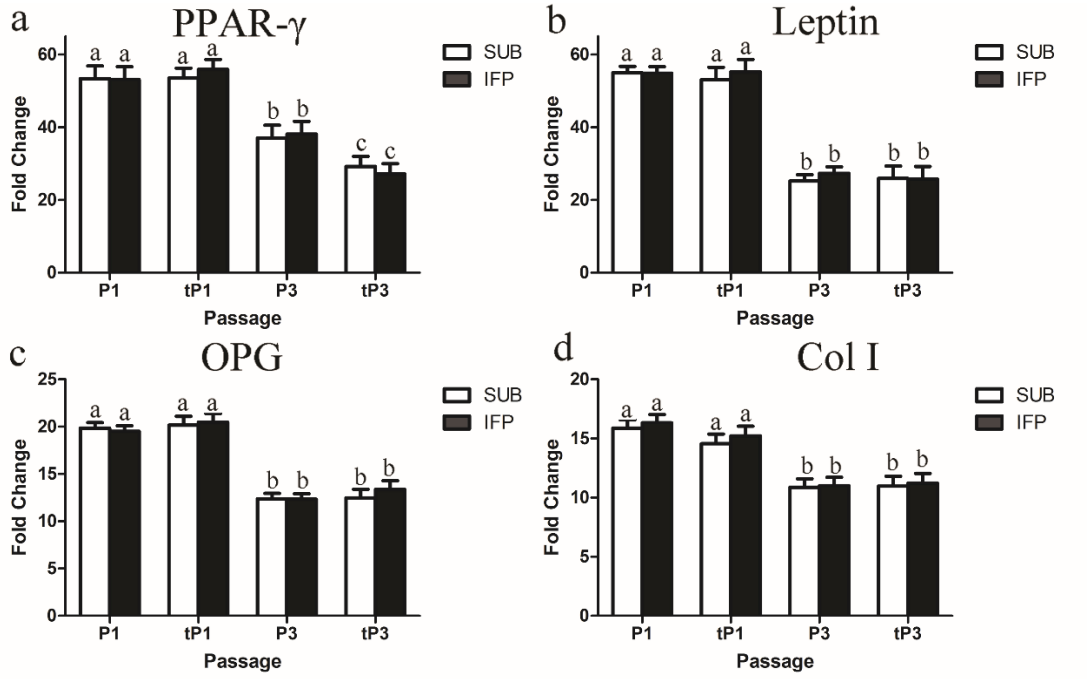

Figure 11 Fold change (mean ± SEM) of adipogenic (a, b) and osteogenic (c, d) lineage target genes in fresh and revitalized (t) canine ASCs from subcutaneous (SUB) and infrapatellar (IFP) adipose tissue cultured in induction medium. Values are relative to the reference gene GAPDH and to cells cultured in stromal medium. OPG = Osteoprotegerin, Col1α1 = Collagen Iα1. Columns with different superscripts within cell tissue source are significantly different ($P < .05$).

The ultrastructure observed in this study was similar to those reported for other species [185, 186] including abundant cytoplasmic mitochondria [185] and many small lipid vacuoles [186] in brown and white adipocytes, respectively. The characteristics are consistent with lipid energy storage [178, 187] and the role of the inner mitochondrial membrane in thermogenesis [188, 189]. Mature adipocytes are post-mitotic, so cell precursors rapidly differentiate in response to energy demands [190, 191]. As such, immature cells at many stages of differentiation assume characteristics of the mature cells as observed in the ASCs in study. This is also consistent with

the current knowledge that white and brown adipocytes are derived from distinct precursor populations [192-194].

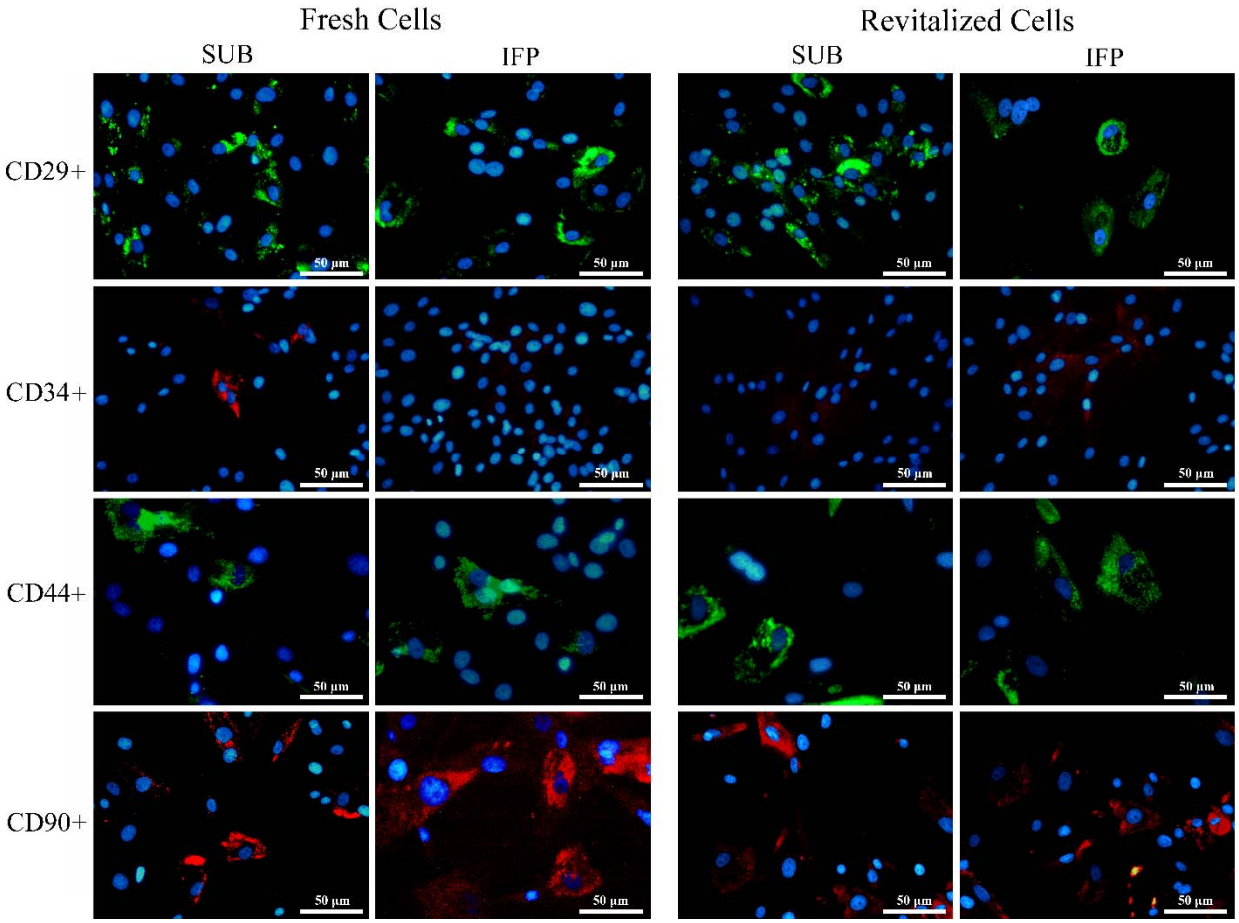

Figure 12. Fluorescent photomicrographs of SUB and IFP fresh and revitalized canine P3 ASCs from subcutaneous (SUB) and infrapatellar (IFP) adipose tissue labeled with cell surface markers indicated. 40 × magnification. Scale bar = 50 µm.

Fewer mitochondria surrounding the nucleus after cryopreservation may indicate greater maturity in revitalized cells. Mitochondrial localization is a characteristic of mammalian cleavage-stage embryos that is strongly indicative of stem cell competence, and alterations may be associated with diminished pluripotency [195, 196]. The percentage of cells with perinuclear mitochondria decreased while that of cells with lipid droplets increased with cell passage in an adult primate adipose derived stem cell line [195]. Reduced perinuclear mitochondria were

associated with lower oxygen consumption and higher adenosine triphosphate consistent with lower energy requirements of differentiated cells with slower metabolism. The decrease in mitochondria after cryopreservation in this study was a subjective assessment, so the magnitude of the change could not be quantified or directly compared between ASC tissue sources. A consistent finding was that mitochondrial numbers were consistent within cells from specific tissue sources and reduced following cryopreservation.

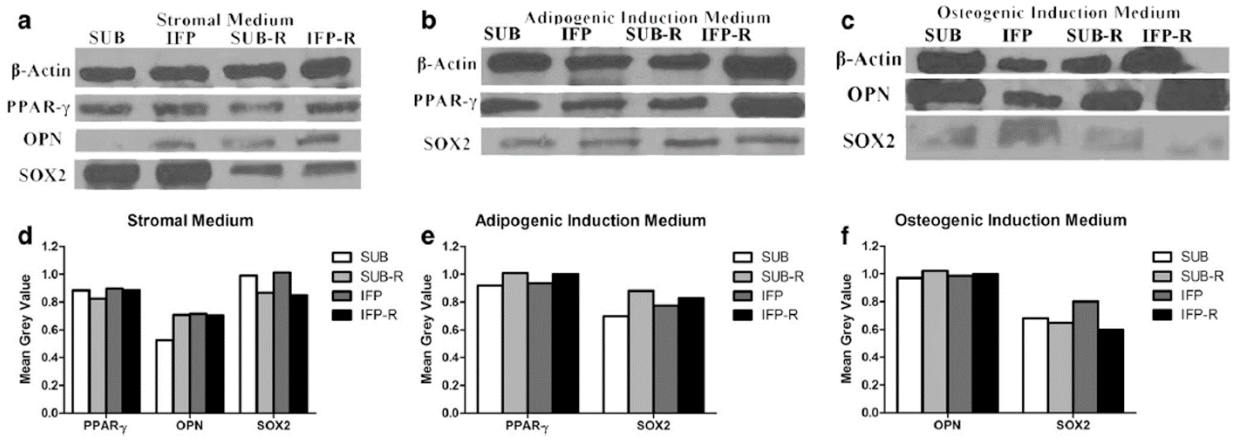

Figure 13. Western blot image of proteins from fresh and revitalized (-R) canine P3 ASCs from subcutaneous (SUB) and infrapatellar (IFP) adipose tissue after culture in stromal (a), adipogenic (b) or osteogenic (c) medium with corresponding graphs indicating relative density (d-f). PPAR-γ = Peroxisome proliferator-activated receptor-γ, SOX2 = Sex determining region Y box-2, OPN = Osteopontin.

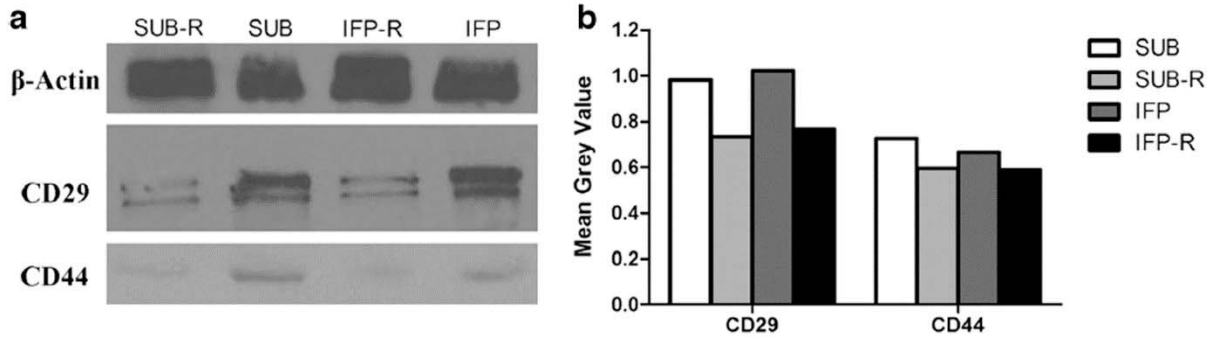

Figure 14. Western blot image (a) and corresponding relative density graph (b) of fresh and revitalized (-R) P3 ASCs following culture in stromal medium.

Current knowledge suggests that loss of mitochondria may be a result of organelle disruption and/or cell selection by the cryopreservation process [37, 43, 197]. The potential for cell selection is further supported by increased numbers of lipid vacuoles post-cryopreservation. The cryoprotectant used in this study, DMSO, is a standard component of cryopreservation media for cell protein and membrane stabilization [21, 37, 43] and to prevent intracellular ice formation [37, 43]. At non-toxic DMSO levels, and despite a slow freezing process, intracellular ice formation is not fully prevented [198-200]. Fewer mitochondria and more abundant lipid vacuoles are associated with greater cell maturity as indicated above [195, 196]. Based on the these findings, it is possible that the higher lipid content of more mature cells within the heterogeneous cell isolate confers a higher transition temperature during freezing [201]. Together with the DMSO, the higher lipid content may protect against ice formation and thereby select for greater cell maturity. Further studies are required for confirmation of this finding.

Additional distinctions between fresh and cryopreserved ASCs were decreases in cell percentages expressing CD29 and CD44, multipotent stromal cell phenotypic markers that are stably expressed in ASCs [75]. Exceptions included variable CD90 expression and an initial increase in the number of CD44+ cells in P1 cryopreserved cells. Previous studies identified increased CD90 expression in revitalized cells versus fresh MSCs from human umbilical cord and rat adipose and bone marrow tissues [202, 203]. It is generally accepted that due to the presence of CD90 in the endothelial population, changes in expression are best interpreted in combination with the expression of other surface markers [75]. The initial increase in CD44 expression in revitalized cells that was not paralleled in CD29 expression could be due to an increase in CD44 expression by cells that do not express CD29, potentially due to high protein concentrations in FBS. The principle ligand of CD44 is hyaluronic acid (HA) [204]. Murine cumulus cell-oocyte

complexes retain HA in the extracellular matrix and expand in the presence of FBS [205]. In contrast, HA is released into the culture medium in the absence of FBS, the cells dissociate and attach to culture ware as individual cells [205]. Hence, high concentrations of FBS in the freezing medium may increase local HA concentrations and stimulate upregulation of the receptor in cells in the passage immediately post revitalization.

In general, there were fewer cells expressing CD29 and CD44 after cryopreservation within passages, with the exceptions discussed above, and passage effect tended to be more profound in cryopreserved cells. Lower CD29 and CD44 expression was confirmed by western blot. Upregulation of apoptotic genes and increased apoptosis is associated with cryoprotectants and the cryopreservation process itself [19, 206]. Additionally, DMSO concentrations of 10% or higher reduce the number of porcine ASC fibroblastic colony forming units and increase cell apoptotic gene expression after cryopreservation [21]. A previous study confirmed that the expression of adhesion molecule CD62L [207] was lost while CD57, an apoptosis protein [208], increased after cryopreservation in CD4+ and CD8+ T cells [206]. Based on this established information, decreases in CD44 and CD29 post cryopreservation suggests a similar and important effect on canine SUB and IFP ASCs that should be considered for cell therapy and tissue regeneration strategies.

Decreases in SOX2 protein expression and PPAR-γ gene expression observed in this study further suggests that cryopreservation may impact ASC plasticity. Both are early transcription factors, SOX2 is associated with the multipotent ASC phenotype [209, 210] and PPAR-γ is nuclear receptor that controls energy metabolism and cell differentiation and is highly expressed in [211, 212]. It is further controls transcription of genes for radical oxygen species detoxification enzymes [213]. Recently, mitochondria were shown to be central to oligodendrocyte differentiation and

major targets of PPAR-γ agonist protection against inflammatory cytokine damage [211]. The fact that PPAR-γ protein expression was not detectably lower in P3 ASCs after cryopreservation is likely because gene and protein expression is not necessarily parallel, and changes in gene expression typically precede alterations in protein levels. Lower expression of both SOX2 and PPAR- γ in addition to the reduced presence of cellular mitochondria may indicate greater cell vulnerability to inflammatory byproducts in addition to decreased differentiation capacity.

As a whole, these in vitro study results indicate that there are few differences between canine SUB and IFP ASCs before and after cryopreservation. The impact of cryopreservation on the cells is strongly supported at the genetic, protein and ultrastructural levels and appears to be consistent with lower expansion capacity and plasticity associated with greater cell maturity. Cryopreservation is vital to storage and transport of progenitor cells [41, 42, 214, 215]. It is especially important given the growing recognition of the importance of cell phenotype for specific therapeutic and tissue regeneration purposes [216-218]. Continued efforts to minimize the impact of cryopreservation on ASC properties as well mechanisms to clearly delineate and anticipate the effects will continue to improve cell-based therapies and tissue regeneration.

CHAPTER 3. COLLAGEN AND HYDROXYAPATITE SCAFFOLDS ACTIVATE DISTINCT OSTEOGENESIS SIGNALING PATHWAYS IN ADULT HUMAN ADIPOSE-DERIVED MULTIPOTENT STROMAL CELLS

3.1. Introduction

Bone grafts are a standard therapy to augment osteogenesis, but autografts can be complicated by limited graft material and donor site morbidity and allografts by potential disease transmission and immunogenicity [219, 220]. Bone graft substitutes offer plentiful, risk free options that are not influenced by donor condition [221]. ASCs enhance the osteoinductive and osteoconductive properties of commercially available, bone graft substitutes [219, 222]. Advantages like a greater number and volume of tissue harvest depots in addition to higher stromal cell density and comparable plasticity to bone marrow derived multipotent stromal cells make ASCs an appealing choice for MSC-scaffold constructs [223]. However, recipient factors like age, sex and health also influence the ability of ASCs to promote bone formation [224, 225]. Customization of ASC-bone graft constructs for individual morbidities will elevate current standards of care.

Osteogenesis is a dynamic, multifaceted process with intersecting cell signaling cascades that direct cell recruitment, differentiation, maturation and behavior [226]. Bone forming capacity is reduced by cell signaling pathway modifications from disease or age [226-228]. Osteoblastic and osteoclastic activity is regulated by the ratio of osteoprotegerin (OPG) and receptor activator of nuclear factor kappa β ligand (RANKL), and alterations are thought to contribute to abnormal bone healing and maintenance in several bone diseases [226]. Activity levels of CB1 and CB2 are implicated in age related changes in bone turn over and mass [227-230]. Notably, OPG stimulation triggers Wnt/β catenin signaling while the cannabinoid receptors appear to work via adrenergic signaling [226, 231, 232]. This knowledge provides an opportunity to explore targeted restoration of specific osteogenic pathways with ASC-bone graft constructs. Specifically, the ability to

confidently restore cell signaling most strongly associated with compromised bone formation of individual patients will contribute to improved and customized treatment options.

Commercially available bone grafts are composed of inorganic and organic components to direct cell differentiation and extracellular matrix (ECM) production [219, 221, 233-236]. The type and amount of inorganic crystals as well as their ratios to each other and proteins stimulate distinct gene expression [142, 234, 237-241]. Cells also behave differently on identical scaffolds when cultured in environments designed to maintain a primordial state versus those to promote differentiation and maturation [242, 243]. Mechanisms to "prime" cells by short term exposure to induction reagents may accelerate differentiation stimulated by the scaffold [244].

We propose that it is possible to reproducibly select for specific ASC osteogenesis signaling pathways with scaffold composition and/or culture medium. To evaluate this potential, in vitro human adult ASC viability, gene expression and ECM deposition and organization was determined on bone graft scaffolds composed of pure type I collagen, type I collagen and one mineral, β tricalcium phosphate, and type I collagen with two minerals, β tricalcium phosphate and hydroxyapatite. Cell-scaffold combinations were determined following culture in stromal (S), osteogenic (O) or short term osteogenic followed by stromal medium (OS) for up to 28 days. The following two-part hypothesis was tested: 1) Identical ASC isolates on distinct bone graft scaffolds demonstrate unique viability, differentiation, ECM production and gene expression in the same culture conditions; 2) Identical ASC-bone graft scaffold combinations have unique cell viability, differentiation, ECM production, and gene expression when cultured in S, O or OS medium. The overarching goal of this investigation was to identify ASC-scaffold combinations for local, targeted restoration of genetic expression and ECM deposition to enhance bone healing in the presence of specific bone pathology.

3.2. Materials and Methods

3.2.1. Ethics Statement All procedures were approved by the Institutional Review Board (Protocol #00006218) and informed consent was obtained prior to tissue use.

3.2.2. Study Design Commercially available human ASCs (LaCell LLC, New Orleans, LA) were culture expanded to cell passage (P) 3. Cell viability was quantified with confocal laser microscopy immediately after loading and 7 and 14 days of culture. Gene expression (alkaline phosphatase (ALP), osteocalcin (OCN), cannabinoid receptors one and two (CB1, CB2), osteoprotegerin (OPG), nuclear factor kappa β ligand (RANKL)) and ECM deposition (double stranded DNA (dsDNA), total protein, sulfated glycosaminoglycan (sGAG), total collagen) in ASC-scaffold constructs were quantified prior to and after 7, 14 and 28 days of culture in S, O and OS medium. Scanning electron microscopy (SEM) was used to assess scaffolds without cells and extra-cellular matrix on constructs after 7 and 14 days of culture. Specifically, the sample set consisted of ASCs from 3 donors that were each loaded on three distinct scaffolds and immediately assessed or evaluated after culture in three different media for 7, 14 or 28 days for all measures except cell viability and SEM, which were each performed after the first two. A minimum of three replicates of each assay were performed for all samples.

3.2.3. Scaffold Materials Bone graft scaffolds were composed of type I bovine collagen (C, Avitene^{tm} Ultrafoam^{tm}, Davol, Inc., Warwick, RI), 15% hydroxyapatite, 85% β-tricalcium phosphate, type I bovine collagen (HT, MasterGraft^{tm} Matrix, Medtronic Sofamor Danek, Inc., Minneapolis, MN) and 20% type I bovine collagen, 80% β-tricalcium phosphate (CT, Vitoss® Scaffold Foam^{tm}, Stryker Corp., Kalamazoo, MI). Scaffolds were aseptically cut into 5x5x3 mm (C), 5x5x5 mm (HT), and 5x5x4 mm (CT) rectangular blocks for constructs.

3.2.4. Cells Frozen ASC aliquots (LaCell, LLC, New Orleans, LA) from 1 male and 2 females (47.3 ± 7.0 years (mean ± SEM), 28.3 ± 4.1 BMI) in cryopreservation medium (LaCryoM-100, LaCell, LLC) were used for this study [41, 42]. Aliquots were thawed at 37ºC with agitation for 2-3 min, combined with 5 ml of stromal medium (S, DMEM/F12 (Hyclone, Logan, UT), 10% characterized fetal bovine serum (Hyclone), 1% antibiotic (MP Biochemicals, Solon, OH)) and centrifuged (300xg, 5 min). Cells were culture expanded to P3 in S medium (37ºC, 5% CO_2) with an initial seeding density of $5x10^3$ cells/cm^2, media changes every three days and passage at ~70% confluence [181].

3.2.5. Cell Loading Passage 3 ASC suspensions (17.0×10^6 cells/120 mL corresponding to 57,000 cells/mm^3 of total scaffold volume) from each donor were loaded onto 3 scaffolds of each composition on 3, 4-inch-long, 22g spinal needles suspended from a rubber stopper in 100 ml spinner flasks (Bellco® Biotechnology, Newark, NJ). The process was repeated 5 times for each donor (15 samples/scaffold/donor). Scaffolds were oriented with the shortest dimension perpendicular to the needle long axis. Spinner flasks were maintained in a humidified incubator (37C, 5% CO_2) for 2 h with a magnetic stir bar rotating at 70 rpm. Following cell loading, loading efficiency was calculated from the number of cells remaining in each flask. Samples were evaluated or transferred to 1 of 3 media in six well culture plates (Thermo Fisher Scientific, Waltham, MA, USA): 1) stromal (S, DMEM/F12 (Hyclone, Logan, UT), 10% characterized fetal bovine serum (Hyclone), 1% antibiotic (MP Biochemicals, Solon, OH)); 2) osteogenic (O, stromal + 10 mM β-glycerophosphate (Affymatrix, Santa Clara, CA), 20 nM dexamethasone (Sigma-Aldrich, St. Louis, MO), 0.05 mM ascorbic acid (Sigma-Aldrich)); or 3) osteogenic for 48 h followed by stromal (OS).

3.2.6. Cell Viability (Days 0, 7, 14) Cell viability was quantified on 20 digital photomicrographs (TIFF,10x) of the construct surface, 250 μm apart, that were generated with a spectral confocal laser scanning microscope digital imaging system (Leica TCS SP2, Leica Microsystems, Buffalo Grove, IL, USA). Constructs were rinsed with phosphate buffered saline and incubated at room termperature in darkness with assay reagents (Invitrogen LIVE/DEAD® Viability/Cytotoxicity kit, Thermo Fisher Scientific) for 30 min [245]. The numbers of live (green) and dead (red) cells in each section were quatified (Image-Pro, Media Cybernetics, Bethesda, MD) to calculate live cell percentage (live cells/total cells x 100) for each construct.

3.2.7. Gene Expression (Days 7, 14, 28) Total RNA was extracted from cell-scaffold constructs (RNeasy Plus Mini Kit, Qiagen, Germantown, MD) and cDNA synthesized (QuantiTect Reverse Transcription Kit, Qiagen). Quantification of target gene levels (ALP, OCN, CB1, CB2, OPG RANKL) was performed with a 384-well plate sequence detection system (ABI Prism 7900HT, Applied Biosystems, Carlsbad, CA) using SYBR Green Supermix (Bio-Rad Laboratories, Hercules, CA) and validated primer sequences (Table 8). The $2^{-\Delta\Delta Ct}$ values were determined relative to the reference gene glyceraldehyde 3-phosphate dehydrogenase (GAPDH) and target gene expression immediately after cell loading (Day 0). The OPG/RANKL ratio was determined in individual samples by dividing the OPG fold change by the RANKL fold change.

3.2.8. Compositional Analysis (Days 7, 14, 28) Cell-scaffold constructs were lyophilized (-55° C, 0.2 mbar, 4 hr) and then incubated in a papain digest (2 mg papain (MP Biomedicals)/g lyophilized sample, 20 mM L-cysteine (MP Biomedicals), 9 mM di-sodium EDTA (Sigma-Aldrich), 3.6 M sodium acetate (Sigma-Aldrich)) at 60° C for 10 hrs. Following centrifugation of the solution (4000 × g, 10 min), the supernatant was collected and stored at -80°C. Samples were thawed for 1 min in a 37°C water bath immediately prior to compositional analysis. All assays were performed

according to manufacturer's instructions or published methods for microtiter plate analysis, performed in triplicate and fluorescence or absorbance quantified with a multiwell plate reader (Synergy HT, BioTek Instruments, Winooski, VT). Composition fold change relative to Day 0 was calculated as C_f/C_i (C_i: content immediately after cell loading; C_f: content after 7, 14, or 28 days of culture).

Table 8. RT-PCR primer sequences

Gene Name	Sequence	Accession No.
GAPDH	F: CGGGATTTGGTCGTATTG R: CTGGAAGATGGTGATGGG	NM_001289746.1
ALP	F: TTCTTCTTGCTGGTGGAG R: GGCTTCTTGTCTGTGTCA	XM_017000903.1
ColIαI	F: AGAGCATGACCGATGGATTC R: CCTTCTTGAGGTTGCCAGTC	XM_005257059.4
OCN	F: GCAGAGTCCAGCAAAGGT R: CCCAGCCATTGATACAGG	NM_199173.5
CB1	F: CGATACACTTGGCATTGACG R: AACCACGAGCAAAGGAGAGA	XM_006715330.3
CB2	F: ATTGGCAGCGTGACTATG R: GAAGGCGATGAACAGGAG	XM_011540629.2
OPG	F: AACCCCAGAGCGAAATAC R: AAGAATGCCTCCTCACAC	NM_002546.3
RANKL	F: ATCGTTGGATCACAGCACATCA R: TGAGCAAAAGGCTGAGCTTCA	XM_017020803.1

GAPDH: glyceraldehyde 3-phosphate dehydrogenase; ALP: alkaline phosphatase; ColIαI: collagen 1α1; OCN: osteocalcin; CB1: cannabinoid receptor type I; CB2: cannabinoid receptor type II; OPG: osteoprotegerin; RANKL: receptor activator of nuclear factor kappa-B ligand.

Double stranded DNA (dsDNA) – PicoGreen: Total dsDNA was quantified using a commercially available kit (Quant-iT PicoGreen dsDNA Assay Kit, Thermo Fisher Scientific). Fluorescence was measured at 480 and 520 nm and dsDNA quantified on a lambda DNA standard curve.

Total Collagen – Hydroxyproline [246]: An equal volume of 6N HCl was added to samples or serial dilutions of trans-4-hydroxy-L-proline (ACROS Organics™, Morris Plains, NJ) and incubated overnight at 110ºC. Samples were incubated for 5 min at room temperature following addition of 500 µl of oxidant solution (0.178g Chloramines T in 15 ml of isopropanol and 10 ml of ddH_2O) and then 25 ml of acetate citrate buffer (120 g sodium acetate trihydrate, 12 ml acetic acid, 50 g citric acid monohydrate, 34g NaOH in 1L ddH_2O, pH 6.0). Subsequently 500 µl of Ehrlich's reagent (1g p-dimethylaminobenzaldehyde (Sigma-Aldrich) in 20 ml isopropanol with 6.6 ml perchloric acid and 15.6 ml ddH_2O) was added and samples incubated at 60ºC for 12 min. Following 4 min of cooling on ice, samples were transferred to a 96 well microtiter plate and absorbance read at 550 nm.

Sulfated Glycosaminoglycan (sGAG) - Dimethylmethylene Blue (DMMB) [247]: Sodium formate was added to 1, 9- DMMB in ethanol and the pH adjusted to 3.0 with formic acid to create the sGAG assay buffer. Samples were combined with buffer in a microtiter plate, and the sGAG concentration determined from absorbance at 520 nm and a chondroitin sulfate standard curve.

Total Protein – Lowry Assay [248]: Samples were mixed with Biuret's reagent (Sigma-Aldrich) and maintained at room temperature for 12 min. The absorbance at 650 nm was measured after 30 min at room temperature following addition of Folin-Ciocalteu's reagent (Sigma-Aldrich).

Total protein concentration was determined on a bovine serum albumin (Sigma-Aldrich) standard curve.

3.2.9. Ultrastructure (Days 0, 7, 14): Standard procedures were used to prepare samples for SEM. Briefly, they were fixed in 0.5% glutaraldehyde in 0.1M sodium cacodylate buffer (pH 7.4) for one hr and then for 48 hr in 0.1% osmium tetroxide. Samples were dehydrated in a series of ethanol solutions (50-100%), and, following critical point drying, sputter coated with gold. Photomicrographs were generated of SEM images (Quanta 200, FEI Company, Hillsboro, OR).

3.2.10. Statistical Analysis*:* All results are presented as least squares (LS) mean ± SEM. Statistical analyses were performed with commercially available software (SAS 9.4, Institute, Cary, NC). A 3×3×3 factorial analysis of variance followed by pairwise tests of least-squares means was used to compare gene expression and composition measures among time points, scaffolds and media ($p < 0.05$). Normality and homogeneity of variance were assessed with Shapiro-Wilk tests and residual plots.

3.3. Results

3.3.1. Cell Viability (Days 0, 7, 14) Overall cell loading efficiency was 80.6 ± 3.4% and viability was similar among scaffolds immediately after loading (Day 0, Fig. 12A). After 7 days of culture, the percentage of live cells was not significantly different among constructs irrespective of medium (Fig. 12B). After 14 days, the percentage of viable cells on CT constructs in S medium was significantly lower than C constructs (Fig. 12C).

3.3.2. Gene Expression (Days 7, 14, 28)

In general ALP expression tended to decrease and OCN increase with culture time while Col1α1 increased with culture S medium (Fig. 16 & 17). The changes in ALP and OCN expression were most pronounced in HT scaffolds cultured in O medium. Summarily, there was highest expression

of ALP in HT constructs cultured in OS and O media after 7 days of culture. By 14 days of culture, ALP expression was highest in HT and C constructs in O medium. After 28 days, the highest ALP expression was in C constructs in O medium. The Col1α1 expression was highest in C and HT constructs in O and OS media after 7 days and in S medium after 14 and 28 days of culture. By day 28, C and HT constructs cultured in O media had the highest OCN expression.

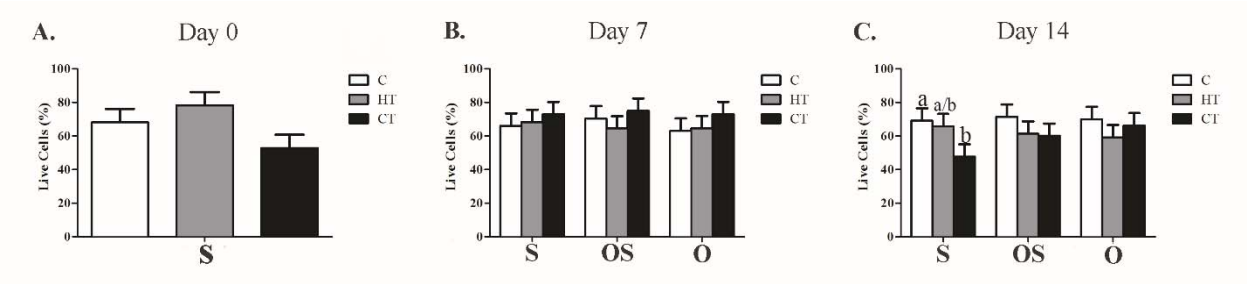

Figure 15 Cell percentages (LS mean ± SEM) for type I bovine collagen (C), hydroxyapatite + β tricalcium phosphate + type I bovine collagen (HT) and β tricalcium phosphate + type I bovine collagen (CT) scaffold-ASC constructs after 0 (A), 7 (B), and 14 (C) days of culture in stromal (S), osteogenic for 48 hours followed by stromal (OS) or osteogenic (O) medium. Significant differences are indicated by different column superscripts within graphs ($p<0.05$).

With time, CB1 and OPG/RANKL expression tended to increase in constructs cultured in O medium (Fig 16 & 18). The CB1 expression was highest in C constructs in O medium at all time points. Expression of CB2 was highest in C and CT constructs after 14 days of culture in all media. The OPG/RANKL expression ratio was highest in on HT constructs in all media after 14 and 28 days, though the greatest expression was reached after 28 days in O medium.

3.3.3. Compositional Analysis (Days7, 14, 28) (Fig 19 & 20)

Double stranded DNA (dsDNA) – PicoGreen): The dsDNA fold change tended to remain the same or increase slightly with time. It was highest on HT constructs in O medium after 7 days, in O and OS media after 14 days and in S and OS media after 28 days of culture.

Gene	Scaffold	S			OS			O		
		Day 7	Day 14	Day 28	Day 7	Day 14	Day 28	Day 7	Day 14	Day 28
ALP	C	1.4±1.7^{A}	6.7±1.7^{B}	6.0±1.7^{B}	3.0±1.7^{A}	7.9±1.7^{B}	9.9±1.7^{B}	3.7±1.7^{A}	18.1 ± 1.7^{B}	15.1 ± 1.7^{B}
	HT	3.4±1.7^{A}	14.7±1.7^{B}	10.2±1.7^{B}	16.7±1.7^{A}	11.4±1.7^{B}	12.7±1.7$^{A/B}$	11.8±1.7$^{A/B}$	18.4 ± 1.7^{A}	9.1 ± 1.7^{B}
	CT	4.6±1.7	4.0±1.7	4.5±1.7	3.2±1.7	4.6±1.7	2.2±1.7	4.6±1.7	5.1 ± 1.7	2.8 ± 1.7
Col1α1	C	1.0±0.8^{A}	3.6±0.8^{B}	4.0±0.8^{B}	2.2±0.8	1.2±0.8	1.1±0.8	2.2±0.8	1.3±0.8	0.6±0.8
	HT	1.4±0.8^{A}	5.3±0.8^{B}	6.6±0.8^{B}	2.0±0.8	0.5±0.8	0.5±0.8	2.5±0.8^{A}	0.5±0.8$^{A/B}$	0.2±0.8^{B}
	CT	0.08±0.8	0.9±0.8	1.1±0.8	0.8±0.8	0.2±0.8	0.4±0.8	0.1±0.8	0.2±0.8	0.2±0.8
OCN	C	1.1±0.6^{A}	3.6±0.6^{B}	5.1±0.6^{C}	1.5±0.6^{A}	4.1±0.6^{B}	4.7±0.6^{B}	1.9±0.6^{A}	4.9±0.6^{B}	6.8±0.6^{B}
	HT	1.3±0.6	1.9±0.6	2.7±0.6	1.1±0.6	1.8±0.6	2.2±0.6	1.3±0.6^{A}	2.3±0.6^{A}	4.8±0.6^{B}
	CT	0.9±0.6	1.4±0.6	1.9±0.6	1.1±0.6	1.9±0.6	2.5±0.6	0.9±0.6	1.7±0.6	2.3±0.6
CB1 ($\times 10^4$)	C	0.0006±0.3	0.0003±0.3	0.01± 0.3	0.002± 0.3	0.007±0.3	0.03±0.3	4±0.3^{A}	4.6±0.3^{B}	5.3±0.3^{B}
	HT	0.0002±0.3	0.0004±0.3	0.03±0.3	0.1±0.3	0.03±0.3	0.02 ±0.3	0.3±0.3^{A}	2.3±0.3^{B}	1.1±0.3^{C}
	CT	0.0001±0.3	0.0002±0.3	0.0003±0.3	0.02±0.3	0.01±0.3	0.002±0.3	0.02±0.3^{A}	0.6±0.3$^{A/B}$	1.2±0.3^{B}
CB2	C	13.5±4.8^{A}	39.9±4.8^{B}	16.9±4.8^{A}	8.1±4.8	15.6±4.8	12.8±4.8	7.7±4.8^{A}	40.3±4.8^{B}	6.0±4.8^{A}
	HT	3.0±4.8	9.0±4.8	5.1±4.8	8.5±4.8	7.8±4.8	8.1±4.8	9.3±4.8	16.5 ± 4.8	18.1±4.8
	CT	6.1±4.8^{A}	36.1±4.8^{B}	21.5±4.8^{C}	6.6±4.8^{A}	32.7±4.8^{B}	16.9±4.8^{A}	3.4±4.8^{A}	22.2±4.8^{B}	7.7±4.8^{A}
OPG /RANKL	C	1.1±2.5	2.6±2.5	3.7±2.5	2.1±2.5	3.0±2.5	7.8 ± 2.5	7.5±2.5^{A}	6.2±2.5^{A}	67.8±2.5^{B}
	HT	4.1±2.5^{A}	13.7±2.5^{B}	15.7±2.5^{B}	4.4±2.5^{A}	16.1±2.5^{B}	14.5±2.5^{B}	2.7±2.5^{A}	49.1±2.5^{B}	90.4±2.5^{C}
	CT	0.3±2.5	0.8±2.5	3.8±2.5	0.2±2.5	1.0±2.5	2.4±2.5	0.7±2.5	3.9±2.5	6.2±2.5

Figure 16. Fold change ($2^{-\Delta\Delta Ct}$) in ALP, Col1α1, OCN, CB1, CB2, OPG/RANKL (mean ± SEM) gene expression in C, HT, and CT ASC-scaffold constructs cultured in stromal (S), osteogenic for 48 hours followed by stromal (OS) or osteogenic (O) medium for 7, 14, and 28 days. Fold change was calculated relative to the reference gene glyceraldehyde 3-phosphate dehydrogenase (GAPDH) and target gene expression in constructs immediately after cell loading. Columns with different superscripts within constructs and media are significantly different among time points.

Total Collagen – Hydroxyproline: Total collagen fold change also increased slightly or remained static with time. Fold change was highest on C scaffolds for all time points and media.

Sulfated Glycosaminoglycan (sGAG) - Dimethylmethylene Blue (DMMB): The sGAG fold change tended to increase with time in C and HT constructs cultured in O and OS media. It was highest on HT constructs in OS and O medium after 7 days of culture and on C constructs after 28 days of culture in the same media.

Total Protein – Lowry Assay: Total protein fold change was primarily evident in C constructs, and it was highest on C constructs in S and O media after 14 days and in OS and O media after 28.

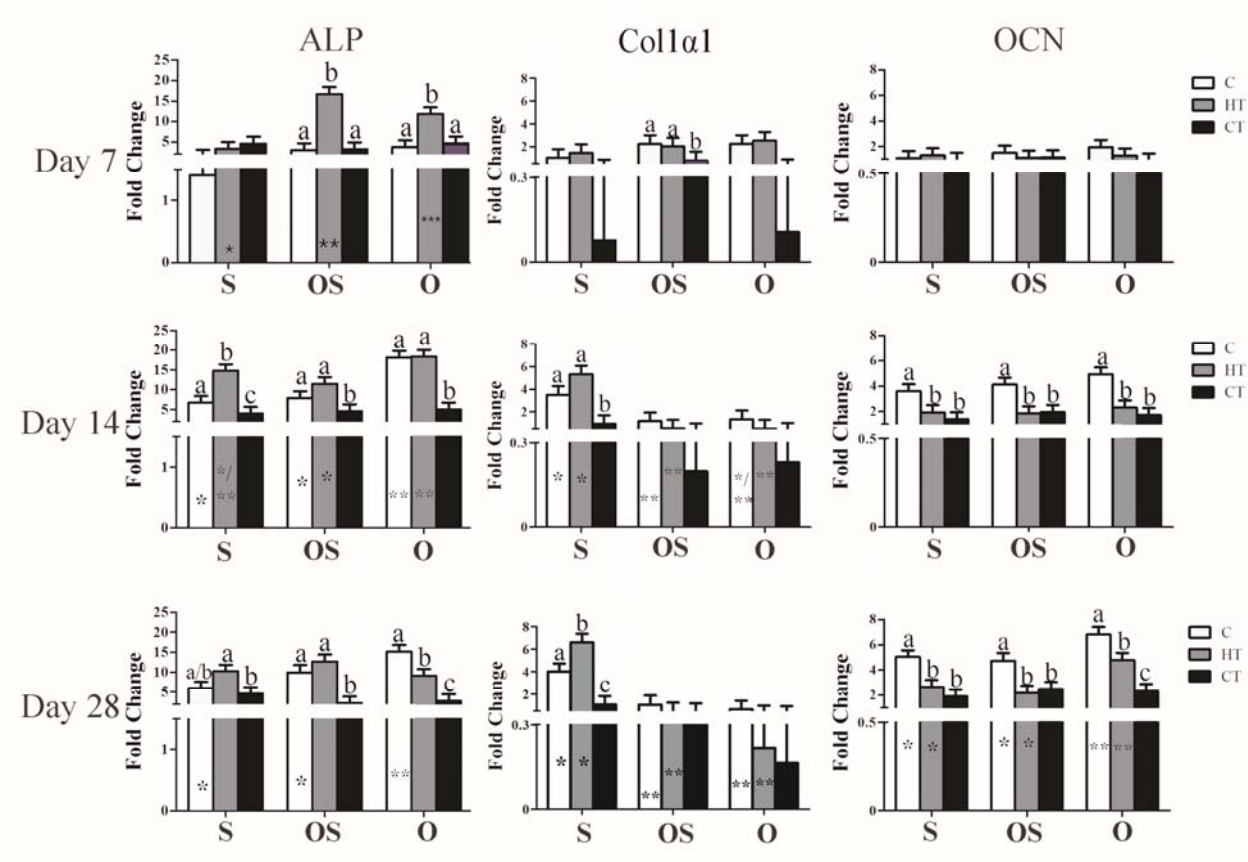

Figure 17 Alkaline phosphatase (ALP), collagen IαI (ColIαI) and osteocalcin (OCN) (LS mean ± SEM) expression in type I bovine collagen (C), hydroxyapatite + β tricalcium phosphate + type I bovine collagen (HT), and β tricalcium phosphate + type I bovine collagen (CT) scaffold-ASC constructs cultured in stromal (S), osteogenic for 48 hours followed by stromal (OS) or osteogenic (O) medium for 7, 14, or 28 days. The $2^{-\Delta\Delta Ct}$ values are reported relative to the reference gene glyceraldehyde 3-phosphate dehydrogenase (GAPDH) and target gene expression in constructs immediately after cell loading. Columns with distinct superscripts are significantly different among constructs within culture medium and those with different numbers of asterisks (*) are significantly different among culture medium within constructs ($p<0.05$).

3.3.4. SEM

Following cell loading, collagen fibrils tended to fuse with each other or other scaffold materials (Fig. 21). Amorphous matrix deposition was apparent in C constructs in S and O medium after 7 and 14 days of culture. In HT constructs, there was considerably more loosely organized, fibrous ECM following culture in S versus O medium and the amount increased with culture time. Mineralized scaffold material tended to be most prevalent in CT constructs. The ECM was more

fibrous in CT constructs cultured in S versus O medium after 7 and 14 days of culture, but deposition was marginal compared to other constructs. Overall ECM deposition and organization was greatest in CT constructs cultured in O medium for 14 days.

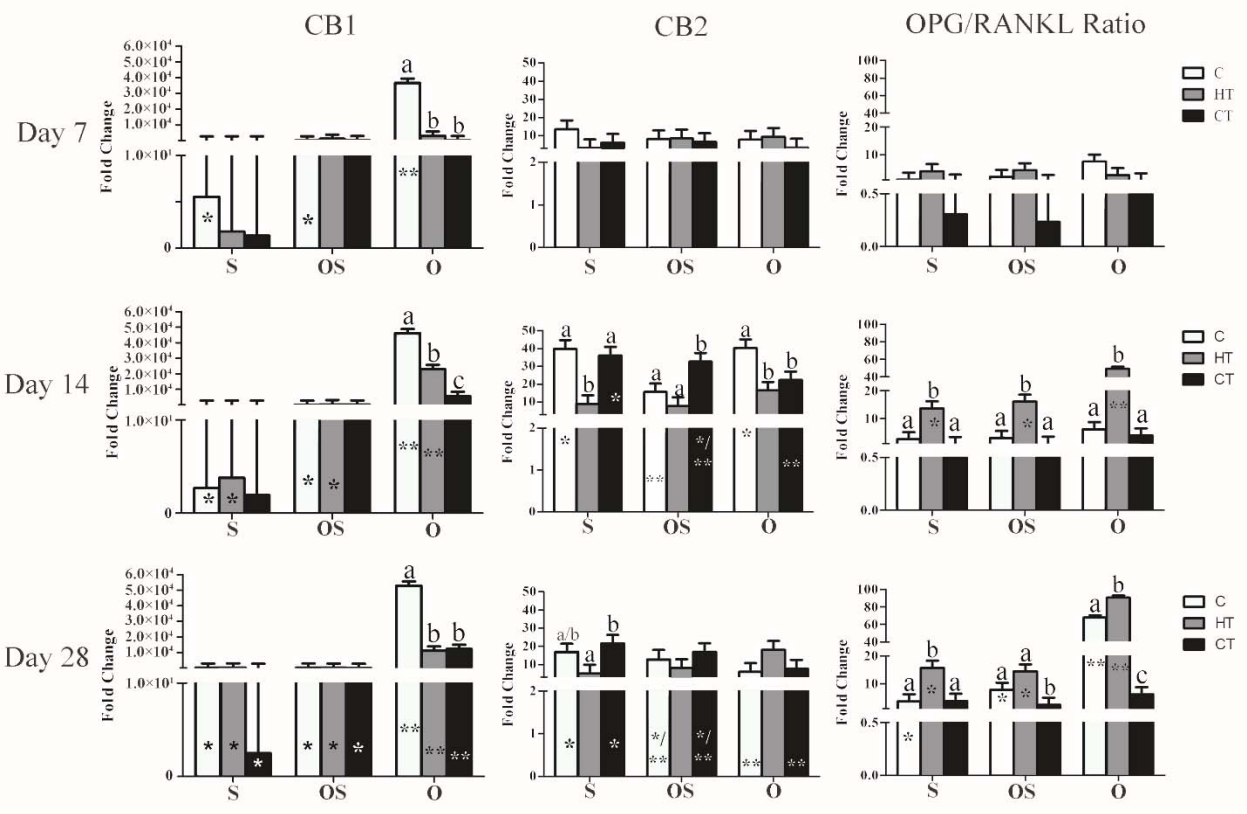

Figure 18. Cannabinoid receptors type I (CB1) and II (CB2), and the ratio of osteoprotegerin and the receptor activator of nuclear factor kappa beta ligand (OPG/RANKL) (LS mean ± SEM) expression in the same scaffolds under identical culture conditions as Figure 2. Columns with distinct superscripts are significantly different among constructs within culture medium and those with different numbers of asterisks (*) are significantly different among culture medium within constructs ($p<0.05$).

3.4. Discussion

The results of this study indicate that HT and C scaffolds in O medium support more robust ASC osteogenesis than CT scaffolds. This was evidenced by early increases in ALP expression, later increases in OCN expression, and ECM deposition and ultrastructure. Similar genetic expression and ECM deposition with higher collagen content on C scaffolds suggests comparable, though

potentially slower osteogenesis and a strong propensity for a more fibrous matrix ultrastructure compared to HT scaffolds. A notable distinction between the cell-scaffold constructs was significantly higher CB1 expression on C scaffolds and OPG/RANKL expression on HT scaffolds throughout the majority of the study. Together these results suggest that it is possible to customize ASC osteogenic cell signaling for enhanced bone formation based on bone pathology.

Component	Scaffold	S			OS			O		
		Day 7	Day 14	Day 28	Day 7	Day 14	Day 28	Day 7	Day 14	Day 28
dsDNA	C	1.2 ± 0.2	1.1 ± 0.2	1.1 ± 0.2	1.1 ± 0.2	1.2 ± 0.2	1.1 ± 0.2	1.2 ± 0.2	1.3 ± 0.2	1.5 ± 0.2
	HT	1.6 ± 0.2^{A}	1.6 ± 0.2^{A}	2.6 ± 0.2^{B}	1.3 ± 0.2^{A}	2.6 ± 0.2^{B}	1.8 ± 0.2^{A}	2.5 ± 0.2^{A}	2.7 ± 0.2^{A}	1.8 ± 0.2^{B}
	CT	1.4 ± 0.2	1.5 ± 0.2	1.8 ± 0.2	1.5 ± 0.2	1.6 ± 0.2	1.4 ± 0.2	1.8 ± 0.2	1.8 ± 0.2	1.9 ± 0.2
Total Collagen	C	1.5 ± 0.1^{A}	1.5 ± 0.1^{A}	2.2 ± 0.1^{B}	1.5 ± 0.1^{A}	2.0 ± 0.1^{B}	2.1 ± 0.1^{B}	2.2 ± 0.1	2.6 ± 0.1	2.2 ± 0.1
	HT	1.1 ± 0.1	1.0 ± 0.1	1.0 ± 0.1	1.4 ± 0.1	1.0 ± 0.1	1.2 ± 0.1	1.1 ± 0.1	1.0 ± 0.1	1.1 ± 0.1
	CT	1.1 ± 0.1	0.9 ± 0.1	0.9 ± 0.1	0.9 ± 0.1	0.9 ± 0.1	0.9 ± 0.1	1.0 ± 0.1	1.0 ± 0.1	0.9 ± 0.1
sGAG	C	1.1 ± 0.2	1.7 ± 0.2	1.7 ± 0.2	1.2 ± 0.2^{A}	1.8 ± 0.2^{A}	3.3 ± 0.2^{B}	1.3 ± 0.2^{A}	2.6 ± 0.2^{B}	2.8 ± 0.2^{B}
	HT	1.2 ± 0.2	1.6 ± 0.2	1.6 ± 0.2	2.1 ± 0.2^{A}	1.2 ± 0.2^{B}	2.1 ± 0.2^{A}	2.5 ± 0.2	2.5 ± 0.2	2.1 ± 0.2
	CT	1.1 ± 0.2	1.4 ± 0.2	1.6 ± 0.2	1.3 ± 0.2	1.4 ± 0.2	1.1 ± 0.2	1.6 ± 0.2	1.8 ± 0.2	1.6 ± 0.2
Protein	C	1.0 ± 0.1	1.3 ± 0.1	1.1 ± 0.1	1.1 ± 0.1	1.1 ± 0.1	1.5 ± 0.1	1.2 ± 0.1	1.7 ± 0.1	1.4 ± 0.1
	HT	1.0 ± 0.1	1.1 ± 0.1	1.0 ± 0.1	1.1 ± 0.1	1.0 ± 0.1	1.1 ± 0.1	1.1 ± 0.1	1.0 ± 0.1	1.1 ± 0.1
	CT	1.0 ± 0.1	1.0 ± 0.1	1.0 ± 0.1	1.0 ± 0.1	0.9 ± 0.1	1.0 ± 0.1	1.1 ± 0.1	1.0 ± 0.1	1.1 ± 0.1

Figure 19. Fold change (mean ± SEM) in dsDNA, total collagen, sGAG and protein in C, HT, and CT ASC-scaffold constructs cultured in stromal (S), osteogenic for 48 hours followed by stromal (OS) or osteogenic (O) medium for 7, 14, and 28 days. Individual values (unitless) were calculated relative to Day 0 as C_f/C_i where C_i is content immediately after cell loading and C_f is content after 7, 14, or 28 days of culture. Columns with different superscripts within constructs and media are significantly different among test time points.

The time course of ALP and OCN expression within HT constructs in O medium is consistent with osteoblastic differentiation and maturation [249, 250]. Hydroxyapatite (HA) in the HT scaffold may have been responsible for the initial enhanced ALP expression over the other scaffolds since HA stimulates human ASC and bone marrow derived multipotent stromal cell (BMSC) ALP expression [251, 252] and ASC osteogenic differentiation [253, 254]. The earliest increase in ALP expression in this study was in O medium; however, the higher ALP in HT

constructs cultured in OS medium for 7 days and S medium for 14 days further supports the effect of the scaffold on the cells. Increased expression of ALP and OCN in C constructs also suggests that collagen promotes osteoblastic ASC differentiation and maturation in O medium, though potentially not as robustly as HA [118, 255]. This is further supported by lack of a decrease in ALP expression in C constructs [245]. Genes for this study were selected to distinguish between early osteoblastic differentiation (ALP), osteoblastic maturation (OCN), and osteoblastic activity (COL1α1) for comparisons among treatments [256-258]. The focus of this study was on early ASC direction and ECM production versus bone formation that is better described by later stage genes [259].

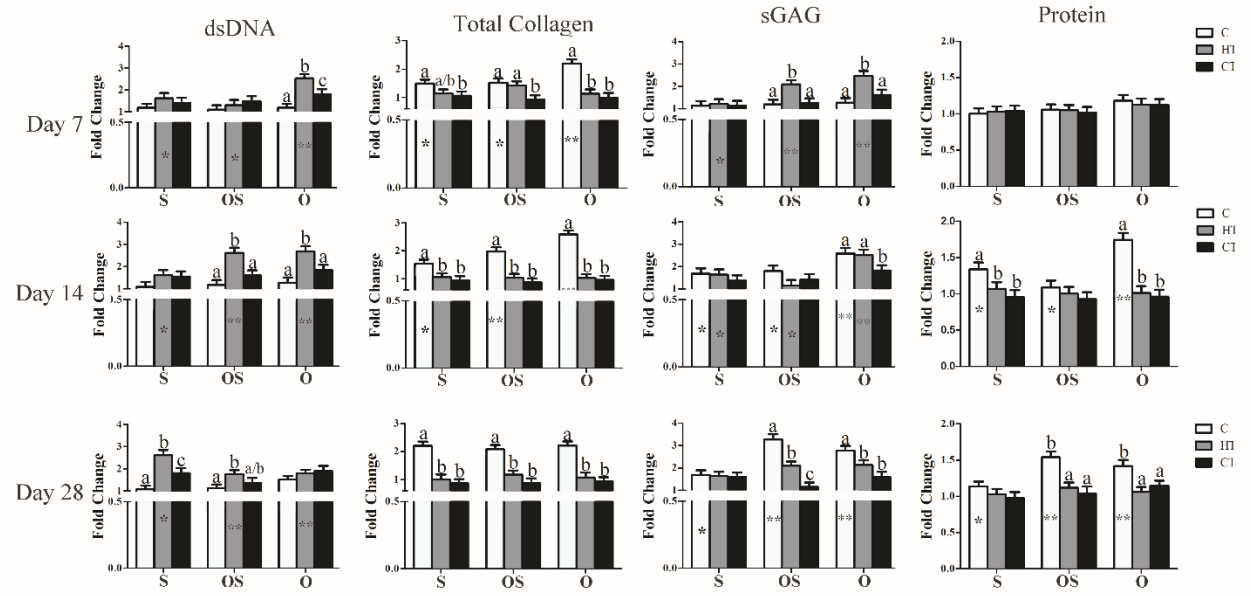

Figure 20. Fold change in dsDNA, total collagen, sulfated glycosaminoglycan (sGAG) and protein content (LS mean ± SEM) in the same constructs and media as Figure 2 after 7, 14 or 28 days of culture. Columns with distinct superscripts are significantly different among constructs within culture medium and those with different numbers of asterisks (*) are significantly different among culture medium within constructs ($p<0.05$).

Lower osteogenic gene expression and ECM deposition within CT constructs may be due tricalcium phosphate dissolution based on previous reports of lower proliferation and viability of undifferentiated cells on comparable scaffolds [260]. Since lower cell viability was only detected

in S medium after 14 days, cell loss may not be the strongest contributor to the observed differences. Another possibility is that the high mineral content caused cell membrane damage or interfered with cell attachment required for differentiation, maturation and ECM production [261-263]. Though surface roughness usually has a positive relationship with osteoblastic differentiation and matrix production, it can be inhibitory beyond a certain point [264-266].

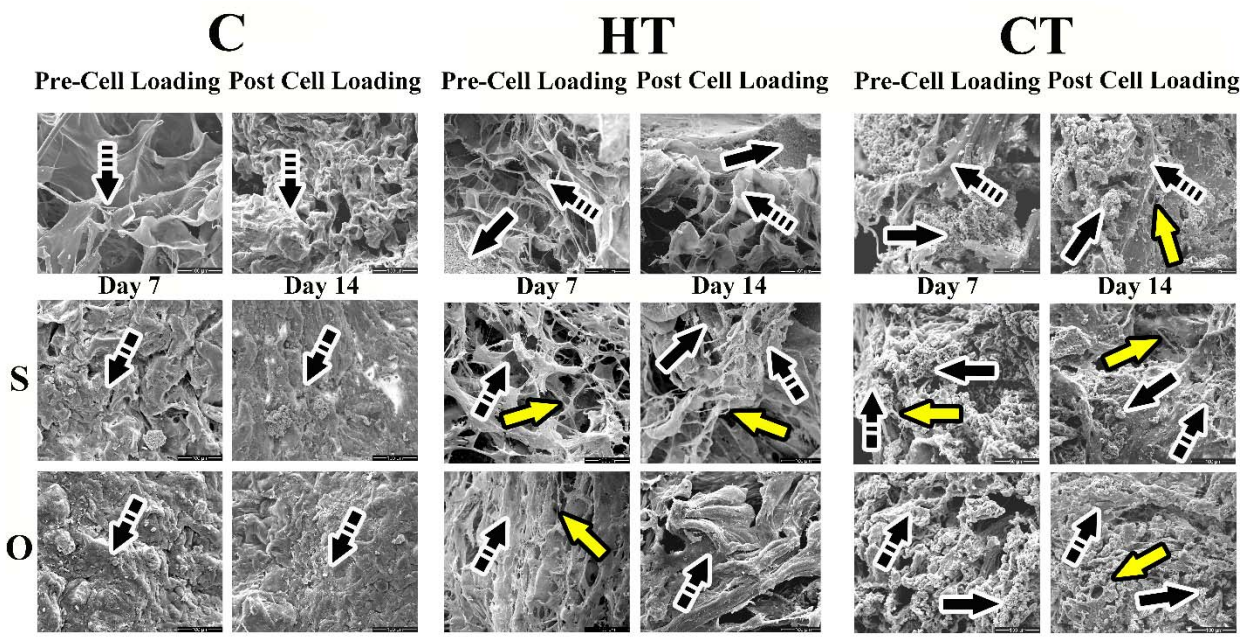

Figure 21. Scanning electron photomicrographs of human ASC-scaffold constructs composed of bovine collagen type I (C), hydroxyapatite + β-tricalcium phosphate + bovine collagen type I (HT) and β tricalcium phosphate + bovine collagen type 1 (CT) before (Pre-Cell Loading) and after (Post Cell Loading) spinner flask cell loading and after 7 (Day 7) and 14 (Day 14) days of culture in stromal (S) or osteogenic (O) medium. Black arrows: mineralized scaffold; yellow arrows: collagen fibrils; two-stripe black arrows: extra-cellular matrix; three-stripe black arrows: scaffold.

Genetic expression is a standard mechanism to evaluate and compare cell characteristics that is important to quantify changes induced by medium or scaffold as in this study [267]. Genetic expression does not entirely reflect cell function in terms of matrix production [268], a central point of directed osteogenesis [263]. Extracellular matrix production is central to the self-perpetuating cycle of ossification [269]. Determination of differences in ECM content provides a mechanism to assess and quantify the process and provide a more comprehensive evaluation of

treatment effects on cell behaviors than genetic analysis alone [270, 271]. Generally, increases in dsDNA suggest cell proliferation associated with lack of differentiation [263]. Proteoglycan, collagen and protein synthesis occurs throughout ossification primarily from osteoblastic ECM production [269]. As such, the ECM content and ultrastructure helps to confirm tissue changes suggested by gene expression.

While there was some evidence of osteogenic stimulation from culture in OS medium, it did not support the same level as continuous O medium culture. The short term exposure in this study may not have been sufficient to induce osteoblastic differentiation in the entire cell population within the scaffolds since isolates may have contained cells at various stages of differentiation.[244] Nonetheless there was a genetic effect of short term osteogenic medium exposure as indicated by higher ALP expression at day 7 on HT scaffolds cultured in OS versus S medium. Similarly, lower Col1α1 expression on C and HT scaffolds in the OS group that mirrored that of scaffolds cultured in O medium after 14 and 28 days of culture suggest cell maturation. Further support of the impact of OS medium included increased ECM protein, sGAG, collagen and dsDNA over S medium at various points in the study. The variable increases in osteogenic gene expression and ECM components are consistent with a cell population with variable maturity [272]. Nonetheless, the observed genetic upregulation and increased ECM components confirm that there is some benefit to short term exposure of ASC-scaffold constructs to osteogenic medium.[271] Customization of medium and culture period will likely increase the effects.

Collagen upregulation and ECM deposition in C constructs in all culture media observed in this study may be a result of collagen type I stimulation of extracellular signal-regulated protein kinase (ERK) [273]. Coating cultureware with collagen increases ERK phosphorylation and expression of ALP and OCN in human ASCs [274]. The results of this study are consistent with

these earlier findings and may indicate that high collagen content scaffolds promote ASC osteoblastic differentiation and ECM production, but slightly less than scaffolds with both collagen and a mixture of inorganic minerals. The importance of this difference in patients with compromised bone formation may not be relevant long term, so upregulation of the specific signaling pathways discussed below may be the strongest mechanism for therapeutic improvements.

Scaffold effects on CB1 and the OPG/RANKL ratio expression were the notable distinction among C and HT constructs cultured in O medium. The importance of CB1 for MSC osteogenic differentiation has been established. It increases with MSC osteoblastic differentiation [228, 275], and BMSCs from CB1 knock outs have a reduced capacity for osteoblastic differentiation [227]. The role of CB1 role in bone homeostasis appears to be mediated primarily through adrenergic signaling and separate from the Wnt signaling pathway [231, 276]. Of importance to clinical translation is that lower CB1 expression is associated with age related bone loss and increased marrow adiposity [227, 228].

The ratio of OPG/RANKL drives osteoblastic differentiation through increases in OPG or decreases in RANKL, and OPG expression is mediated through Wnt/β-catenin pathways [98, 277-281]. Disruption of the OPG/RANKL ratio is more closely aligned with bone pathology versus bone aging associated with changes in CB1 expression [282, 283]. In contrast to the CB1 signaling pathway apparent in C constructs discussed above, an increase in OPG/RANKL expression was consistently apparent in HT constructs. The source of the difference may be that HA increases low-density lipoprotein receptor-related protein 5 (LRP5) and β-catenin expression, and both stimulate canonical Wnt [98, 278, 279, 284].

Increased CB2 expression after 14 days of culture in all media and constructs suggests less association with ASC osteogenesis than other genes. The role of CB2 in the regulation of bone metabolism is not well defined, and existing information suggests both a supportive and an inhibitory effect of CB2 on MSC osteogenesis [114, 228, 230, 285].

These results support the capability of human ASCs to be directed toward different osteogenic pathways by scaffold substrate characteristics. This information may help guide targeted research for distinct bone pathology. Local therapy based on predominant needs of the recipient may be a safe and effective alternative to systemic activation of both cannabinoid and Wnt signaling, which are both associated with serious side effects [229, 281, 286-288]. The complexity of and overlap between signaling pathways, however, requires further work to confirm distinct pathways at multiple levels between treatments.[277]

The parallel outcome measures in this study indicate that HT scaffolds in osteogenic medium have the highest in vitro ASC osteogenesis followed by closely C. Further, osteogenesis appears to be mediated through distinct cell signaling pathways by C and HT scaffolds. This may indicate a significant value of considering patient characteristics when selecting bone grafts, especially when combining them with exogenous ASCs. Since underlying bone pathology may limit in vivo response to scaffolds with or without exogenous cells, the findings must be confirmed in vivo prior to general application. Nonetheless, it is possible that native osteogenesis may benefit more from some bone graft materials augmented by ASCs than others. Further, this information creates a foundation for criteria to create autologous, viable bone grafts from adult ASCs to locally treat deficient bone forming capacity.

CHAPTER 4. POLYMER-MINERAL SCAFFOLD AUGMENTS IN VIVO EQUINE MULTIPOTENT STROMAL CELL OSTEOGENESIS

4.1. Introduction

Viable graft composed of adult multipotent stromal cells (MSCs) and biocompatible scaffold is a promising approach to enhance natural bone formation and augment current treatment strategies for equine traumatic bone injury [221, 251, 289]. Autologous autograft promotes bone formation by local cells, but harvest morbidity in addition to variable cell survival and graft quantity and quality help fuel the search for regenerative medicine alternatives [219, 236, 290]. Osteogenic capabilities of equine bone marrow- (BMSCs) and adipose-derived (ASCs) multipotent stromal cells vary with culture conditions and scaffold carriers [184, 245, 291, 292]. Given the inherent responsiveness of undifferentiated cells to surroundings [219, 221, 267], it is vital to confirm in vitro MSC characteristics in vivo. This is especially true since cell-based therapies are designed to enhance bone healing in potentially unfavorable conditions.

The natural bone fracture environment has over 200 noncollagenous matrix proteins and collagen and hydroxyapatite (HA) nanostructure that guides native progenitor cell osteogenesis [267]. Through structure and composition, functional scaffolds create a biomimetic environment for endo- and exogenous cells [267, 293-297]. Mineral based scaffolds have good biomimetic characteristics, but brittle mechanical properties complicate implant customization, surgical stabilization and biological incorporation [298]. Scaffolds composed of both synthetic polymers and minerals like HA and tricalcium phosphate (TCP) have biomimetic characteristics of inorganic matrix but greater flexibility [298, 299]. A scaffold composition that supports consistent, predictable tissue formation by MSCs from distinct tissues and donors is appealing for clinical application.

Poly-L-lactic acid (PLLA) and polyethylene glycol (PEG), biocompatible, nontoxic polyester polymers, are often copolymerized for FDA-approved implants [300]. Distinct PLLA:PEG ratios have predictable hydrolytic degradation [109, 301-305]. Addition of HA to PLLA scaffolds neutralizes acid from PLLA hydrolysis [299] and enhances murine osteoblast cell line survival, growth and osteogenic gene expression [306]. Composite PLLA/TCP scaffold increases endogenous alkaline phosphatase activity in human ASCs over PLLA alone [297]. Information about equine MSC-scaffold osteogenesis is relatively limited [307], but this contemporary knowledge supports potential for polymer-mineral scaffold carriers to support the process [109, 302].

Homogenous distribution of viable MSCs throughout scaffold carriers is crucial for organized tissue matrix production and organization [308]. Bioreactor dynamic cell loading under optimal conditions limits cell loss and ensures distribution [124] important for neovascularization and de novo tissue formation [223]. Spinner flask bioreactors limit cell cluster formation, facilitate uniform cell seeding and support nutrient and waste exchange [309, 310]. Additionally, exposure to fluid flow for as little as 15 minutes upregulates murine MSC osteogenic gene expression [311, 312]. Hence, spinner flasks provide an efficient mechanism for consistent construct loading that may help drive osteoblastic differentiation and maturation.

Given the potential of equine ASCs and BMSCs to augment bone generation [313-315], targeted work is necessary to identify polymer-mineral bioscaffold carriers [316-318] that reliably promote equine MSC osteogenesis in vivo. This study was designed to quantify osteogenesis by equine ASCs and BMSCs on scaffold carriers composed of TCP/HA (40:60, HT, Scaffdex^{TM}, Ltd, Tampere, Finland), PEG/PLLA (60:40, GA) and PEG/PLLA/TCP/HA (36:24:24:16, GT) in an athymic mouse model. The tested hypothesis was that osteogenesis is comparable on GA and GT

scaffolds with either ASCs or BMSCs and greater than on HT scaffolds with either cell type. It was further hypothesized that the same scaffolds with MSCs have greater osteogenesis than those without.

4.2. Materials and Methods

4.2.1. Ethics Statement

All animal procedures were approved by the Institutional Animal Care and Use Committee prior to study initiation (protocols #13-050 and 07-049).

4.2.2. Study Design

Cell passage (P) 1 cryopreserved equine bone marrow (BMSC) and adipose-derived (ASC) multipotent stromal cells were culture expanded to P3. Cells were loaded onto one commercially available mineral (HT) and two novel polymer-mineral scaffolds (GA, GT) via a spinner flask bioreactor. Passage (P) 3 immunophenotype and cell viability on scaffolds after 7 and 21 days of static culture were determined. Scaffolds with and without cells were implanted subcutaneously in athymic mice. Radiographs were performed immediately and then every three weeks up to 9 weeks. Explants were evaluated for composition (double stranded DNA (dsDNA), total collagen, sulfated proteoglycan, protein), osteogenic target gene mRNA expression (alkaline phosphatase (ALP), bone sialoprotein (BSP), osteocalcin (OCN), osteoprotegerin (OPG)), calcium and phosphorus content and ultra- and microstructure. All materials and reagents were from Sigma-Aldrich, St. Louis, MO unless otherwise noted.

4.2.3. Scaffold Preparation (PEG/PLLA, GA; PEG/PLLA/TCP/HA, GT)

PEG/PLLA (60:40): Solutions of 10% PEG (molecular weight (MW) 1,900 – 2,200 g/mole) and 10% PLLA (MW 100,000 – 150,000 g/mole) in 1, 4-dioxane (AcroSeal^{TM}, ACROS Organics) were combined at a ratio of 6:4 (v/v) with stirring at 85^{o}C to create a homogenous mixture.

PEG/PLLA/TCP/HA (36:24:24:16): TCP was added to 10% PEG at a ratio of 4:6 (TCP:PEG, w/w) and HA to 10% PLLA at a ratio of 4:6 (HA:PLLA, w/w) under the same conditions as above. Solutions were combined at a ratio of 6:4 (TCP-PEG:HA-PLLA) and then solidified in polydimethylsiloxane tubes (inner diameter: 10 mm; depth: 10 mm) by cooling to -80ºC overnight. They were subsequently lyophilized for 48 hours. Tubular scaffolds were sliced into discs (diameter: 10 mm; depth: 3 mm) that were individually packaged and sterilized with ethylene oxide at 57ºC for 2 hrs.

4.2.4. Tissue Harvest, Cell Expansion, Cryopreservation

Sternal bone marrow and subcutaneous adipose tissue were harvested from seven thoroughbred geldings (6.3 ± 1.7 years; mean ± standard error of the mean (SEM)) as previously described [245]. Briefly, horses were sedated (detomidine HCl, 0.04 mg/kg intravenously (IV)), the sternebrae aseptically prepared, and 6 ml of 2% lidocaine chloride infiltrated into the soft tissues. With 14 G Jamshide needles, bone marrow was aspirated into heparinized syringes (1000 IU/60 ml bone marrow aspirate). Next, skin and subcutaneous tissues dorsolateral to the base of the tail were infiltrated with 2% lidocaine chloride. Skin was incised for 10 cm parallel to and approximately 15 cm lateral to the dorsal sacrum, and exposed subcutaneous adipose tissue (15-20 ml) was sharply excised. The skin was apposed with #2 nylon.

Cells were isolated as published with minor modifications [245]. Bone marrow aspirate combined with an equal volume of stromal medium (Dulbecco's modified Eagle's medium F-12 (DMEM/F-12, Hyclone, Logan, UT), 1% antibiotic/antimycotic solution (MP Biomedical, Irvine, CA), 10% fetal bovine serum (FBS, Hyclone)) was separated via centrifugation (350 × g, 4ºC, 30 min) with Ficoll-Paque® PLUS (Stem Cell Technologies, Vancouver, Canada). The cell layer was removed and centrifuged (260 × g, 4ºC, 5 min) to form a cell pellet that was seeded in T75 flasks

(5×10^3 cells/cm^2) for culture. Stromal medium was refreshed after 24 hours and then every 3 days. In this study, P0 is the first cell passage of primary cells. Procedures performed at temperatures other than room temperature are indicated.

Minced adipose tissue was combined with an equal volume of phosphate buffered saline (PBS, Hyclone). After the mixture separated into two phases over 5 min, the infranatant was digested in 1% bovine serum albumin (BSA, Fisher Bioreagents, Fair Lawn, NJ) and 0.1% collagenase type I (Worthington Biochemical Corporation, Lakewood, NJ) in DMEM/F-12 for 2 hours at 37ºC. After filtering (100 µm nylon cell strainers, BD Falcon, Bedford, MA) and centrifugation (260 × g, 5 min), cells in DMEM with 1% BSA were added to an equal volume of red blood cell lysis buffer (0.16 mol/L NH_4Cl, 0.01 mol/L $KHCO_3$, 0.01% ethylenediaminetetraacetic acid (EDTA)) for 5 min. The stromal vascular fraction (SVF) was collected after centrifugation (260 × g, 5 min) and cultured like above.

At 70% confluence, cells were detached with 0.05% trypsin (Hyclone), suspended in cryopreservation medium (80% FBS, 10% DMEM/F-12, 10% dimethylsulfoxide (DMSO, Fisher Scientific, Fari Lawn, NJ)) at $1\text{-}1.5\times10^6$ cells/ml and aliquoted into 1.5 ml cryovials (Fisher Scientific). Cells were cooled to -80ºC (~-1ºC/min, CoolCell®, BioCision, Larkspur, CA) overnight and then transferred to liquid nitrogen for 33-45 days. To thaw, cryovials were placed in a 37ºC water bath for 1-2 min followed by centrifugation (380 × g, 5 min), a PBS wash, another centrifugation (380 × g, 5 min) and then stromal medium culture as before.

4.2.5 Immunophenotype - Flow Cytometry

Passage 3 revitalized ASCs and BMSCs from 3 equine donors were combined in equal proportions within cell type for immunophenotype detection. Aliquots of 1×10^5 cells in 150 µl PBS were incubated for 30 minutes at room temperature with 200 µg/ml of labeled or unlabeled antibody

(CD34-PE, CD29, CD73-FITC, CD44-FITC, CD90-PE, CD105-PE) specific or validated cross-reactive for equine antigens (Table 9). Cells were rinsed with PBS, centrifuged (350×g, 5 min), and fixed with 4% neutral buffered formalin. For CD29, cells were incubated with labeled anti-immunoglobulin (IgG-FITC) for 30 min, rinsed with PBS, centrifuged (350×g, 5 min), and fixed with 4% neutral buffered formalin. Cell fluorescence was quantified using a FACSCalibur flow cytometer and Cell Quest Pro software (BD Biosciences, San Jose, CA). Autofluorescence was determined on antibody negative samples.

4.2.6. Construct Seeding and Culture

Passage 1 revitalized ASCs and BMSCs were culture expanded to P3 and then loaded onto scaffolds (1×10^6 cells/scaffold) for 2 hours with 70 rpm stirring in spinner flask bioreactors (37^o C, 5% CO_2). Spinner flasks consisted of 100 ml flasks (Bellco® Biotechnology, Newark, NJ) containing 120 ml of serum-free stromal medium and three separate 4-inch-long, 22 gauge spinal needles suspended from a rubber stopper at the top of each flask that each passed through the center of one scaffold (Fig. 22). Individual loading processes for scaffolds without cells, pooled aliquots identical to those used for immunophenotype, and for each cell tissue source and donor included one scaffold of each composition situated at the middle of the fluid. After 2 hours, loading efficiency was determined and cell-scaffold constructs divided into six equal pieces for immediate evaluation, culture in stromal medium or implantation as described below.

4.2.7. Cell Number - 3-(4, 5-dimethylthiazol-2-yl)-2,5-diphenyl tetrazolium bromide (MTT)

Commercially available MTT (Cell Proliferation Kit I) was used to determine cell number immediately after cell loading or following 7 or 21 days of stromal medium culture in 24 well culture plates (n=3 replicates/cell tissue source/scaffold composition/time point). Briefly, constructs were gently rinsed with PBS and placed into fresh plates followed by incubation with

500 µl of a 5:1 mixture of stromal medium and MTT solution (5 mg/ml in PBS) for 2 hrs (37° C, 5% CO_2). Subsequently, 500 µl of DMSO was added to each well, absorbance read at 540 nm (Synergy HT, BioTek Instruments, Winooski, VT), and the cell number determined from equine ASC or BMSC standard curves. Cell number fold change was calculated as C_f/C_i (C_f: cell number after 7 or 21 days of culture; C_i: cell number immediately after scaffold loading).

Table 9. Antibodies for Flow Cytometry

Antibody	Label	Marker expression	Manufacturer	Species	Target species	Diluent
CD29	N/A	β1 integrin	BD Biosciences	Mouse	Canine	PBS
CD44	FITC	Cell-surface Glycoprotein, hyaluronic acid receptor	eBioscience	Mouse	Canine	PBS
CD73	FITC	5'-Nucleotidase	eBioscience	Mouse	Human	PBS
CD90	PE	Thy-1, fibroblasts, MSC, hematopoietic progenitor (HSC)	eBioscience	Mouse	Canine	PBS
CD105	PE	Type 1 Glycoprotein	eBioscience	Mouse	Human	PBS
CD34	PE	HSC	BD Biosciences	Mouse	Canine	PBS
Rabbit anti-mouse IgG	FITC	N/A	Sigma	Rabbit	Mouse	PBS

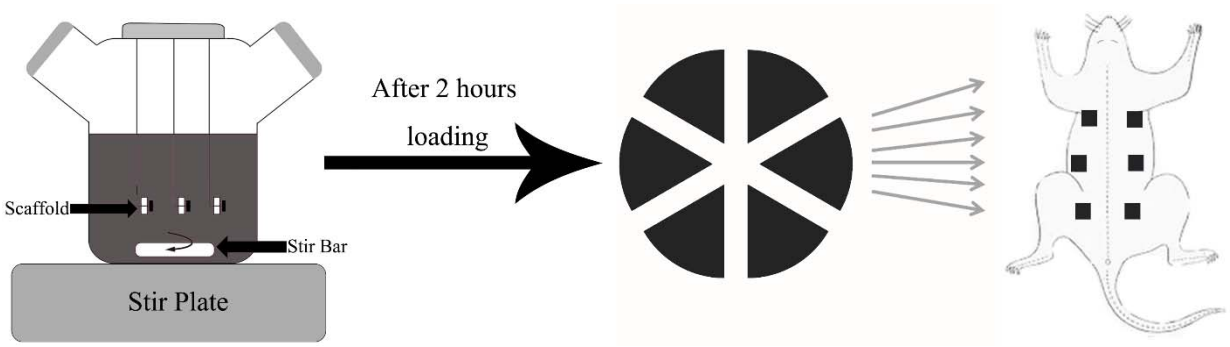

Figure 22. Schematic of spinner flask bioreactor cell loading, scaffold division and implantation.

4.2.8. Scaffold Surgical Implantation

Six equal pieces of scaffolds containing ASCs, BMSCs or no cell (n=1/horse/cell tissue source/scaffold composition) were surgically implanted in the dorsal subcutaneous tissues of male, athymic mice (nu/nu, Charles River Laboratories, Wilmington, MA). Implants were harvested nine weeks after surgery and evaluated for gene expression (n=2/mouse), composition (n=2/mouse), ultra-structure, (n=1/mouse) and microstructure (n=1/mouse).

Mice were premedicated (glycopyrrolate, 0.02 mg/kg; butorphanol, 0.5 mg/kg, both subcutaneously) and anesthetized with isoflurane on oxygen delivered via a Baine circuit and mask. Following aseptic preparation, six 5 mm skin incisions were created equidistantly along the dorsum extending from the scapula to the sacrum approximately 1 cm ventral to each side of the spine. Following minimal blunt dissection, scaffolds were placed beneath the skin, subcutaneous tissues closed with #3-0 nylon and skin apposed with tissue glue.

4.2.9. Radiographs – Mineral Deposition

Radiographs (Sound Technologies, Carlsbad, California) were performed immediately and 3, 6 and 9 weeks after surgery with mice in ventral recumbency and anesthetized as described above. Mineral deposition was subjectively assessed based on changes in radiopacity.

4.2.10. Microcomputed Tomography (μCT) – Porosity, Bone Volume/Total Volume

Two- and three dimensional images generated from a micro-computed tomography (μCT) scanner (μCT 40; Scanco Medical AG, Bassersdorf, Switzerland) and graphics software were used to quantify specimen percent porosity (Mimics®, Materialise, Ann Arbor, MI) and bone volume/total volume (BV/TV, μCT Evaluation Program V6.6), respectively, 9 weeks after implantation. Imaging technique (55kV, 145μA) and 2-dimensional 16-bit gray-scale threshold were identical among samples. Percent porosity was measured on slices at 25, 50, and 75% of the total specimen height. The mean of the 3 values was used as the measure for each specimen. To distinguish between high contrast scaffold versus low contrast, newly deposited tissue, two thresholds were used for 3-D image reconstructions of GT (170, 370 mgHA/ccm) and HT (380, 590 mgHA/ccm) samples. The difference in the BV/TV at each threshold was considered a measure of new tissue deposition. A single threshold (270 mgHA/ccm) was used for GA constructs which did not contain high contrast material.

4.2.11. Compositional Analysis-DNA, Hydroxyproline, Sulfated Gyclosaminoglycan, Protein

Compositional analysis was performed identically to previous reports [135, 274, 319, 320]. Briefly, constructs were lyophilized at -55^{o}C and 0.2 mbar for 4-5 hours and then 20 mg of each sample was digested (9 mM di-sodium ethylenediaminetetraacetic acid, 20 mM sodium acetate, 20 mM L-cysteine (MP Biomedicals, Solon, OH), 2 mg papain (MP Biomedicals)/g lyophilized sample) at 60^{o}C for 10 hrs [77, 120]. Digested samples were vigorously vortexed and then centrifuged (4000 ×g, 10 min). Supernatants were stored at -80^{o}C until analysis. Double stranded DNA (dsDNA) was determined with a commercially available kit (Quant-iT^{TM} PicoGreen$^{®}$ Kit, Invitrogen, Carlsbad, CA) [77]. Hydroxyproline content as a measure of total collagen was quantified via Ehrlich's colorimetric assay and absorbance at 550 nm based on trans-4-hydroxy-L

proline (ACROS Organics™, Morris Plains, NJ) standards [77, 321]. Sulfated glycosaminoglycan (sGAG) was quantified with a dimethylmethylene blue (DMMB) assay, absorbance at 520 nm and a chondroitin sulfate standard curve [77, 247]. Lowry's total protein assay with Biuret's and Folin-Ciocalteu's reagents, absorbance at 650 nm, and bovine serum albumin standards was use to quantify sample protein [322].

4.2.12. Scanning Electron Microscopy (SEM) - Ultrastructure, Phosphate, Calcium

Samples were fixed with 2.5% glutaradehyde in 0.1 M sodium carcodylate buffer (pH 7.4), post fixed in 0.1% osmium tetroxide, and then dehydrated in a series of ethanol-distilled water solutions [245]. After critical point drying, they were sputter coated with gold and imaged (FEI Quanta 200, Netherlands). Surface calcium and phosphorus was measured in the center of each sample by energy-dispersive X-ray spectroscopy (EDS, 20kV, 3% accuracy) [323].

4.2.13. RT-PCR - Gene Expression

Total RNA was isolated from harvested samples (RNeasy Plus Mini Kit, Qiagen, GmbH, Germany), the concentration determined spectrophotometrically (NanoDrop ND-1000; NanoDrop Technologies, Wilmington, DE, USA), and cDNA synthesized (QuantiTect Reverse Transcription Kit, Qiagen). Equine and murine osteogenic target gene levels (alkaline phosphatase (ALP), osteocalcin (OCN), bone sialoprotein (BSP) and osteoprotegerin (OPG)) (Table 10) were quantified with real-time RT-PCR using SYBR Green (Qiagen) technology and an MJ Research Chromo 4 Detector (Bio-Rad Laboratories, Hercules, CA). Primers were designed according to species-specific genetic sequences. Each primer was tested with bone RNA to confirm lack of cross reactivity. The ΔCt values were determined relative to the reference gene glyceraldehyde 3-phosphate dehydrogenase (GAPDH).

Table 10. Primer sequences

Species	Lineage	Primer	Sequences	Accession No.
Equine	Housekeeping	GAPDH	F: AAGAAGGTGGTGAAGCAGG R: CTCAGTGTAGCCCAGGATG	NM_001163856.1
	Osteogenic	ALP	F: GGAGTATGAGATGGACGAG R: GTAGTGAGAGTGCTTGTGCC	XM_005607380.2
		OCN	F: TGGCCCTGACTGCATTCTG R: CCCTCCTGCTTGGACATGAA	XM_005610022.1
		OPG	F: CCCCCCTTGTCCTGACCACT R: CGCCCTTCCTCACATTCG	XM_001916099.4
		BSP	F: GAAGAATCGGACGCTGAG R: ATCGTAGACAGGGTGGTG	XM_001496125.4
Murine	Housekeeping	GAPDH	F: ACCCAGAAGACTGTGGATGG R:ACACATTGGGGGTAGGAACA	XM_017321385.1
	Osteogenic	ALP	F: TGATGTGGAATACGAACTGG R: TGGGAATGCTTGTGTCTG	XM_006538500.2
		OCN	F: CCATCTTTCTGCTCACTCTG R: TTATTGCCCTCCTGCTTG	NM_007541.3
		OPG	F: CACTCGAACCTCACCACAGA R: GCTCGATTTGCAGGTCTTTC	NM_008764.3
		BSP	F: CAGCCATGAGTCAAGTCAGC R: CTTGTGGCTCTGATGTTCCA	NM_001204203.1

4.2.14. Light Microscopy - Microstructure

Following fixation in 4% neutral buffered formalin, serial sections (5µm) of paraffin embedded specimens were stained with hematoxylin & eosin (H&E) and Masson's trichrome. Digital images were generated of all specimens (Leica DM 4500B, Allendale, NJ).

4.2.15. Statistical Analysis

Statistical analyses were performed with the JMP statistical package (v13.0.0, SAS Institute, Cary, NC). Mixed ANOVA models were used to evaluate cell number fold change, composition (dsDNA, total collagen, sulfated proteoglycan, protein), gene expression, porosity and BV/TV among scaffold compositions within cell tissue sources and between cell tissue sources within scaffold compositions. Fixed effects included scaffold composition and cell tissue source. Equine donor and mouse were random effects. Tukey's post hoc tests were applied for multiple group comparisons ($p < 0.05$).

4.3. Results

4.3.1. Immunophenotype - Flow Cytometry

The majority of P1 ASCs and BMSCs were CD29+, CD105+, CD34-, CD73- (Fig. 23). There were higher percentages of C90+, CD105+, CD44+ ASCs (Table 11).

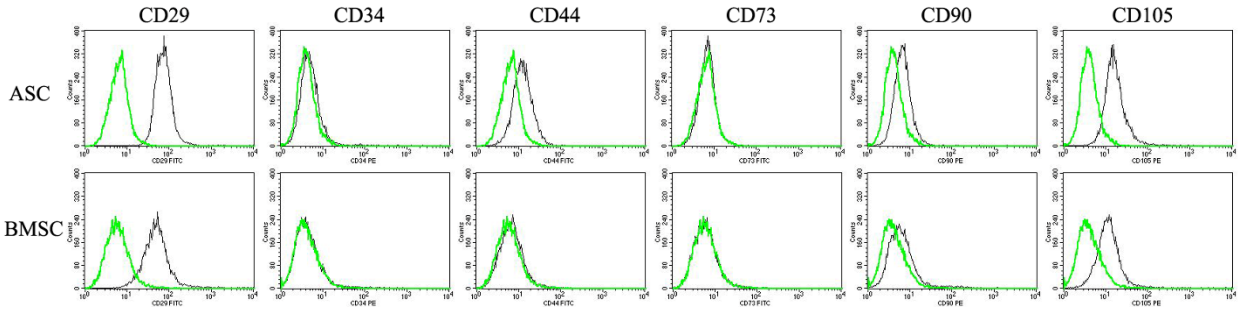

Figure 23. Immunophenotypes of P3 equine ASCs or BMSCs after culture expansion post-cryopreservation. The black lines represent labeled cells and the green autofluorescence.

4.3.2. Cell Number - 3-(4, 5-dimethylthiazol-2-yl)-2, 5-diphenyl tetrazolium bromide (MTT)

The ASC and BMSC loading efficiencies were 81.2 ± 11.4% and 83.4 ± 4.4%, respectively. The ASC and BMSC number increased significantly in HT constructs between 7 and 21 days of culture and BMSCs increased similarly in GT constructs (Fig. 24). After 7 days, the increase in BMSC number was greater in HT versus the other scaffolds, and after 21 days, the increase in GA was lower than the other two.

Table 11. Percentages of CD29+, CD44+, CD90+, CD105+, CD34-, CD73- P3 equine ASCs or BMSCs after culture expansion post-cryopreservation.

	CD29+	CD34-	CD44+	CD73-	CD90+	CD105+
ASC	99	83.5	11.0	99.8	46.2	87.7
BMSC	90.3	97.9	1.5	99.9	28.2	58.8

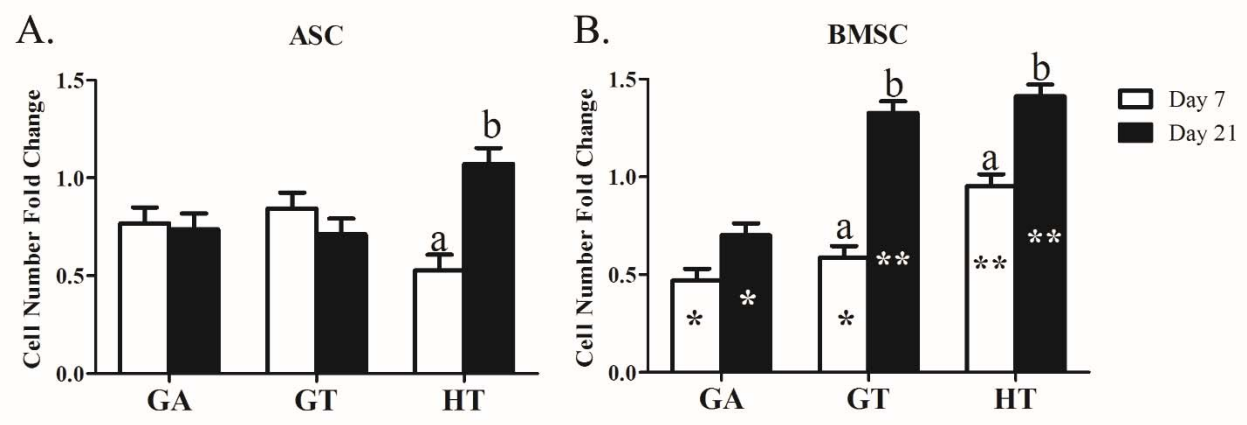

Figure 24. Fold change in ASC (A) or BMSC (B) number after 7 or 21 days of static culture in stromal medium on scaffolds composed of TCP/HA (40:60, HT), PEG/PLLA (60:40, GA) or PEG/PLLA/TCP/HA (36:24:24:16, GT). Columns with distinct superscripts are significantly different between culture times within scaffold composition and those with different asterisk (*) numbers are significantly different among scaffold compositions within culture time ($p<0.05$).

4.3.3. Radiographs – Mineral Deposition

All GA scaffolds and GT scaffolds with ASCs or without cells remained radiolucent throughout the study. Those GT scaffolds with BMSCs became radiopaque 6 weeks after implantation.

Scaffolds composed of HT were radiopaque throughout the study, and scaffold margins became rounded with time (Fig. 25).

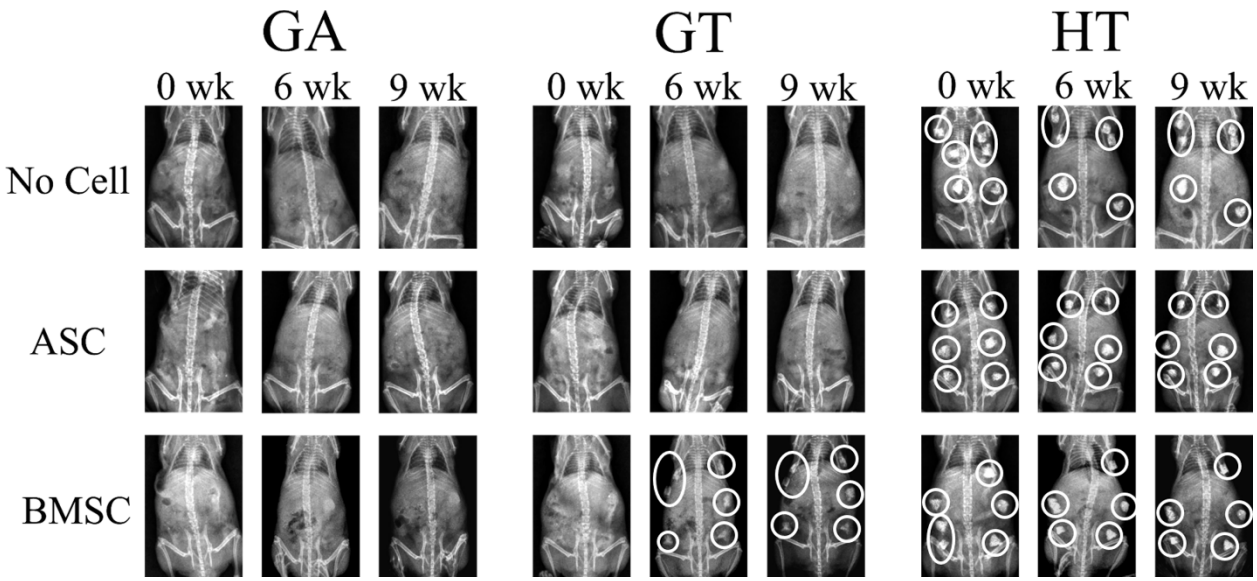

Figure 25. Radiographs of mice with carrier scaffolds composed of TCP/HA (HT), PEG/PLLA (GA) or PEG/PLLA/TCP/HA (GT) with no cells or equine ASCs or BMSCs 0, 6, and 9 weeks after surgical implantation. White circles surround radiopaque implants.

4.3.4. Microcomputed Tomography (μCT) – Porosity, Bone Volume/Total Volume

There were measurable differences between BV/TV of GT and HT constructs at low and high thresholds, while BV/TV in GA constructs were only detectable at a high threshold (Fig. 26). The HT constructs had the highest percent porosity (Fig. 27A). Within scaffold compositions, GA and GT scaffolds with cells had higher porosity than those without, while HT scaffolds without cells had higher porosity than HT-BMSC constructs. Direct comparisons among scaffold BV/TV is not possible due to distinct thresholds used to create reconstructions. Within scaffold compositions, GT- and HT-BMSC constructs had the highest BV/TV, and GT-ASC constructs had higher BV/TV than those with no cells (Fig. 27B).

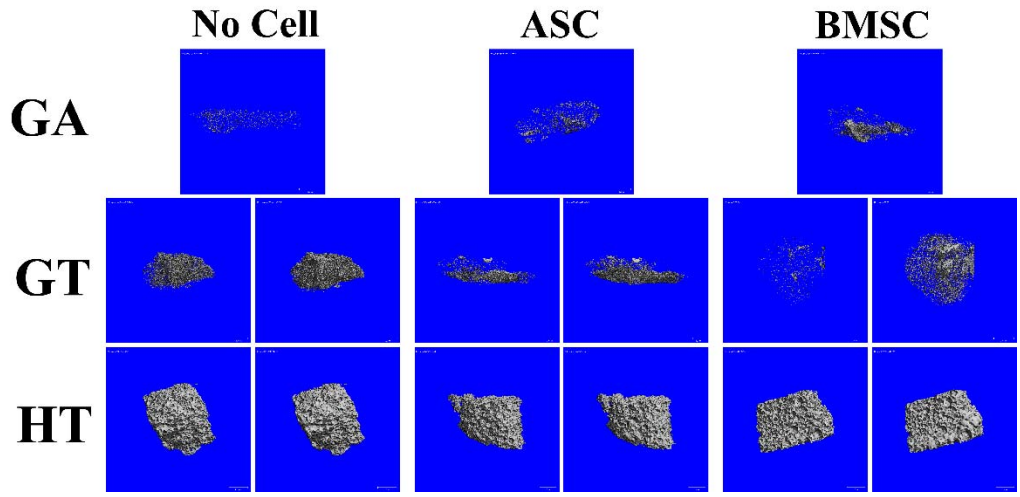

Figure 26. Three-dimensional explant reconstructions demonstrating models generated with low (left) and high (right) thresholds to distinguish between high contrast scaffold structure (left) versus low contrast, newly deposited tissue (right). A single threshold was used for GA constructs due to the limited presence of high contrast material in the specimens. See Fig. 20 for acronym definitions.

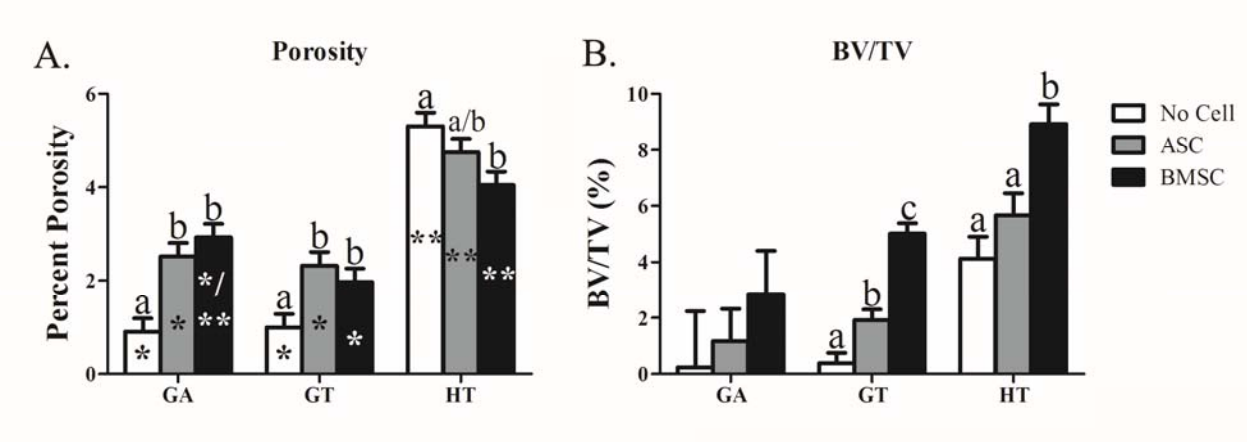

Figure 27. Percent porosity (A) and BV/TV (B) (mean ± SEM) of equine ASC and BMSC constructs 9 weeks after subcutaneous implantation in a murine model. Columns with distinct superscripts are significantly different among cell tissue source within scaffolds and those with different asterisk numbers (*) are significantly different among scaffolds within cell tissue source ($p<0.05$). See Fig. 20 for acronym definitions

4.3.5. Compositional Analysis- DNA, Hydroxyproline, Sulfated Gyclosaminoglycan, Protein

Significant differences in extracellular matrix within scaffold composition included higher hydroxyproline (collagen) in GT-ASC constructs versus those without cells (Fig. 28B), higher protein in GT-ASC constructs versus no cells or BMSCs and higher protein in HT scaffolds

without cells versus either ASC or BMSC constructs (Fig. 28D). Differences among scaffolds within cell types included higher dsDNA in GT versus GA or HT scaffolds without cells, in GT versus HT scaffolds with ASCs and in GA versus HT scaffolds with BMSCs (Fig. 28A). Hydroxyproline was higher in HT versus GA scaffolds without cells and GT versus GA or HT scaffold with ASCs (Fig. 28B). Both GA and GT scaffolds with ASCs or BMSCs had higher sGAG than HT with the same cells (Fig. 28C). Protein was higher in HT versus GA scaffolds without cells and GT versus GA or HT with ASCs (Fig. 28D).

4.3.6. Scanning Electron Microscopy (SEM) - Ultrastructure, Phosphate, Calcium

Collagen fibrils and amorphous matrix were apparent in all explants (Fig. 29). A notable distinction was the presence of solid regions in various stages of mineralization and surrounded by randomly oriented collagen fibrils in scaffolds with cells. The well delineated regions were distinct from the more proteinaceous ECM of scaffolds without cells. Subjectively, BMSC construct ECM was the most dense among explants.

Within HT-BMSC and GA and GT constructs, calcium and phosphorus percentages were higher and lower, respectively, in scaffolds with versus without cells (Fig. 30), and ratios did not change appreciably in HT-ASC constructs. The calcium phosphorus ratio was closest to that of HA (1.6) in GA-BMSC and GT-BMSC constructs [324].

4.3.7. RT-PCR - Gene Expression

Equine – There was no detectable equine gene expression in scaffolds without cells. Osteogenic gene expression tended to be highest in scaffolds with BMSCs and vary among scaffold compositions. Within scaffold compositions, BMSC constructs had higher ALP and OCN than ASC constructs (Fig. 31 A, B). The OPG and BSP expression was highest in GT- and HT-BMSC constructs, respectively (Fig. 31 C, D). Within cell tissue source, ALP was higher in HT- versus

GA-ASC constructs (Fig. 31A). Both ALP and OCN were lowest in HT-BMSC constructs (Fig. 31A, B). The OPG in GA-ASC constructs was higher and lower than GT- and HT-ASC constructs, respectively. The BSP was lower in HT- versus GA- and GT-ASC constructs. Additionally, GT-BMSC constructs had higher BSP than GA-BMSC constructs.

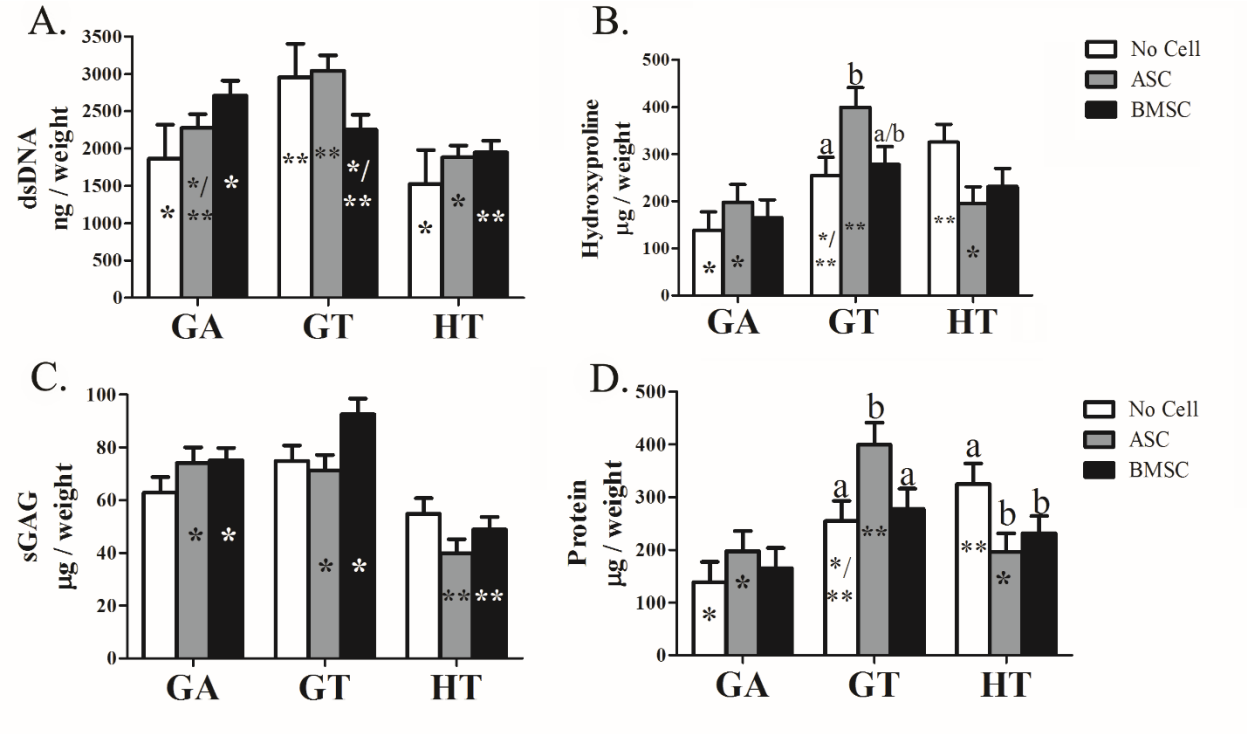

Figure 28. The dsDNA (A), hydroxyproline (collagen) (B), sulfated glycosaminoglycan (sGAG) (C) and protein (D) content (LS mean ± SEM) equine ASC and BMSC constructs 9 weeks after subcutaneous implantation in a murine model. Columns with distinct superscripts are significantly different among cell types within scaffolds and those with different asterisk (*) numbers are significantly different among scaffolds within cell types ($p<0.05$). See Fig. 20 for scaffold composition.

Murine – Osteogenic gene expression tended to be highest in scaffolds with BMSCs compared to those with no cells or ASCs. Differences among scaffold compositions varied and tended to parallel the equine gene expression. Among cell tissue source within scaffold composition, the highest expression levels included ALP in GA- and GT-BMSC constructs (Fig. 32A), OCN in all BMSC constructs (Fig. 32B), OPG in GT-BMSC constructs (Fig. 32C) and BSP

in GT- and HT-BMSC constructs. Lowest expression levels included ALP expression in GT-ASC constructs (Fig. 32A) and BSP in all scaffolds without cells (Fig. 32D). Among scaffold compositions, ALP tended to be lower in GA and GT versus HT scaffolds with ASCs or without cells and in HT versus GA and GT scaffolds with BMSCs (Fig. 32A). The OPG expression followed the same general pattern with the exception that it was lower in GA- versus HT-BMSC constructs (Fig. 32B). The BSP was highest in HT scaffolds without cells and lowest in GA-BMSC constructs.

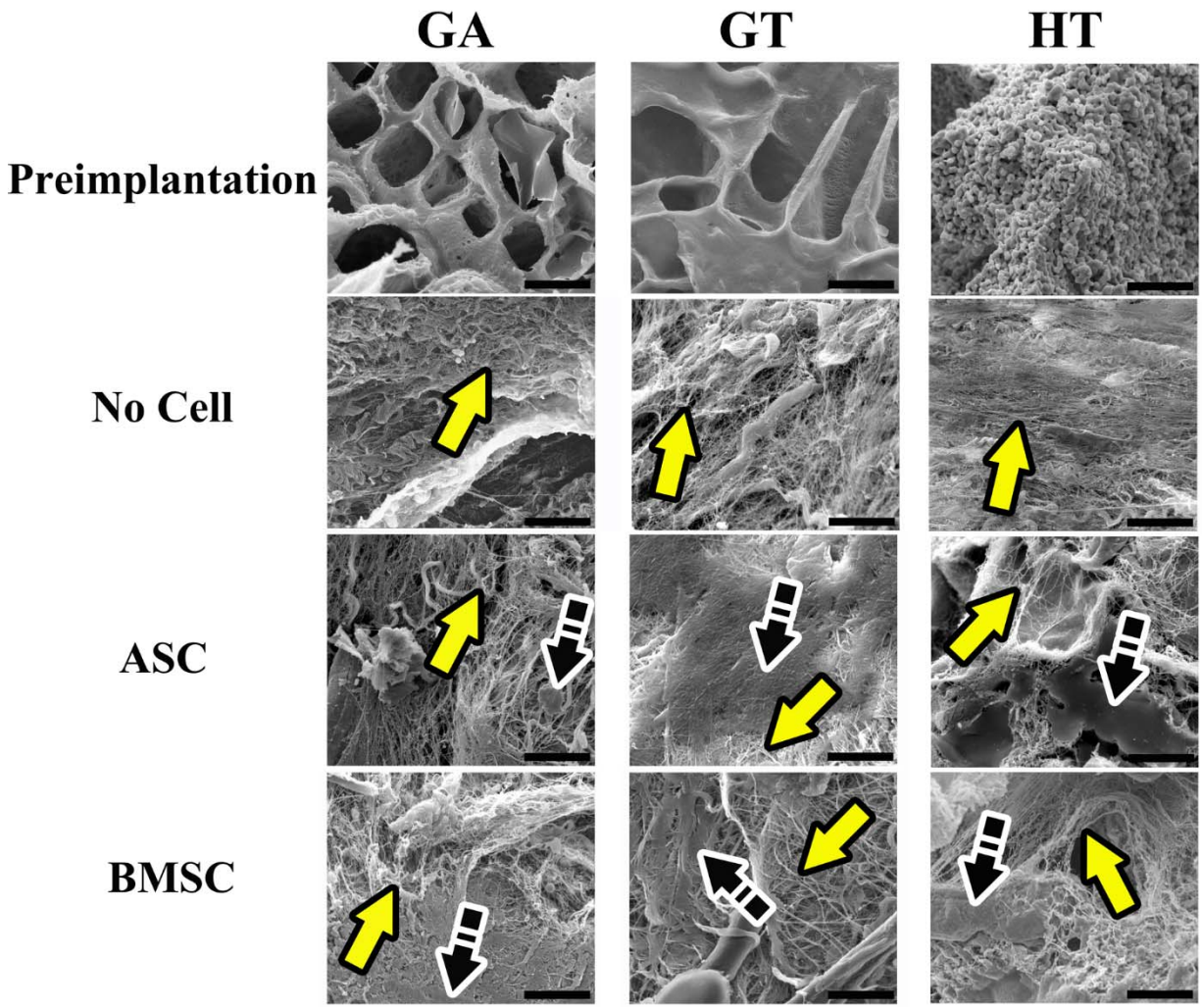

Figure 29. Scanning electron photomicrographs of scaffolds before cell loading (Preimplantation) and 9 weeks after implantation without (No Cell) or combined with equine ASCs (ASC) or BMSCs

(BMSC). Magnification = 3000x ; bar = 20 µm. Yellow arrows = collagen fibrils; Two-stripe black arrow = solid (mineralizing) region. See Fig. 20 for acronym definitions.

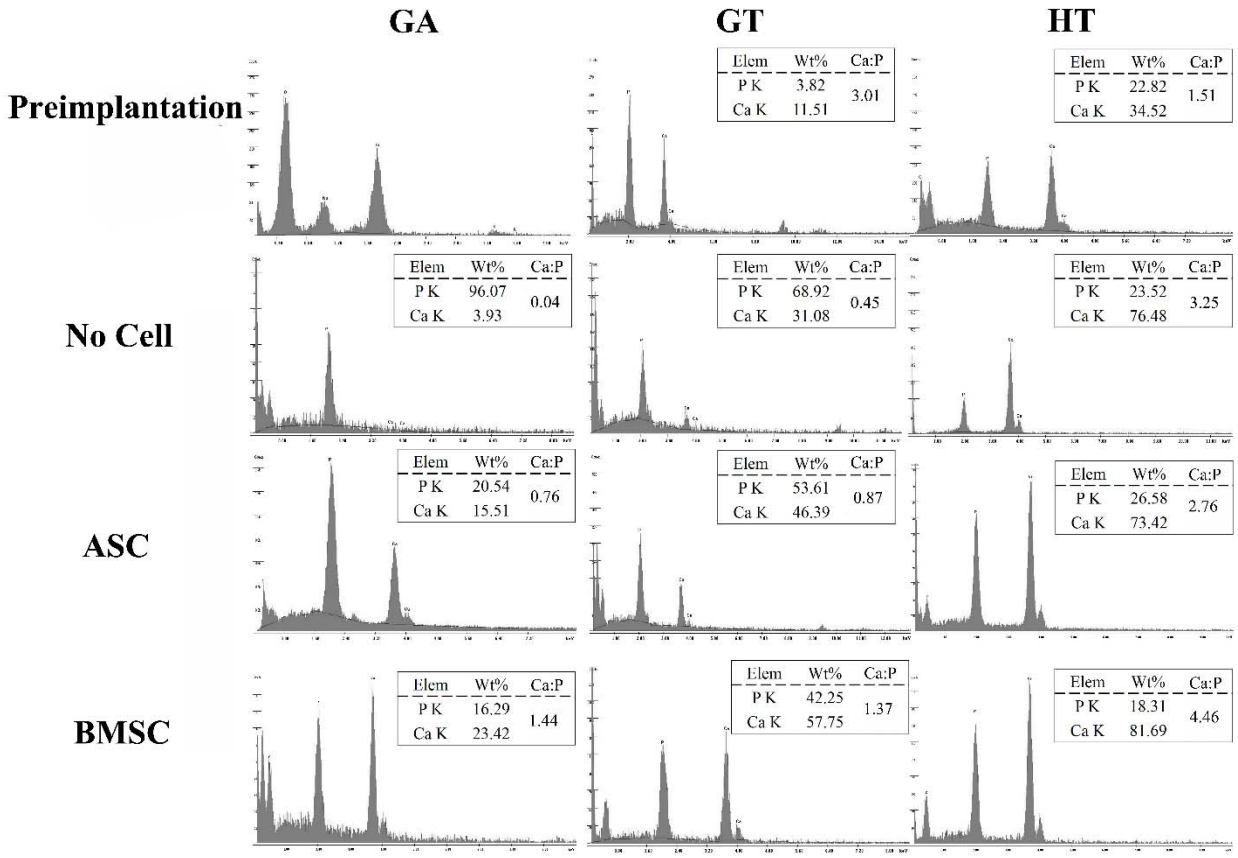

Figure 30. Energy dispersive x-ray microanalysis of explants before (Preimplantation) cell loading or combined with equine ASCs (ASC) or BMSCs (BMSC) 9 weeks after implantation. See Fig. 20 for acronym definitions.

4.3.8. Light Microscopy - Microstructure

Regardless of composition, scaffolds with cells had more ECM than those without, most ECM deposition was on the implant periphery, and osteoid was apparent in all BMSC constructs. Specific to constructs, there was more amorphous, proteinaceous ECM apparent on GT- versus GA-ASC constructs, and GT-BMSC constructs had more osteoid ECM than GA-BMSC (Fig. 33).

4.4. Discussion

The overarching conclusions from this study are that addition of mineral to polymer scaffolds enhances equine MSC osteogenesis over polymer alone, but mineral (HT) scaffolds provide superior support for equine MSC osteogenesis compared to either polymer composition. Parallel outcomes disprove both parts of the first hypothesis since osteogenesis was best on HT scaffolds regardless of cell tissue source and BMSCs showed more robust osteogenesis than ASCs. Further, GT scaffolds supported better osteogenic differentiation and ECM deposition than GA. However, the second hypothesis that the scaffolds with MSCs have greater osteogenesis than those without is true.

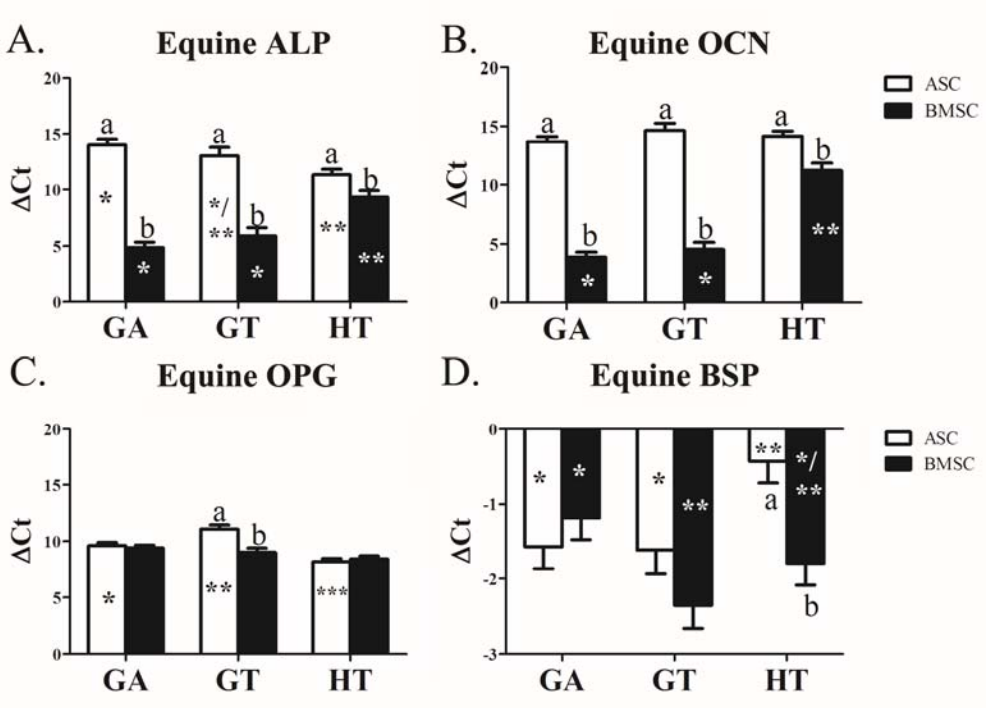

Figure 31. Equine alkaline phosphatase (A; ALP), osteocalcin (B; OCN), osteoprotegerin (C; OPG), and bone sialoprotein (D; BSP) levels (mean ± SEM) in equine MSC-scaffold constructs 9 weeks after implantation. Columns with distinct superscripts are significantly different between cell tissue source among scaffolds and those with different asterisk numbers (*) are significantly different among scaffolds between cell tissue source ($p<0.05$). See Fig. 20 for acronym definitions.

This study also confirms the presence of exogenous mRNA in implants 9 weeks after placement. Most previous work confirms persistence of implanted cells with inert cell labels or plasmid gene expression that can be incorporated into endogenous cells following exogenous cell senescence [325]. Few studies confirm the presence of exogenous mRNA to suggest, if not confirm, viable cell osteogenic gene expression. Another major finding is the largely parallel equine and murine genetic expression including higher osteogenic gene expression by murine cells in BMSC constructs. Higher osteogenic potential of BMSCs compared to ASCs is consistent with established information and largely attributed to epigenetic factors [291, 326]. Observed upregulation of osteogenic gene expression by murine cells in equine BMSC constructs may be a consequence of both growth factor production, ECM deposition, and direct and indirect signaling by exogenous cells [9, 11, 245, 284, 327-334]. These findings are consistent with knowledge of native cell recruitment and direction by MSC implants [267, 335, 336], and they further emphasize the need to construct implants for optimum direction of both exo- and endogenous cell contributors to osteogenesis.

Study findings and current knowledge show that polymer-mineral scaffold support of equine MSC osteogenesis will be improved with further optimization. Previous reports indicate that addition of mineral to polymer scaffolds enhances MSC osteogenesis in other species, sometimes more than mineral alone [297, 323, 337]. A biomimetic environment is created, in part, by composition, surface topography, microarchitecture and mechanical properties [267]. Flexible polymer scaffolds with less structural organization in this study may have weaker osteogenic signaling that the rigid, porous ceramic structure. Calcium ions released from calcium phosphate based minerals play a major role in influencing osteoblastic differentiation [338], and the presence of either HA or TCP enhances mRNA levels of BSP in human BMSCs without osteogenic medium

[243]. Based on equine MSC osteogenic gene expression on scaffolds with calcium phosphate (HA and TCP) in this study and on collagen in previous work, polymer scaffolds with three-dimensional bone microstructure overlaid with minerals and collagen may better support osteogenesis [238, 245]. Scaffolds specifically designed for ASC osteogenesis could also possibly increase contributions to osteogenesis.

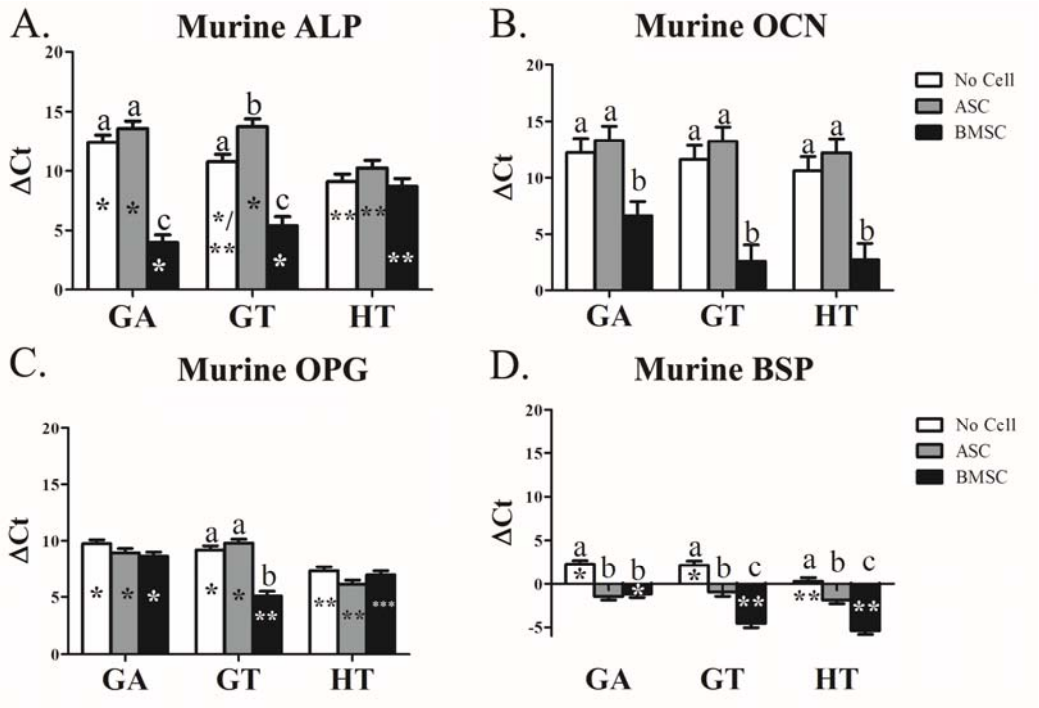

Figure 32. Murine alkaline phosphatase (A; ALP), osteocalcin (B; OCN), osteoprotegerin (C; OPG), and bone sialoprotein (D; BSP) levels (mean ± SEM) in equine MSC-scaffold constructs 9 weeks after implantation. See Fig. 10 for acronym definitions.

Higher ECM and osteoid deposition on the scaffold periphery have resulted from cell distribution and in vivo conditions. Cell distribution was not confirmed, so cells may have concentrated on the scaffold periphery from spinner flask centrifugal forces and lack of continuous scaffold pores [126, 140, 339, 340]. Better interstitial flow on the construct surface in vivo could have promoted better cell survival that in the center despite small implant size [302, 309, 341]. While not directly translatable to in vivo, reduced in vitro MSC numbers at 7 and 21 days compared

to initial number in half of the constructs may account for lower in vivo ECM deposition. The cause of cell loss was not evaluated, but increased cell numbers in some scaffolds is inconsistent with scaffold cytotoxicity. The MSC affinity for culture plastic in vitro or surrounding tissues in vivo may have been equal or greater than that for scaffold components [265, 342]. Explant dsDNA content does not suggest cell loss likely due to murine cells from the local environment in vivo. Future studies to evaluate cell distribution and orthotopic ECM deposition will help resolve these points.

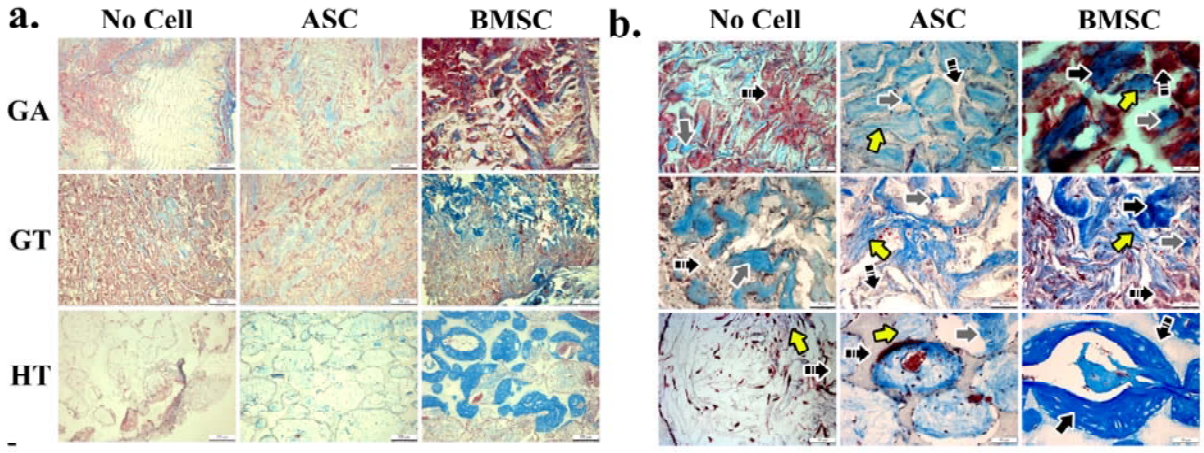

Figure 33. Light photomicrographs of equine MSC-scaffold explants 9 weeks after surgery. Masson's trichrome stain; magnification, 10x; scale bar = 200 μm (A); Magnification 40x; scale bar = 50 μm (B). Black arrow = osteoid, yellow arrow = collagen fibers; gray arrow = proteinaceous ECM; Two-triple black arrow = scaffold. See Fig. 20 for acronym definitions.

Presence of equine MSCs significantly enhanced ECM deposition in scaffolds regardless of composition, though SEM and light microscopy confirmed osteoid deposition was highest with either BMSCs and/or high scaffold mineral content. Changes in EDS calcium and phosphate may indicate early ion deposition for mineralization [343]. Compositional analysis confirmed proteinaceous ECM in MSC constructs that was observed with light microscopy. Lower ECM composition in HT constructs is likely from ECM deposition throughout GT and GA scaffolds versus HT scaffold pore surfaces. The HT scaffold porosity may have decreased from ECM

deposition within pores and polymer scaffold porosity increased from ECM deposition and organization.

The results of this study are limited to ectopic versus orthotopic ossification that is more representative of implant efficacy to support osteogenesis in native bone [344, 345]. Athymic mice have diminished osteogenic capabilities compared to immunocompetent animals [346, 347], so scaffolds and cell-scaffold constructs may behave differently in an equine fractures. Nonetheless, subcutaneous implantation is an accepted approach with numerous intra-animal replicates to compare in vivo ECM deposition and genetic expression among scaffolds and cell-scaffold constructs [348, 349]. The study length exceeded the time for natural, early fracture stabilization [350] to evaluate long term differences in cell-construct in vivo behaviors. Results that differ between this and other studies can be attributable to study duration, distinct in vivo and in vitro environments [351, 352], species [353, 354] and revitalized MSCs, a point that has been shown to impact cell behavior [18, 23, 24] within immunophenotypes [6, 7, 355]. Nonetheless, the number of sample replicates, duration, and parallel outcome measures in this study provide robust tests of the stated hypotheses.

As a whole, these in vivo study results confirm that addition of mineral to polymer carrier scaffold enhances strong osteogenic capabilities of equine MSCs without osteogenic preconditioning prior to implantation and that BMSCs appear to have better osteogenic ECM production and organization than ASCs Findings from these investigations confirm that contributions of both exogenous cells and recruitment of host MSCs are vital to MSC construct osteogenesis. The contributions in the present study may provide important information to help overcome equine bone healing challenges. The novel scaffold carriers evaluated in this study are

appropriate for continued development of synthetic graft materials and viable tissue implants to augment equine fracture strategies.

CHAPTER 5. THE EFFECTS OF COLLAGENASE CONCENTRATION ON EQUINE ADIPOSE DERIVED-MULTIPOTENT STROMAL CELL ISOLATION

5.1. Introduction

The most common technique to isolate adipose derived multipotent stromal cells (ASCs) is based on enzymatic digestion to separate the stromal vascular fraction (SVF) from the tissue. The cells are subsequently cultured on plastic culture plate which selects for ASCs based on plastic adherence [356]. Nevertheless, there is no standard protocol with uniform parameters for the isolation [356]. Collagenase type I digests for ASC isolation are widely used, and the collagenase concentrations are variable [96, 357]. This can result in irregularities between cell isolates even if everything else is the same [356]. Commercial collagenase to dissociate tissues may leave foreign protein residuals like collagenase type I, protease, polysaccharidases, and lipase [358]. In a previous study in our laboratory, a 0.1% collagenase digest was used to isolate ASCs from equine subcutaneous adipose tissue and the concentration could efficient yield nucleated cells and the cells isolated exhibited in vitro proliferation and multipotent capabilities [291]. Reduction of collagenase concentration used in the digest solution will reduce the foreign protein residuals.

In the horse, the adipose SVF and ASCs are used to treat joint related diseases and tendon/ligament related injuries [359, 360]. However, common isolation and culture techniques fail to ensure homogenous cell populations, and nonprogenitor cell contamination may impair treatment efficacy and induce inflammation [359-361]. There are many cell subpopulations in the SVF and cultured ASCs that include endothelial cells, erythrocytes, fibroblasts, lymphocytes, monocyte/macrophages, preadipocytes, pericytes and hematopoietic stem and progenitor cells [75, 362, 363]. The identity of MSCs can be determined by immunophenotype based on surface protein expression [364]. Fluorescence activated cell sorting (FACS) allows single cell selection so it is

frequently used to isolate specific cell subpopulations [365]. In vitro, ASCs retain CD44 and CD105 expression and lack the expression of major histocompatibility complex class II (MHCII) [364], and they can be selected based on these characteristics. Cell sorting techniques to remove nonprogenitor cells and purify cell isolates may result in more predictable cell behavior.

In published reports, the majority of equine reports utilize fresh cells [366]. However, current knowledge supports that MSCs change with extensive culture including decreasing expansion capacity and plasticity with increasing passage [367, 368], and the risk of microbe or exogenous cell contamination also increases with culture time [41, 42]. As an alternative to continuous culture, cryopreservation is often employed for cell preservation. Several studies indicate that slow cooling and cryoprotectants (CPs) such as dimethyl sulfoxide (DMSO) and fetal bovine serum (FBS) fully retain stem cell properties [25, 43, 77]. However, the actual impact of slow cooling and freezing with CPs, particularly on the maintenance of multipotentiality in the cell population after cryopreservation, is not clear [14]. Additionally, the chemical toxicity of cryoprotectants should also be considered [43]. Several side effects of DMSO (e.g. nausea, vomiting, flushing, fever, chills, dyspnea, cardiac symptoms, transient hypertension and hypotension and anaphylaxis) are associated with the infusion of DMSO-cryopreserved hematopoietic progenitor cell applications [54]. Conventional cryopreservation methods usually result in some irreversible cell damage and mortality due to intracellular ice formation and CP toxicity [14, 43]. Identification of an ideal medium for cryopreservation is the first step in using cryopreserved MSCs in equine veterinary patients. To achieve this goal, reduction of the CP toxicity and fully quantifying the effects of cryopreservation on short-term proliferation and genetic profile of equine ASCs is necessary.

The three-part tested hypothesis tested in this study was that 1) equine ASC yield, plasticity, and expansion rate decreases with increasing collagenase in the tissue digest; 2) MHCII-, CD44+, CD105+ ASCs have higher expansion and plasticity compared to MHCII+, CD44+, CD105+; and unsorted cells; and 3) ASC expansion potential and plasticity decreases with increasing cryopreservation medium DMSO concentration. The yield of nucleated cells, immunophenotype profile, in vitro expansion capabilities, and plasticity of equine ASCs isolated from adipose tissue digested with distinct collagenase concentrations were determined. The same was assessed after FACS was employed to select MHCII-, CD44+, CD105+ and MHCII+, CD44+, CD105+ cells from fresh and cryopreserved ASCs. Additionally, the in vitro expansion, immunophenotype profile, and plasticity were evaluated in equine ASCs cryopreserved in media with 5% or 10% dimethyl sulfoxide (DMSO).

5.2. Materials and Methods

5.2.1. Ethics Statement

All animal procedures were approved by the Institutional Animal Care and Use Committee (Protocol #07-049).

5.2.2. Study Design

Subcutaneous adipose tissues from dorsolateral to the base of the tail were collected from 4 adult, thoroughbred gelding horses (10.7±5.9 years of age, mean ±standard error of the mean (SEM)). Different type I collagenase concentrations, 0.1%, 0.05%, and 0.025%, wt were used in adipose tissue digests for ASC isolation. Stromal vascular fraction (SVF) cells from the series collagenase digests were equally divided into two portions, fresh and cryopreserved. Identical cell aliquots were cryopreserved in two different cryopreservation media: 1: 80% fetal bovine serum (FBS), 10% dimethyl sulfoxide (DMSO), and 10% Dulbecco's Modified Eagle Medium: Nutrient

Mixture F-12 (DMEM) (C1); or 95% FBS and 5% DMSO (C2) in liquid nitrogen for 30-60 days. Two distinct cell subpopulations were sorted from fresh and cryopreserved cells via FACS, CD44+, CD105+, the major histocompatibility complex class II (MHCII) - and CD44+, CD105+, MHCII+ cells. Cell doublings (CDs) and doubling times (DTs) were determined for all the cell groups. Fibroblastic (CFU-F), osteoblastic (CFU-Ob), and adipocytic (CFU-Ad) colony-forming unit frequency percentages and lineage-specific target gene mRNA expression levels were determined (peroxisome proliferator-activated receptor γ (PPAR-γ), leptin – adipogenesis; alkaline phosphatase (ALP), bone sialoprotein (BSP) – osteogenesis, sex determining region Y-box 2 (SOX2), Nanog - progenitor) after culture in lineage-specific induction or stromal media. The oncogene mRNA expression levels were determined (β catenin, Notch 1, and FAS) after culture in stromal media. Materials were from Sigma-Aldrich, St. Louis, MO unless otherwise noted.

5.2.3. Cell Isolation, Expansion and Cryopreservation

Subcutaneous adipose tissue was harvested from 4 adult euthanized thoroughbred gelding horses (10.7±5.9 years of age, mean ±standard error of the mean (SEM)). Cells were isolated according to published procedures with minor modifications [245]. Adipose tissue was weighed and rinsed with phosphate buffered saline (PBS, Hyclone, Logan, UT) and minced. The minced tissues were mixed with an equal volume of PBS for 3 minutes. The mixture was allowed to separate into two phases and the upper phase was digested with one of three type I collagenase digestion concentration digests: Group 1, 1% bovine serum albumin (BSA, Fisher Bioreagents, Fair Lawn, NJ) and 0.1% collagenase type I (Worthington Biochemical Corporation, Lakewood, NJ) in Dulbecco's modified Eagle's medium: F-12 (DMEM/F-12, Hyclone, Logan, UT); Group 2, 0.5% BSA and 0.05% collagenase type I in DMEM/F-12; Group 3, 0.25% BSA and 0.025% collagenase type I in DMEM/F-12). The commercial collagenase type I was from the same batch and contained

no less than 125 activity units per mg. All digests were for 90 min with agitation at 37ºC. The digest was then filtered with 100 μm nylon cell strainers (BD Falcon, Bedford, MA) and then centrifuged (260 × g, 5 min) to form the cell pellet. The cell pellet was suspended in 1% BSA in DMEM and the mixture was centrifuged (260 × g, 5 min) and an equal volume of red blood cell lysis buffer (0.16 mol/L NH_4Cl, 0.01 mol/L $KHCO_3$, 0.01% ethylenediaminetetraacetic acid (EDTA)) was added. The mixture was maintained at room temperature for 5 min and centrifuged (260 × g, 5 min) to remove red blood cells. The resulting stromal vascular fraction (SVF) pellet was resuspended in stromal medium (10% FBS (Hyclone), 1% antibiotic/antimycotic solution in DMEM) followed by culture (37 ºC, 5% CO_2) in T75 flasks (Fisher Scientific, Fair Lawn, NJ). Medium was refreshed after 24 hours to remove unattached cells and then every 3 days [18]. The cell yield was evaluated with 0.1% trypan blue staining by hemocytometer. Subsequent passages were performed at 70-80% cell confluence. For purposes of this study, the primary cell isolated was the SVF and the first cell passage of primary cells was P0. Aliquots (~ 1×10^6 cells) of each SVF were suspended in two freezing media, Cryo 1: 10% DMEM, 10% dimethyl sulfoxide (DMSO, Fisher Scientific), 80% FBS; and Cryo 2: 5% DMSO and 95% FBS). CoolCell® was employed to maintain the cooling rate at about -1°C/min and the container was kept at -80 ºC overnight when samples were moved to liquid nitrogen. The cryopreserved cells were kept in liquid nitrogen for a minimum of 30 - 60 days and then moved to a 37ºC water bath for 1-2 min until the ice dissolved. The cryopreserved cells were seeded in T75 flasks as P0 after the cryopreservation period.

5.2.4. Antibody Labeling

The Dylight 488 and Dylight 633 antibody labeling kits (Thermo Fisher Scientific, Somerset, NJ) were used to label equine specific antibodies against CD44 and MHCII, respectively, according to

the manufacturer's instructions. Briefly, 100 µl antibody solution (1 mg/ml) was mixed with 8 µl borate buffer and the mixture was incubated with DyLight Reagent for 60 min at room temperature protected from light. The labeling reaction was mixed with the resin and then centrifuged (1000 × g, 1 min) to collect the purified antibody.

5.2.5. Fluorescence Activated Cell Sorting (FACS)

Fresh and cryopreserved P0 cells were equally divided to two cohorts: unsorted cells and sorted cells. The sorted cells were incubated with antibodies that are equine specific or validated for equine cross reactivity (CD44-488, CD105-PE, MHCII-633) for 30 min at room temperature. The target cell populations (negative cells: CD44+, CD105+, MHCII-; positive cells: CD44+, CD105+, MHCII-) were sorted and quantified by flow cytometry using a FACS Calibur flow cytometer and Cell Quest Pro Software (BD Biosciences, San Jose, CA). Both cell populations were cultured in stromal medium.

5.2.6. Cell Expansion

Cells were cultured in 12-well plates (Thermal Fisher Scientific) at an initial density of 5,000 cells/cm^2. The cell number was evaluated after 2, 4, and 6 days of culture. Cell doublings (CDs) and doubling times (DTs) were determined with duplicate cultures and calculated with the standard formulae (CD= ln(Nf/Ni)/ln(2) and DT =CT/CD; Ni: initial cell number; Nf: final cell number; CT: culture time) [18]. Cell counts were performed with the alamar blue metabolism assay. Alamar blue (Thermo Fisher Scientific) was added to the culture medium for a final concentration of 10%. The mixture was incubated about 4 hours at 37^{o}C in darkness. Absorbance corresponding to cell number was read at 570 nm and 600 nm. Day 2 and 4 cell numbers were used as the Ni for Day 4 and 6, respectively.

5.2.7. Multipotentiality – Limiting Dilution Assays

Limiting dilution assays were used to evaluate fibroblastic (CFU-F), osteoblastic (CFU-Ob), and adipocytic (CFU-Ad) colony-forming unit frequencies [96]. For all cell populations, 8 replicates of 5000, 2500, 1250, 625, 312 or 156 cells/well were seeded in 96-well plates and cultured in stromal medium for 7 days. The CFU-F colonies were fixed with 4% paraformaldehyde and stained with 0.1% toluidine blue. For CFU-Ob, cells were cultured in stromal medium for 7 days followed by culture in osteogenic medium (DMEM/F-12, 10% FBS, 1% antibiotic/antimycotic solution, 10 mmol/L β-glycerophosphate, 20 nmol/L dexamethasone, and 50 μg/ml sodium 2-phosphate ascrobate) for another 4 days. Cells were rinsed 3 times with 150 mM NaCl and then fixed with 70% ethanol and stored at 4 ^{o}C overnight. Cells were stained with a 2% alizarin red solution for 10 min at room temperature and followed rinsed 5 times with distilled water. To determine CFU-Ad, cells were cultured in stromal medium for 7 days followed by culture in adipogenic induction medium (DMEM/F-12, 3% FBS, 5% rabbit serum, 1% antibiotic/antimycotic solution, 33 μmol/L biotin, 17 μmol/L pantothenate, 100 nmol/L insulin, 1 μmol/L dexamethasone, 500 μmol/L isobutylmethylxanthine (IBMX), 5 μmol/L rosiglitazone (TZD)) for 3 days. The same medium without IBMX and TZD was used as maintenance medium to culture the ells for additional 3 days. The cells were fixed in 1% PFA at room temperature and stained with 0.3% oil red O for 15 min. Wells were considered positive for fibroblastic, adipocytic or osteoblastic when there were ≥ 10 toluidine blue stained, ≥ 10 oil red O-stained, or ≥ 1 alizarin red stained colonies, respectively. The ratio of negative to total wells per row was used to compute the CFU frequencies according to Poisson's ratio ($F=e^{-x}$; F: ratio of negative to total wells; e: natural logarithm constant 2.71; x: CFU/well) [18, 96, 181].

Table 11. Primer Sequences

Lineage	Primer	Sequences	Accession No.
Housekeeping	GAPDH	F: AAGAAGGTGGTGAAGCAGG R: CTCAGTGTAGCCCAGGATG	NM_001163856.1
Stromal	SOX2	F: CTCTGGTAGTGCTGGGACATGTG R: AGTACAACTCCATGACCAGCTC	XM_003363345.3
	Nanog	F: ACTGTCTCTCCTCTGCCTTC R: TCTTCCTTCTTTGCCTCG	XM_014740545.1
Osteogenic	ALP	F: GGAGTATGAGATGGACGAG R: GTAGTGAGAGTGCTTGTGCC	XM_005607380.2
	BSP	F: GAAGAATCGGACGCTGAG R: ATCGTAGACAGGGTGGTG	XM_001496125.4
Adipogenic	PPAR-γ	F: CCACTGACCAAAGCGAAG R: TGAGCGAAACTGACACCC	XM_001492430.3
	Leptin	F: GTTGAAGCTGTGCCAATCCG R: CATCTTGGACAAACTCAGGAC	XM_014738998.1
Oncogenic	FAS	F: ACACAGACAAGCCACATC R: GCAATCAGTAACAGGAACAG	XM_014733084.1
	Notch1	F: TTCGTGCTGCTCTTCTTC R: TGGTCTGTCTGGTCATCC	XM_014736246.1
	β-catenin	F: CAGGTGGTGGTGAATAAGG R: GTTGTGGAGAGTTGTAATGG	NM_001122762.1

5.2.8. Gene Expression – RT-PCR

Total RNA was extracted from cells (EZNA^{TM} Total RAN kit II, Omega bio-tek, Norcross, GA, USA) and the concentration determined spectrophotometrically (NanoDrop ND-1000; NanoDrop Technologies, Montchanin, DE). The RNA was transcribed to cDNA using Maxima First Strand cDNA synthesis kit (Thermo Scientific) and target gene mRNA levels, glyceraldehyde 3-phosphate dehydrogenase (GAPDH), PPAR-γ, Leptin, ALP, BSP, SOX2, Nanog, FAS, β-catenin, and Notch1 (Table 11), were quantified with RT-PCR using SYBR Green (Absolute Blue qPCR kit, Thermo Scientific) technology and HT7900 (Applied Biosystems, Darmstadt, Germany). The ΔCt values were determined relative to the reference gene GAPDH.

5.2.9. Statistical Analysis

Statistical analyses were performed with the JMP statistical package (SAS Institute, Cary, NC). Mixed ANOVA models were used to evaluate cell yield, cell immunophenotype percentages, CD, DT, CFU frequency percentages and gene expression among cell types. Tukey's post hoc tests were applied for multiple group comparisons ($p<0.05$).

5.3. Results

5.3.1. ASC Isolation

Cell yields were $2.6 \pm 0.5 \times 10^5$, $2.1 \pm 0.5 \times 10^5$, and $1.2 \pm 0.5 \times 10^5$ nucleated cells/g adipose tissue for 0.1%, 0.05%, and 0.025% type I collagenase solution, respectively. The cell yield from 0.025% collagenase was significantly lower than for 0.1% (Fig. 34).

5.3.2. Immunophenotype

The percentages of negative (MHCII-, CD44+, CD105+) cells from the series of collagenase digests were not significantly different (Fig. 35a). Additionally, there were no significant differences between percentages of negative cells among fresh cells, or those cryopreserved with

either medium, Cryo 1 or Cryo2 (Fig. 35). A similar pattern was found in the percentages of positive (MHCII+, CD44+, CD105+) cells (Fig. 35b).

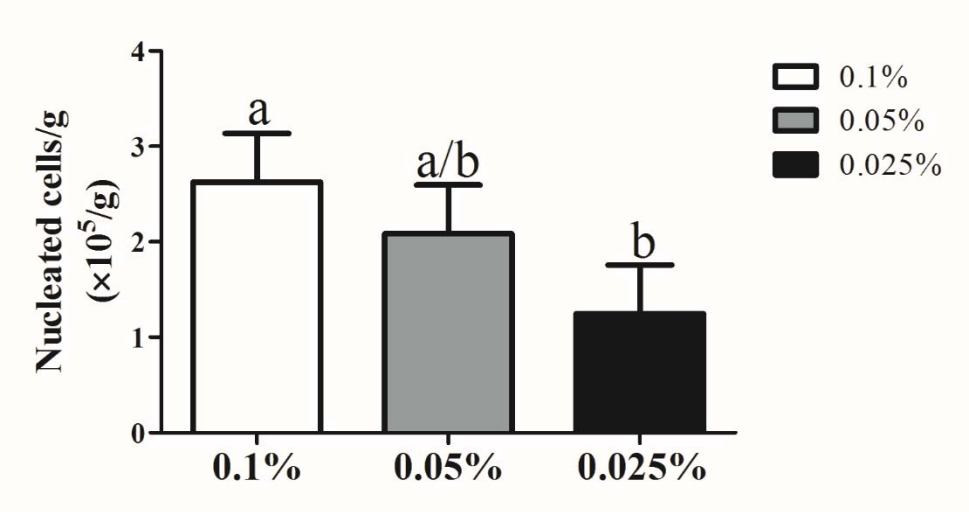

Figure 34. Equine adipose tissue ASC yield (mean ± SEM, n=4) from three different type I collagenase digest concentration (0.1%, 0.05%, 0.025%). Columns with different superscripts are significantly different from each other ($p<0.05$)

5.3.3. Cell Expansion

Fresh cells isolated with distinct collagenase concentrations had similar CD and DT values. Cryopreserved cells had similar CD and DT values for 5 and 10% DMSO cryopreservation medium (Fig. 36). Since the percentages of positive and negative cells (Fig. 35) and in vitro expansion rates (Fig. 36) from different collagenase concentrations were similar, immunophentoypes from different digests were combined within fresh and cryopreserved cells.

Following cell sorting after cryopreservation, there were very few MHCII+, CD44+, CD105+ cells (7077 ± 8953 cells), and the cell isolates did not grow well. Therefore, CD and DT values are not included in the results. The CDs of fresh, unsorted cells were significantly higher compared to other cell populations (Fig. 37a), while the corresponding DT in fresh unsorted cells was significantly lower than other cell populations (Fig. 37b). After cryopreservation, negative

cells had similar growth parameters as the unsorted, cryopreserved cells. However, the fresh positive and negative cell populations had significantly lower and higher CD and DT versus fresh, unsorted cells, respectively.

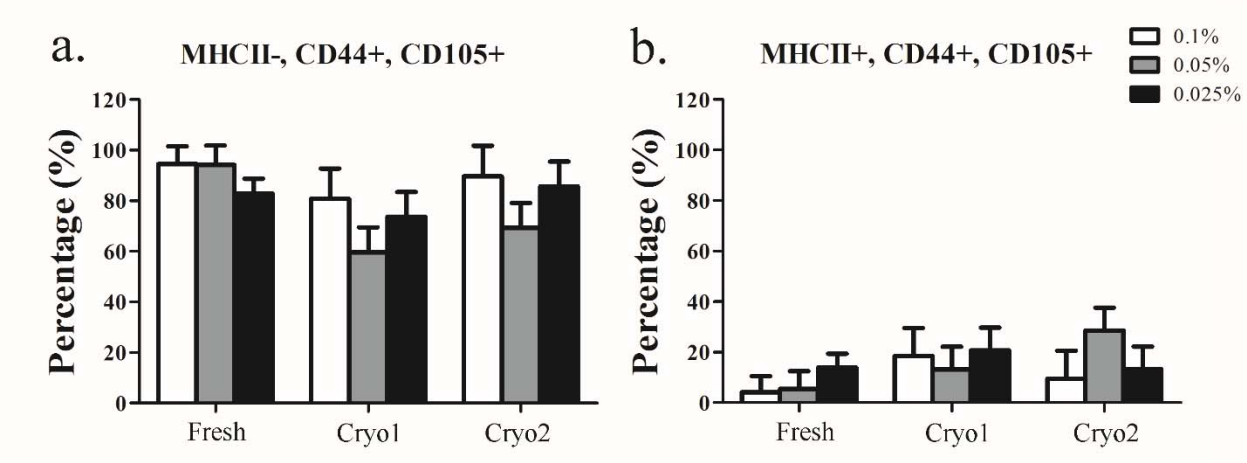

Figure 35. Percentages (LS mean ± SEM) of fresh and cryopreserved cells isolated with digests containing type I collagenase concentrations 0.1, 0.05, or 0.025% with immunophenotype CD44+, CD105, and MHCII- (a), or MHCII+ (b). Cryo1: 80% FBS, 10% DMSO in DMEM/F-12; Cryo2: 95% FBS, 5% DMSO.

5.3.4. Multipotentiality- Limiting Dilution Assays

All cell populations maintained a fibroblastic-like morphology when cultured in stromal medium (Fig. 38a). In osteogenic medium, calcium deposits in cell coloies stained with alizarin red (Fig. 38b). After adipogenic medium culture, robust lipid droplets stained with oil red O (Fig. 38c).

The CFU frequency percentage indicates the percentage of cells from a cell population that have can form CFU-F, -Ob, or –Ad colonies. Fresh MHCII-, CD44+, CD105+ cells had significantly higher CFU-F than cryopreserved cells or cryopreserved cells (Fig. 39a). After cryopreservation in medium with either 5 or 10% DMSO, unsorted cells had the significantly lowest CFU-Ob frequency among all cell isolates (Fig. 39b).

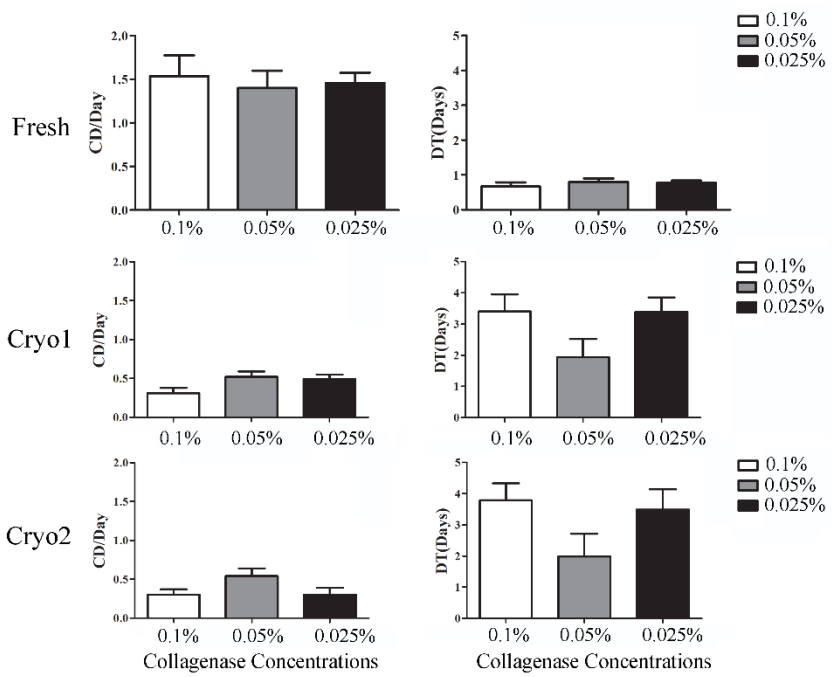

Figure 36. Cell doublings (CD) and doubling times (DT) (LS mean ± SEM) from fresh and cryopreserved cells isolated with 0.1, 0.05, or 0.025% collagenase I digests. Cryo1: 80% FBS, 10% DMSO in DMEM/F-12; Cryo2: 95% FBS, 5% DMSO.

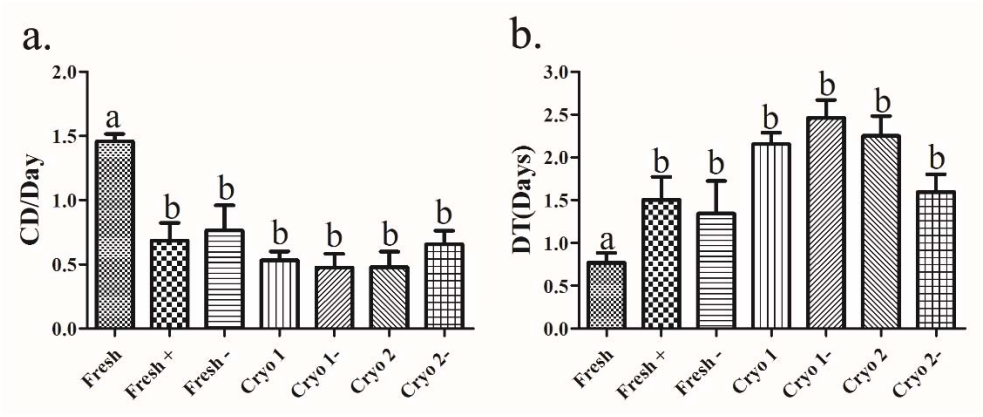

Figure 37. Cell doublings (CD) (a) and doubling times (DT) (b) (mean ± SEM) of fresh and cryopreserved equine ASC isolates that were unsorted, MHCII+, CD44+, CD105+ (+) or MHCII-, CD44+, CD105+ (-). Cryo1: 80% FBS, 10% DMSO in DMEM/F-12; Cryo2, 95% FBS, 5% DMSO. Columns with distinct superscripts are significantly different ($p<0.05$).

5.3.5. Gene Expression

Lineage-specific Gene Expression

When the cells were cultured in stromal medium, fresh MHCII-, CD44+, CD105+ cells had lower SOX2 and Nanog (Fig. 40A and B) expression compared unsorted cells. The MHCII-, CD44+, CD105+ cells had greater SOX2 expression (Fig. 40A), but lower Nanog expression (Fig. 40B) after cryopreservation with 10% DMSO compared to unsorted cells with the same cryopreservation medium. After cryopreservation in medium with 5% DMSO MHCII-, CD44+, CD105+ Nanog expression was higher than unsorted cells (Fig. 40B). For the induced cells, fresh MHCII-, CD44+, CD105+ cells had higher ALP expression (Fig. 40C) than unsorted and the same immunophenotype had higher ALP (Fig. 40C) and BSP (Fig. 40D) expression versus unsorted cells after cryopreservation with 5% DMSO. After culture in adipogenic medium, the PPAR-γ and leptin expression (Fig. 40 E and F) in fresh and Cryo1 unsorted cells were significantly higher than fresh MHCII-, CD44+, CD105+ and Cryo1 MHCII-, CD44+, CD105+cells, respectively.

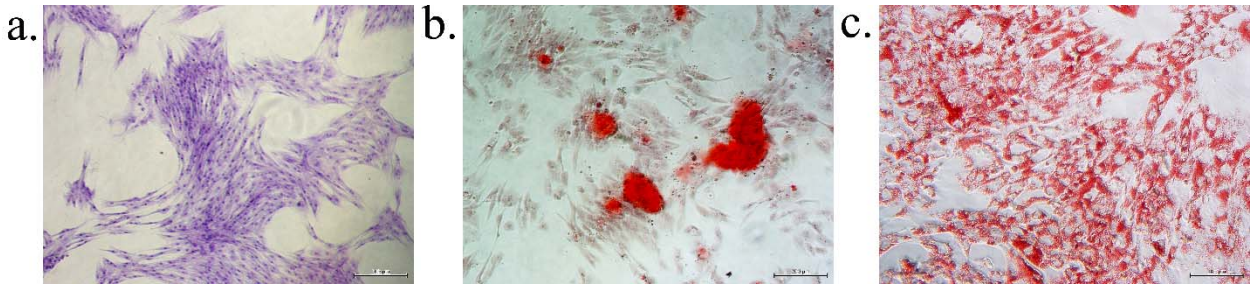

Figure 38. Photomicrographs of equine ASCs after 7 days of culture in stromal medium with toluidine blue staining a, 5 ×; with alizarin red staining of calcium deposition after 4 days of culture in osteogenic medium b, 5 ×; with oil red O lipid staining after 3 days of culture in adipogenic induction medium followed 3 days of adipogenic maintenance medium, c, 5 ×. Scale bar = 200 μm.

For the cells cultured in stromal medium, the significant differences among cell types within cell subpopulations included Cryo2 negative cell subpopulation had the highest SOX2 and Nanog expression than other negative cell subpopulations. Cryo1 negative cell subpopulation had higher SOX2 expression than fresh negative cell subpopulation (Fig 40A). For unsorted cells, fresh cells had higher and lower SOX2 expression versus Cryo1 and Cryo2 cells, respectively (Fig.

40A and B). For the induced cells, the mRNA level of ALP in fresh negative cells was greater versus cryopreserved negative cells regardless of cryopreservation methods (Fig. 40C) within cell subpopulations. However, the Cryo2 negative cells had higher BSP expression versus other negative cell subpopulations (Fig. 40D). On the other hand, after adipogenesis, the cryopreserved negative cells had greater leptin expression versus fresh negative cells, while the fresh and Cryo1 unsorted cells had greater leptin expression versus Cryo2 unsorted cells (Fig. 40F).

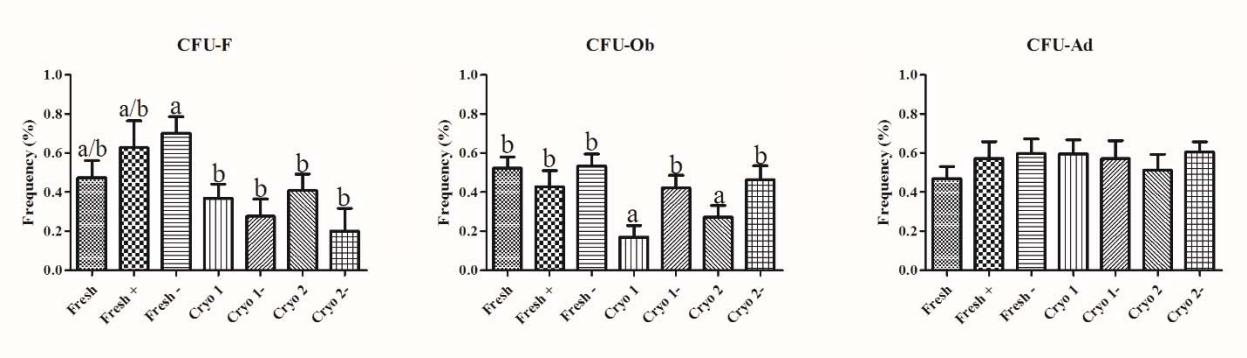

Figure 39. Colony forming unit (CFU) frequencies (LS mean ± SEM) for the same cell populations as Figure 32 following culture in stromal (CFU-F), osteoblastic (CFU-Ob), or adipogenic (CFU-Ad) medium. Columns with different superscripts are significantly different among cell populations ($p<0.05$).

Oncogene expression

The mRNA levels of FAS and β-catenin in Cryo2 negative cells were significantly lower than Cryo2 unsorted cells (Fig. 41A and C). The negative fresh cell subpopulation had lower β-catenin expression than fresh unsorted cells (Fig. 41C). Significant differences within cell subpopulations among treatments included higher FAS expression by Cryo1 negative cells versus Cryo2 negative cells. Fresh, unsorted cells had higher Notch1 and β-catenin expression versus unsorted Cryo1 and Cryo2 cells, respectively (Fig. 41B and C).

5.4. Discussion

The findings of this in vitro study indicate that the collagenase concentrations used to digest equine adipose tissue do significantly affect percentages of MHCII-, CD44+, CD105+ and MHCII+,

CD44+, CD105+ isolated despite the fact that higher collagenase concentrations result in higher nucleated cell numbers. Post-isolate expansion rates are not impacted by collagenase concentration, either. Additionally, MHCII+ and – cells have lower proliferation rates compared to fresh, unsorted cells after cryopreservation with 5 or 10% DMSO. Perhaps of greatest importance is that cryopreservation may reduce the oncogene expression (β-catenin, Notch1) and enhance cell plasticity, especially when cells are cryopreserved in 5% DMSO.

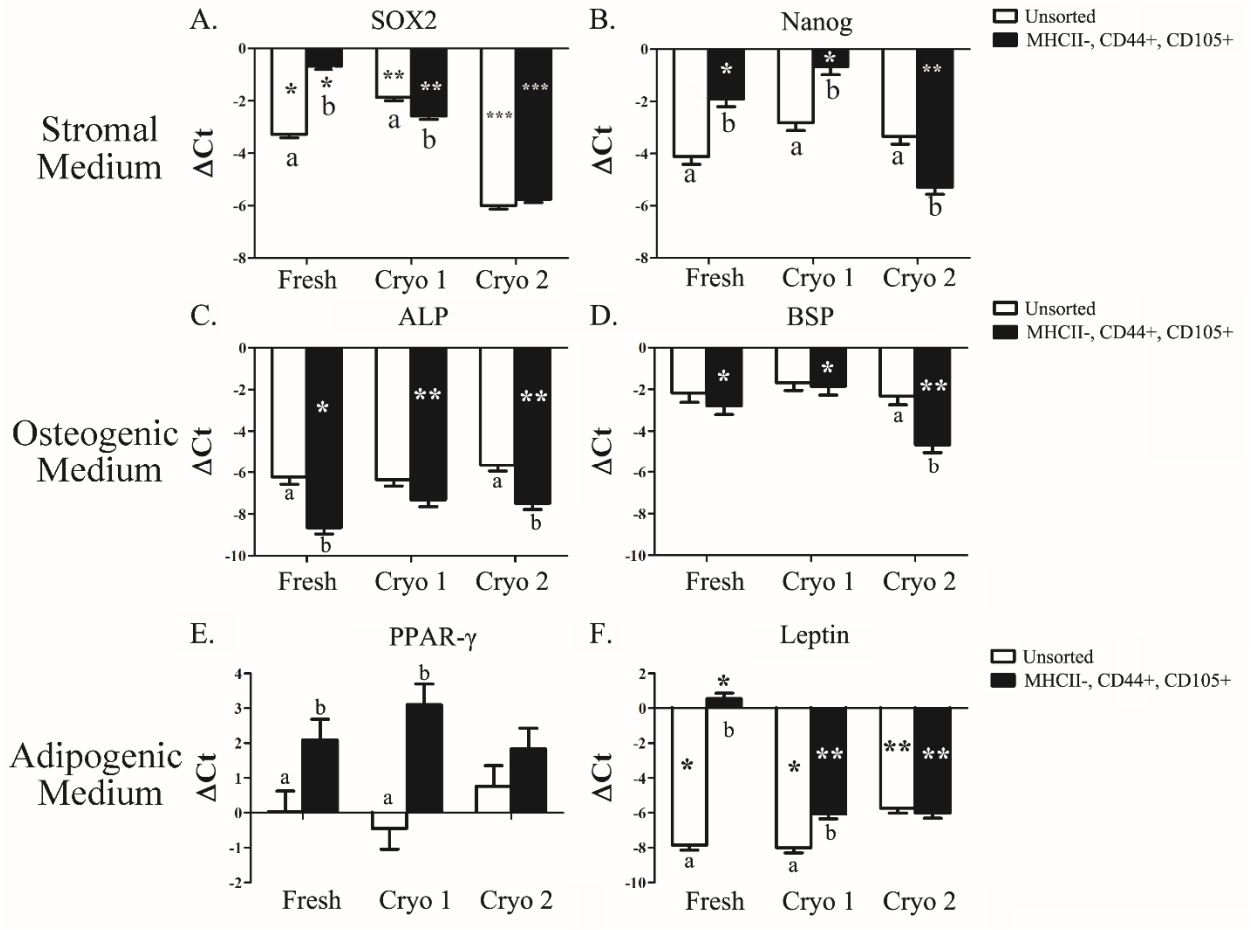

Figure 40. The relative expression (LS mean ± SEM) of stromal (A, B), osteogenic (C, D), and adipogenic (E, F) target gene mRNA levels in the same cell populations as Figure 32. The ΔCt values are reported relative to the reference gene glyceraldehyde 3-phosphate dehydrogenase (GAPDH). Columns within distinct superscripts are significantly different among cell subpopulations within treatments and those with different numbers of asterisks (*) are significantly different among treatments within cell subpopulations ($p<0.05$).

A collagenase digest of 0.1% collagenase type I and 1% BSA has been used to isolate equine ASCs for several years [291]. MSCs are surrounded by a connective tissue matrix with several cell subpopulations including adipocytes, nerve tissue, stromal vascular cells, and immune cells [369]. The commercial collagenase type I widely used in ASC isolation is made up of multiple enzymes like collagenase, proteases, polysaccharidases, and lipase to dissociate the collagen fibers, proteins, polysaccharides, and lipids to release the cells. Higher concentrations are thought to support better tissue digestion, but they also run the risk of more foreign protein residues [358]. The results of this study show comparable ASC isolation with the lower collagenase concentration under identical conditions supporting use of less concentrated collagenase in the digest.

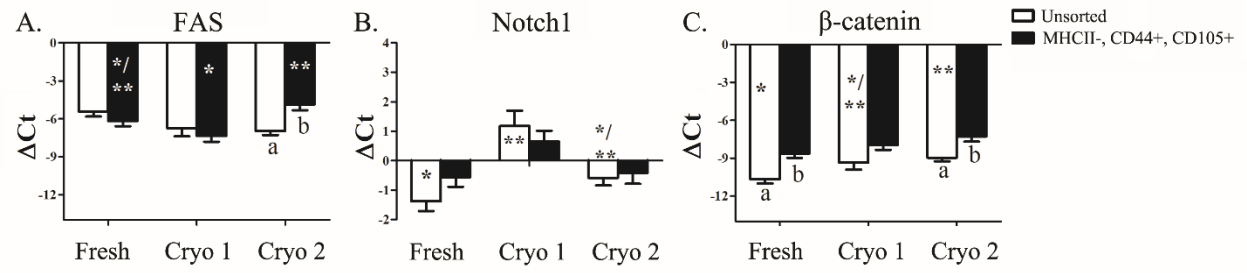

Figure 41. Fas cell surface death receptor (FAS) (A), Notch 1 (B), and β-catenin (C) (LS mean ± SEM) expression in the same cell populations as Figure 33 after 7 days culture in stromal medium. The ΔCt values are reported relative to the reference gene glyceraldehyde 3-phosphate dehydrogenase (GAPDH). The ΔCt values are reported relative to the reference gene glyceraldehyde 3-phosphate dehydrogenase (GAPDH). Columns within distinct superscripts are significantly different among cell subpopulations within treatments and those with different numbers of asterisks (*) are significantly different among treatments within cell subpopulations ($p<0.05$). See Fig. 32 for acronym definitions.

An important findings of this work is the slower proliferation rates of CD44+, CD105+, MHCII+ and MHCII- cells fresh and cryopreserved cells compared to paired, unsorted cells. CD44 and CD105, non-integrin receptors [370], are common stromal cell surface markers [371]. Preadipocyte and endothelial cell subpopulations isolated from human SVF cells have higher proliferation rates compared to the unsorted cells [343, 372]. These cells were unlikely to be present in the populations studies as they do not express CD44 and CD105 [371]. However, the

presence of these cells in unsorted populations could explain the observed higher expansion rates. Cryopreserved cells had lower proliferation rates than the fresh cells regardless of cryopreservation medium similar to previous reports of human and canine ASC [6, 23, 24] while there was few effect on the negative cells, suggesting the negative cells are more stable and predictable than other cell subpopulations in unsorted cells during cryopreservation.

Lower CFU-F and CFU-Ob in cryopreserved cells is consistent with established knowledge in many species including human [23], though results vary among studies from no effect vitro [373]. Another interesting finding in this study is that the osteogenic differentiation in equine unsorted ASCs was not impaired by the cryopreservation in vitro. However, the osteogenesis in negative cells was affected. Several studies demonstrated that the effects of cryopreservation on osteogenesis were limited and the osteogenic capability is impaired in the late passage [6, 25, 85]. However, some conflicting results showed the deleterious effects of cryopreservation on osteogenic differentiation of human ASCs [23]. In the present study, the effects of cryopreservation on negative cells were distinct between the early and late osteogenic genes. ALP serves as the early marker of osteogenic differentiation whereas BSP is characteristic of the terminally differentiated osteoblast [374]. Notably the lower ALP expression in negative cells from Cryo2 treatment suggested the negative cells from cryopreserved cells were more mature especially the cells were cryopreserved in the Cryo2 composed of 5% DMSO. Additionally, the effects of cryopreservation on the negative cells from Cryo1 treatment are distinct to that from Cryo2 treatment, which indicates the osteogenic differentiation was impaired due to higher DMSO concentration in the cryopreservation medium. Overall the adipogenic capability in the negative (MHCII-, CD44+, CD105+) cells was weaker than that in unsorted cells. Since several cell subpopulations resident in the unsorted cells such as pre-adipocyte and hematopoietic

stem/progenitor cells these cell subpopulations also had multipotent capabilities which may contribute to the adipogenic differentiation [75, 371]. Additionally, the differentiation abilities in human pericytes isolated from adipose tissue are greater than their MSC counterparts [375].

Generally, SOX2 was the stemness markers to evaluate the multipotency of MSCs [15, 16], while in some studies SOX2 is involved in human tumor and cancer initiation [376]. We found that cryopreserved cells showed enhanced SOX2 expression level. The enhanced SOX2 expression after cryopreservation may indicate the oncogenic potential in equine ASCs was initialed and enhanced. Some studies demonstrated that the overexpression of SOX2 in porcine bone marrow stem cells (BMSCs) resulted in higher proliferation [9]. However, in another study, the human cryopreserved ASCs showed increased expression of SOX2 after 3 month cryopreservation in the cryopreservation medium (5% DMSO or 10% DMSO in DMEM/Ham F-12 with or without FBS) compared to fresh cells, while their proliferation rate was not affected [15]. In this study, the proliferation rate in the cryopreserved cells was impaired which indicated the effects of SOX2 on ASCs are distinct with other studies may due to the species differences. In fact, the proliferation and differentiation activity of MSCs is mainly affected by other factors, including culture environment and oxygen tension level [15, 16]. Nanog is another transcription factor used to regulate the maintenance of the pluripotent state in adult stem cells [377]. The expression of Nanog is highly controlled in normal human cells while in different types of cancer Nanog has high expression [378, 379]. The expression of Nanog was enhanced in negative cells from cryopreserved cells kept at 5% DMSO may indicate the embryonic potential in the cell subpopulation was enhanced. In short, cryopreserved equine cells maintained their SOX2 and Nanog expression which are considered as the pluripotency genes [376], but the proliferation rate

was hampered. More importantly, the enhanced oncogenic potential in cryopreserved cells also needs to be considered.

In the whole study, the expression of Notch1 and β-catenin was lower in the cryopreserved unsorted cells than that the fresh cells. Lower β-catenin expression in cryopreserved cells may result from the present of DMSO. DMSO as a permeable CP is widely used in MSC cryopreservation [6, 43]. The hydrophobic interactions of DMSO can denature and deactivate vital proteins as well as protect them [50]. β-catenin is an integral structural component of cadherin-based adherens junctions and the imbalance in the structural [380]. The decreased expression of β-catenin may result from the denaturation and deactivation. The Wnt/β-catenin and Notch signaling pathways may contribute to the regulation of stem cell/progenitor cell self-renewal in many tissues [381]. The dysregulation of β-catenin and Notch1 is associated with a number of tumors, including epidermal tumors and T-cell leukaemias [381]. In adult organs, Wnt signaling works as indispensable roles in tissue homeostasis, cell renewal, and regeneration and β-catenin triggers the transcription of Wnt-specific genes responsible for the control of cell fate decisions [380]. After cryopreservation the decreasing expression of β-catenin and Notch1 could result in the fate of cryopreserved cell is out of control and enhance the oncogenic potential in these cells.

FAS (also called CD95 and APO-1) is regulated as the prototypical cell death receptor of the tumor necrosis factor receptor (TNFR) superfamily and initiates apoptosis [382, 383]. The down regulation of FAS has been demonstrated to promote tumor growth and cells are rendered apoptosis resistant [101, 242, 384]. In the present study, the mRNA level of FAS in negative cells from Cryo2 cells was lower than other negative cell subpopulations. In the previous study, FAS ligand expression is rather restricted to the cells of T cell lineage [383] and the FAS-FAS ligand interactions can trigger the cell death by apoptosis [385, 386]. Additionally, the FAS is required

for MSCs therapy by recruitment of T cells [387]. The downregulation of FAS expression can result in reduced multiple cytokines (e.g. monocyte chemoattractant protein-1 (MCP-1), transforming growth factor-β (TGF-β)) secretion, and fail to upregulate the levels of Tregs and induce T cell apoptosis in human bone marrow mesenchymal stem cells (BMMSCs) [387]. The present results suggest the negative cells (MHCII-, CD44+, CD105+) from Cryo2 cells had the relative low risk to be recognized by the immune system and low diminished apoptotic potential.

Overall, based on the results in the present study, we found that negative cells (MHCII-, CD44+, CD105+) from the ASCs isolated from equine subcutaneous adipose tissue have more predictable in vitro behaviors compared to the unsorted cells. As the current knowledge, ASCs are composed of several cell populations, including endothelial cells, preadipocytes, pericytes and other cells [75, 332, 363]. The percentages of these cell populations are variable due to individual characteristics [75]. Therefore, selected negative cells from the heterogeneous population may provide a predictable cell population and cryopreservation enhanced osteogenesis in the negative cells. Additionally, the embryonic potential may be enhanced in the negative cells after cryopreservation and the risk of apoptosis is lower than other cell populations, especially 5% DMSO was employed, which indicated 5% DMSO is recommended for the equine ASC cryopreservation. The oncogene expression (Notch1 and β-catenin) in negative cells is more stable than unsorted cells regardless of cryopreservation medium.

As a whole, the results from this in vitro study showed that lower collagenase concentration (0.05%) is recommended for equine ASC isolation. More important findings in the present study is the selected specific cell subpopulation from a heterogeneous population based on cell immunophenotype profile can provide predictable and stable in vitro cell properties. To reduce the cytotoxicity of cytoprotectants and retain embryonic potential, 5% DMSO for the

cryopreservation of equine ASCs is recommended. Further, the relationship of tumor development and cryopreserved cells in genetic levels must be confirmed before the cryopreserved cells are used in clinical trials.

CHAPTER 6. FELINE ADIPOSE DERIVED MULTIPOTENT STROMAL CELLS HAVE TRANSDIFFERENTIATION ABILITY TO FORM FUNCTIONAL ISLET-LIKE CELL CLUSTERS

6.1. Introduction

Diabetes mellitus is one of the most prevalent feline endocrinopathies, and about 15-20% of feline diabetes cases are caused by decreased β-cell numbers or insulin resistance [308, 320, 388, 389]. The condition affects all breeds and sexes and is associated with reproductive sterilization [390, 391], obesity, physical inactivity [392], and advancing age [393] and drug side effects [308, 320, 388]. To date, no single cause or effective cure has been identified. Serious complications associated with unregulated glucose levels include increased bone fractures [394], cardiovascular disease [395], and neurological dysfunction [396], among others. Contemporary treatment consists of diet and weight management with exogenous insulin administration to replace that normally produced by pancreatic β cells [397]. Available insulin formulations do not share the feline amino acid sequence. Though insulin maintains biological activity across species, sequence differences may affect activity and stimulate the immune system [398, 399]. Additionally, insulin administration must be customized for individual patients, a challenging and time-consuming process. The time and costs associated with establishing and revising insulin therapy and daily injections can be a burden on the owners.

Due to their ability to differentiate into multiple tissues from the same embryonic layer [85, 400, 401], adult multipotent stromal cells (MSC) are increasing in popularity to restore issues lost to trauma or disease. Current knowledge also supports the additional ability of MSCs to "transdifferentiate" into tissues that originate from other embryonic layers [402-404]. A contemporary example of transdifferentiation is the differentiation of adipose-derived multipotent stromal cells (ASCs) of mesodermal lineage into insulin producing cells (IPCs) of endodermal

lineage. This has been accomplished in several species [106, 108, 404, 405], and creates an opportunity to restore natural dynamic glucose regulation provided by β-cells without the morbidity and potential complications of pancreatic tissue transplants [406, 407].

A mechanism to isolate specific ASC immunophenotypes from adipose tissues removed with reproductive organs during routine feline sterilization procedures was recently developed in our laboratory [85]. This study was designed to quantify the transdifferentiation capability of feline ASCs isolated from the reproductive organs. The tested hypothesis was that fresh feline ASCs cultured in pancreatic β cell induction medium had better insulin production and glucose response compared to that cultured in stromal medium.

6.2. Materials and Methods

6.2.1. Study design

Feline ASCs were isolated by the method developed in our published study from adipose tissue removed during routine sterilization of 8 male and 8 female adult cats [85]. For the purposes of this study, the stromal vascular fraction was the primary cell isolate, and passage (P) 0 was the first cell passage. Fresh cells were expanded to P3 and then paired samples were cultured in stromal or three-step islet cell induction medium. The zinc concentration, insulin production, and ultrastructure was compared between stromal cells and the induced cells from stage 3. Multipotent capacity and lineage specific gene expression (insulin, NK6 homeobox 1 (NK6.1), proto-oncogene tyrosine-protein kinase ROS1 (ROS1), somatostatin (STS), ISL LIM homeobox 1 (Isl1), glucagon (GCG), paired box 6 (Pax6), AKT serine/threonine kinase 1 (AKT1), Ras-related protein Rab-2A (RAB2A), hexokinase 1 (HK1), and glucose transporter 2 (Glut2)) was compared between culture conditions in male and female donors. All materials and reagents were from Sigma-Aldrich, St. Louis, MO unless otherwise noted.

6.2.2. Cell Isolation

Adipose tissues were harvested from reproductive organs removed for elective sterilization and cells were isolated as published with minor modifications [85]. Tissue was minced and digested with 0.3% type I collagenase (Worthington Biochemical Corporation, Lakewood, NJ) in Kreb's Ringer buffer (KRB) for 30 minutes, 1,000 rpm stirring with a stir bar at 37oC. After filtering (100 μm nylon cell strainers, BD Falcon, Bedford, MA) and centrifugation (260 × g, 5 min), the resulting SVF pellets were resuspended in 5 ml red blood cell lysis buffer (0.16 mol/L NH4Cl, 0.01 mol/L KHCO3, 0.01% ethylenediaminetetraacetic acid (EDTA)) for 5 min. The SVF was collected after centrifugation (260 × g, 5min) and seeded in 10-mm cell culture dishes in stromal medium (Dulbecco's modified Eagle's medium F-12 (DMEM/F-12, Hyclone, Logan, UT), 1% antibiotic/antimycotic solution (MP Biomedical, Irvine, CA), 10% fetal bovine serum (FBS, Hyclone)). Stromal medium was refreshed after 24 hours and then every 3 days. After 70-80% confluence, the SVF cells were detached with 0.05% trypsin (Hyclone) and cells were seeded in T75 flasks with the density of 5 ×103 cells/cm2 for P0 and all subsequent passages. Procedures performed at temperatures other than room temperature are indicated.

6.2.3. Multipotentiality

To confirm multipotentiality, P1 fibroblastic colony formation and adipogenic and osteogenic differentiation tested cell isolates. For fibroblastic colony formation, P1 cells were cultured in stromal medium for 7 days, fixed with 4% formalin, and stained with 0.1% toluidine blue. To assess adipogenesis, cells were cultured in stromal medium to 70-80% confluence, washed with phosphate buffered saline (PBS, Hyclone) and then cultured in adipogenic medium (Table 12) for 10 days. They were then fixed with 4% neutral paraformaldehyde (PFA) and stained with oil red O. For osteogenesis, the cells were cultured in stromal medium as above the then in osteogenic

preinduction medium for 10 days followed by osteogenic induction medium (Table 18) for another 10 days. Colonies were fixed with 70% ice cold ethanol and stained with 2% alizarin red.

6.2.4. Differentiation of feline ASCs into IPCs.

Cell isolates were culture expanded to P3. At 70-80% confluence, they were seeded in 6-well ultralow attachment plates (Corning, Corning, NY) at 1×10^6 cells/well and cultured for 7 days in stromal medium. A three-stage protocol was used to induce β-cell islet-like clusters (Table 12). The cells in ultralow attachment plates were incubated in serum free medium (SFM) 1 for 2 days as stage 1 and then in SFM 2 for another 6 days as stage 2. Cells were then manually transferred to a standard 6-well plate (Thermo Fisher Scientific, Waltham, MA, USA) culture in stage 3 induction medium for another 4 days. All media were refreshed every 2 days. Paired cells were cultured in stromal medium in standard 6 well plates throughout the induction process.

6.2.5. Dithizone Staining – Zinc Concentration

Following the induction process, cells were incubated with dithizone (DTZ, Fisher Scientific, Fairlawn, NJ) solution (10 µl DTZ working solution (1 mg/ml in dimethyl sulfoxide (Fisher Scientific)) in 1 ml of the culture medium) for 30 min at 37 ^{o}C. Cells were washed in PBS after incubation and imaged with light microscope.

6.2.6. Immunohistochemistry – Intra-cellular Insulin

The Dylight 633 antibody labeling kit (Thermo Fisher Scientific, Somerset, NJ) was used to label the antibody goat anti insulin according to the manufacturer's induction. Briefly, 100 µl antibody solution (1 mg/ml) was mixed with 8 µl supplied borate buffer and the mixture was incubated with Dylight Reagent for 60 min protected from light. The labeling reaction was mixed with resin and then centrifuged (1000 × g, 1 min) to collect the labeled antibody.

Table 12. Composition of induction medium for differentiation

Medium	Composition
Adipogenic medium	Minimum essential medium alpha (α-MEM), 10% rabbit serum, 10% FBS, 10nM dexamethasone, 5 μg/ml insulin, 50 μM 5,8,11,14-eicosatetraynoic acid (ETYA, Cayman, Ann Arbor, MI), 100 μM indomethacin
Osteogenic medium	Osteogeinc pre-induction: DMEM, 10% FBS, 100 nM dexamethasone, 0.25 mM L-ascorbic acid;Osteogenic induction medium: osteogenic preinduction medium supplemented with 10 mM β-glycerophosphate
β-cell induction medium	Stage 1: SFM 1 (2 days): DMEM, 17.5mM glucose, 1% BSA (bovine serum albumin), 1× insulin-transferrin-selenium (ITS, Gibco BRL, Gaithersburg, MD), 4nM activin A (R&D Systems Inc., Minneapolis), 1 mM sodium butyrate, 50 μM 2-mercapethanol, 1% N-2 supplement (R&D Systems Inc.), 1% B-27 supplement (Gibco), 5 μg/ml laminin (Corning), 50 ng/ml recombinant human hepatocyte growth factor (HGF, EMD Millipore, Temecula, CA), 20ng/ml basic fibroblast growth factor (bFGF, Gibco); Stage 2: SFM 2 (2 days): DMEM, 17.5mM glucose, 1% BSA, 1 × ITS, 0.3mM taurine (ACROS Organics, Morris Plains, NJ), 5 μg/ml laminin, 20 ng/ml bFGF, 1% N-2 supplement, 1% B-27 supplement, 50 ng/ml HGF; Stage 3: SFM 3 (2 days): DMEM, 17.5 mM glucose, 1.5% BSA, 1.5 × ITS, 3 mM taurine, 100 nM glucagon-like peptide 1 (GLP-1, TOCRIS bioscience, Ellisville, MO), 1 mM nicotinamide (ACROS Organics), 1 × non-essential amino acids (NEAA, Gibco), 10 nM pentagastrin (TOCRIS bioscience), 1% N-2 supplement, 1% B-27 supplement, 50ng/ml HGF, 20ng/ml bFGF, 5 μg/ml laminin, 10 ng/ml betacellulin (R&D Systems)

Cells were washed with PBS and fixed overnight in 4% neutral PFA. They were permeabilized with 0.5% Triton X-100 in PBS and then incubated with the labeled antibody goat anti insulin (1:200 in PBS, Santa Cruz Technologies, CA) for 30 min. After incubation, the cells were washed with PBS and then cytoskeletal actins was stained with β actin-FITC for 30 min (1: 500 in PBS, Neomarkers, Fremont, CA). Photomicrographs were obtained for all labeled cells with confocal laser scanning microscopy (CLSM, Leica TCS SP2, Leica, Wetzlar, Germany).

6.2.7. Glucose Challenge Assay – Glucose Sensitivity

The induced islet-like cell clusters were collected and washed twice with PBS. The islet-like cell clusters were incubated with KRB buffer for 1 hour at 37^{o}C,followed by incubation with KRB buffer supplemented with different glucose concentrations (25 and 55 mM) for 30 min at 37^{o}C. Following incubation, the medium was collected and stored at -80^{o}C until further use. The stored medium was analyzed for insulin content using a feline specific enzyme-linked immunosorbent assay (ELISA) kit (Mybiosource, San Diego, CA). The cells cultured in stromal medium were used as a control.

6.2.8. Transmission Electron Microscopy – Ultrastructure

Following a PBS rinse, cells were fixed in 2% PFA and 2.5% glutaraldehyde in 0.1 M PBS for 10 min. The samples were centrifuged (350 × g, 5 min) and then fixed with fresh fixative with gentle agitation for 2 hours. They were mixed with equal amounts of 3% agarose and the mixture was placed to a glass slide. When the mixture solidified, it was sliced into cubes. The cubes were washed with 0.1 M PBS and 0.08M glycine 5 times (15 min/time) followed by incubation with 2% osmium tetroxide in 0.1 M PBS in the darkness for 1 hour to fix the cells. The samples were washed with H_2O and dehydrated in a series of ethanol-distilled water solutions. The dehydrated samples were infiltrated with 1:1 ethanol and LR white resin for 2 hours, and then infiltrated with

100% LR white resin for another 2 hours. Embedded samples were placed into the bottom of a beem capsule and incubated in an 18 ºC oven for 24 hours. Ultra-thin sections (90 nm) were cut and stained with 2% uranyl acetate and lead citrate. Some sections were directly evaluated with transmission electron microscopy (JEOL JEM-1400, Japan). The other sections were blocked in 5% BSA in PBS for 30 min and then incubated with goat anti insulin in 0.1% BSA in PBS (1:20) for another 90 min. After incubation, the sections were washed in 0.1% BSA in PBS 6 times (5 min/time) and then incubated in secondary antibody (rabbit anti goat IgG-Gold, Sigma-Aldrich) in 0.1% BSA in PBS for another 90 min. After incubation, the sections were washed with 0.1% BSA buffer and PBS, respectively. The sections were then fixed in 2% glutaraldehyde in PBS for 5 min and contrasted with 2% uranyl acetate and lead citrate after being thoroughly washed in distilled water. Gold labeled sections were observed with TEM

6.2.9. Scanning Electron Microscopy – Surface Ultrastructure

Cells were collected by filtration and fixed in 2% PFA and 2% glutaraldehyde in 0.1 M PBS for 15 min. The solution was extracted into a 10 ml syringe with a Swinney filter holder fitted with a 2 μm pore polycarbonate with 13 mm diameter. Entrapped cells on the filtered were fixed as before another 15 min and then rinsed with 0.1 M PBS and distilled water. The filter was removed from the syringe and dried with hexamethyldisilazane (HMDS, Electron Microscopy Sciences, Fort Washington, PA) for 30 min, 1:1 100% ethanol and HDMS, and 2 changes for 30 min each with 100% HDMS. Finally the HDMS was removed and the samples were placed in a hood overnight to air-dry. The dried samples were mounted onto aluminum SEM stubs, coated with platinum in an EMS 550X sputter coater and imaged with JSM-6610 High vacuum mode SEM (JEOL Ltd., Japan).

6.2.10. RT-PCR – Gene Expression

Total RNA was isolated from cells harvested from each induction stage (EZNA® MicroElute Total RNA kit, Omega, Bio-Tek, Norcross, GA). The quality and concentration was determined spectrophotometrically (NanoDrop ND-1000; NanoDrop Technologies, Wilmington, DE), and cDNA synthesized (Maxima First-Strand cDNA synthesis kit, Thermo Scientific, Waltham, MA). Feline pancreatic target gene levels (insulin, Isl1, HK1, Glut-2, NK6.1, ROS1, STS, GCG, Pax6, AKT1, and RAB2A) (Table 13 &14) were quantified with real-time RT-PCR using the Thermo Fisher Absolute^{TM} Blue QPCR Rox Mix technology and an ABI Prism 7900 HT Sequence Detection System (Applied Biosystems, Foster City, CA) using feline-specific primers. The ΔCt values were determined relative to the reference gene β-actin.

6.2.11. Statistical Analysis

All results are presented as least squares (LS) mean ± SEM. Statistical analyses were performed with the JMP statistical package (v 13.0.0, SAS Institute Cary, NC). Mixed ANOVA models were used to evaluate insulin levels between glucose concentrations within genders and between genders within glucose concentrations. The same models were used to evaluate target gene expression among induction stages within genders and between genders within induction stages. Tukey's post hoc tests were applied for multiple group comparisons ($p<0.05$).

6.3. Results

6.3.1. Multipotentiality

All cell isolates displayed osteogenic and adipogenic differentiation based on histochemical staining. Cells had a fibroblastic shape when cultured in stromal medium (Fig. 42A). Colony calcium stained with alizarin red following culture in osteogenic medium (Fig. 42B), and lipid droplets stained with oil red O after adipogenic medium culture (Fig. 42C).

Table 13. Insulin specific primer sequences

Lineage	Primer	Sequences	Accession No.
Housekeeping	β-actin	F: AGCCTTCCTTCCTGGGTATG R:ACAGCACCGTGTTAGCGTAG	XM_006941899.3
Transcription Factor	Nkx 6.1	F: AACGAAATACTTGGCGG R:CCAGAGGCTTGTTGTAGTCG	XM_019829291.1
	Pax6	F: GGCAATCGGTGGTAGTAA R: CTTGGTATGTTATCGTTGG	XM_019812231.1
	Isl 1	F: CAAGGACAAGAAGCGGAG R: CTGGGTTTGCCTGTAAGC	XM_003981424.3
	Glut 2	F: TTGGCTTGGATGAGTTACG R: GACTTTCCTTTGGTTTCCG	XM_003991916.3
Protein	Insulin	F: CTTCGTCAACCAGCACC R: ACAGCATTGCTCCACGA	XM_019811180.1
	Glucagon	F: TGAACACCAAGAGGAACAA R: ACCAGCCAAGCAATGAAT	XM_006935320.2
	Somatostatin	F: CCAGACAGAGAACGATGCC R: CAGGGTTTGAGTTAGTGGA	XM_003991805.4

6.3.2. Cell Morphology

All cells cultured in ultralow attachment plates formed cell clusters. Following transfer to a standard six well culture plate, cells cultured in stromal medium attached to the plate in colony

formation within 24 hours (Fig. 43A). The vast majority of those cultured in induction medium did not attach at any point and remained as detached cell clusters (Fig. 43 B and C).

Table 14. Insulinoma primer sequences

Lineage	Primer	Sequences	Accession No.
Oncogene	ROS1	F:AACAACAGCCTCTACTACAG R: TATCCTCCGACCGAATCC	XM_019831130.1
	Akt1	F: CCAACACCTTCATCATCCG R: CCATCATTTCCTCCTCCTG	NM_001322435.1
	RAB2A	F: ACAGACAAGAGGTTTCAGC R: TATGACCGTGTGATGGAAC	XM_019822712.1
	HK1	F: TGAGAAGATGGTGAGTGGC R: GGCAGAGCGAAATGAGAC	XM_006937834.3

6.2.3. Dithizone Staining – Zinc Concentration

The cells cultured in induction medium formed clusters that stained DTZ, confirming zinc accumulation (Fig. 44B, C), and those cultured in stromal medium did not stain (Fig. 44A). As before, cells cultured in stromal medium attached to standard culture ware while those cultured in induction medium did not (Fig. 44A).

6.2.4. Immunohistochemistry

The cells cultured in stromal medium lacked insulin expression, while the cells cultured in induction medium had strong insulin expression (Fig. 45).

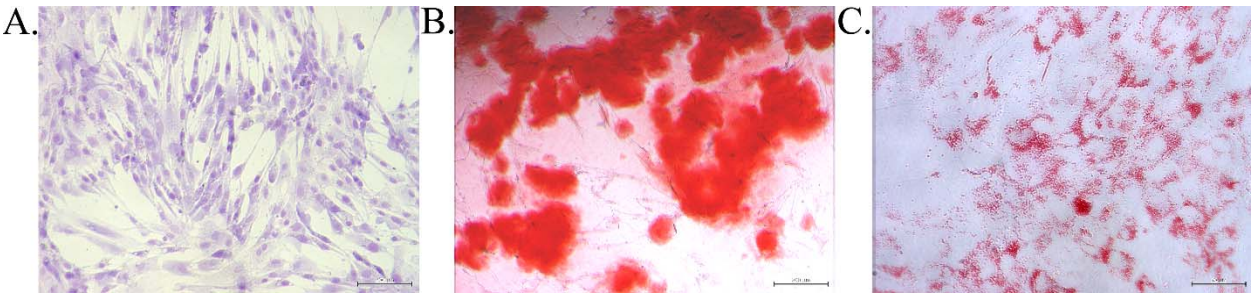

Figure 42. Photomicrographs of feline ASCs following culture in stromal medium A, 5 ×, scale bar = 500 μm; with alizarin red staining of calcium deposition after cultured in osteogenic medium B, 5×, scale bar=500μm; with oil red O lipid staining after culture in adipogenic medium C 40×, scale bar = 50 μm.

Figure 43. Light photomicrographs of fresh feline P3 ASCs from male (A, B) and female (C) after culture in stromal (A), pancreatic β-cell induction (B, C) medium and transferred to the normal culture plate. 5× magnification. Scale bar=500 μm.

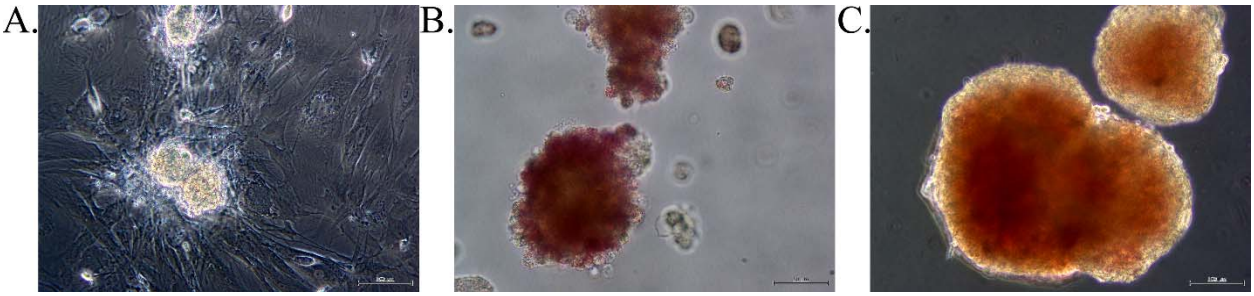

Figure 44. Light photomicrographs of fresh P3 feline ASCs from males (A, B) and females (C) after culture in stromal (A) or pancreatic β-cell induction (B, C) medium. Dithizone staining of zinc. 20 × magnification, scale bar = 100 μm (A, B); 40× magnification, scale bar = 50 μm.

6.2.5. Glucose Challenge Assay

Male and female ASCs cultured in induction medium released insulin in response to glucose (Fig. 46). Insulin secretion was slightly higher (55.7 versus 62.7) at the higher glucose concentration.

6.2.6. Transmission Electron Microscopy – Ultrastructure

Cell ultrastructure was distinct between cells cultured in stromal versus induction medium. Notable differences were the presence abundant perinuclear mitochondria in the cells cultured in stromal medium (Fig. 47A) and secretory granules in the induced cells (Fig. 47B).

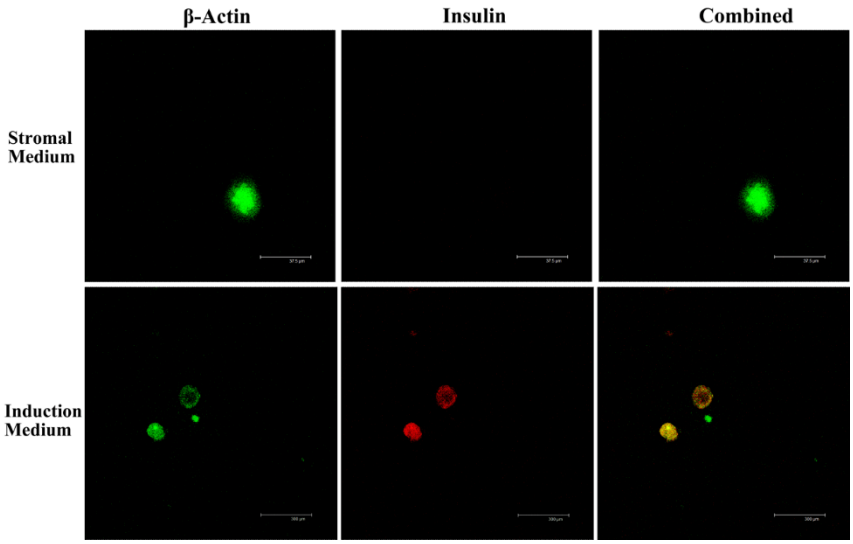

Figure 45. Fluorescent photomicrographs of cells cultured in stromal or induction medium and labeled with antibodies against insulin (red) and actin (blue).

6.2.7. Electroimmunohistochemistry – Insulin Localization

Insulin labeling was localized to the cytoplasm of cells cultured in induction medium, while there was no labeling in those cultured in stromal medium (Fig. 48).

6.2.8. Scanning Electron Microscopy – Surface Ultrastructure

Cells cultured in stromal medium tended to form loose, spherical clusters while those in β cell induction medium formed larger, highly organized clusters with an irregular shape (Fig. 49). Proteinaceous material was apparent on the surface of differentiated cell clusters (Fig. 49B).

6.2.9. Gene Expression

Transcription factor expression: The mRNA levels of transcription factors (Nkx 6.1, Pax6, Isl1, and Glut-2) at Stage 1 tended to be lower than other induction stages (Fig. 50). The mRNA levels

of Pax6 and Glut2 in female samples had lower expression than male at induction stages 1 and 2 and induction stage 1, respectively (Fig. 50B and D).

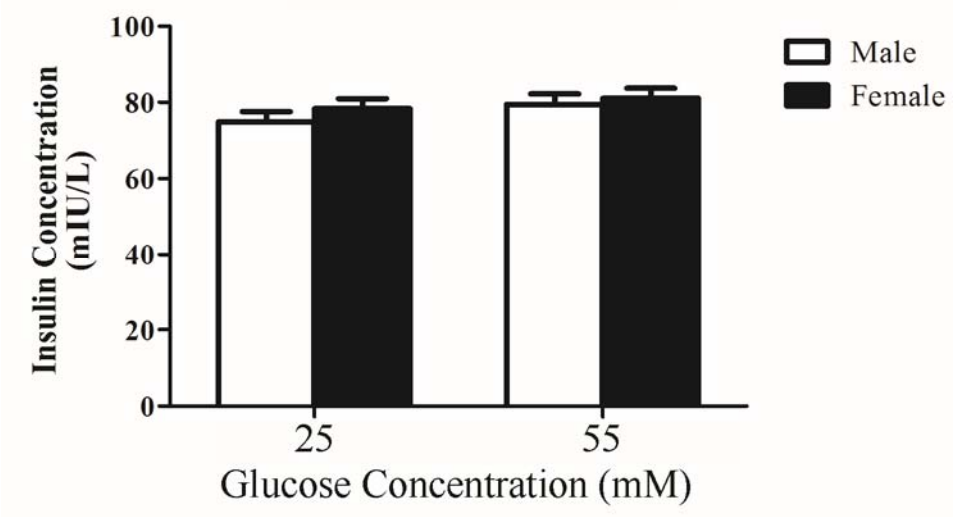

Figure 46. Glucose challenge assay. The insulin secretion from differentiated islet-like cell clusters at stimulated (25 and 55 mM) concentrations of glucose are illustrated.

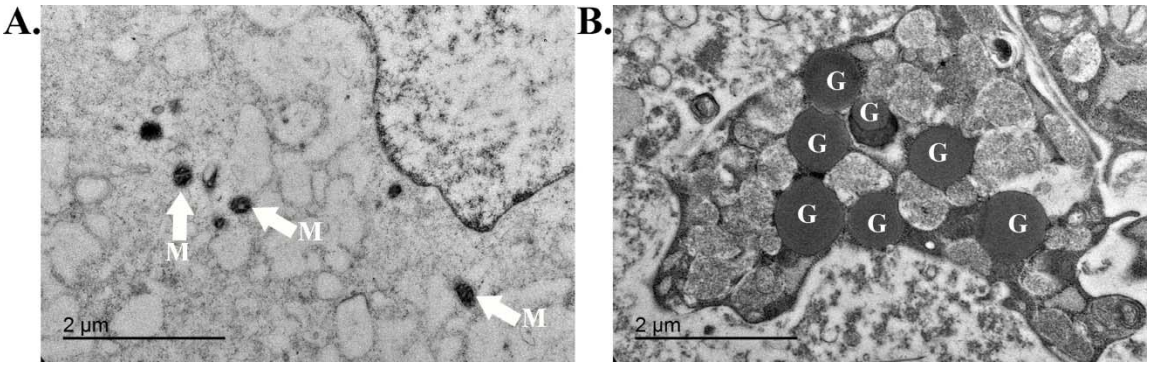

Figure 47. Transmission electron photomicrographs of feline ASCs culture in stromal (A) or induction (B) medium. Legend: M – mitochondria, G – secretory granules. Scale bar = 2 µm.

Pancreatic β-cell target gene expression: Insulin expression detectable only after stage 2 and 3 induction (Fig. 51 A). Glucagon expression was higher after stage 3 induction versus the other stages (Fig. 51 B). Somatostatin levels were lower after stage 1 induction compared to the others (Fig 51 C).

Oncogene expression: There was no difference in ROS1, AKT1, RAB2A, or HK1 expression among induction stages (Fig. 51).

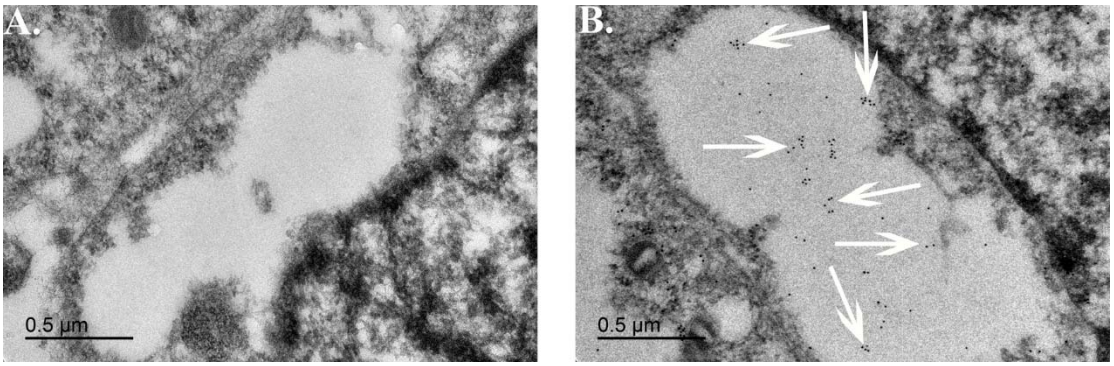

Figure 48. Transmission electron photomicrographs demonstrating insulin labeled with anti-insulin antibodies (arrows) in feline ASCs cultured in stromal (A) or induction (B) medium. Scale bar = 0.5 µm.

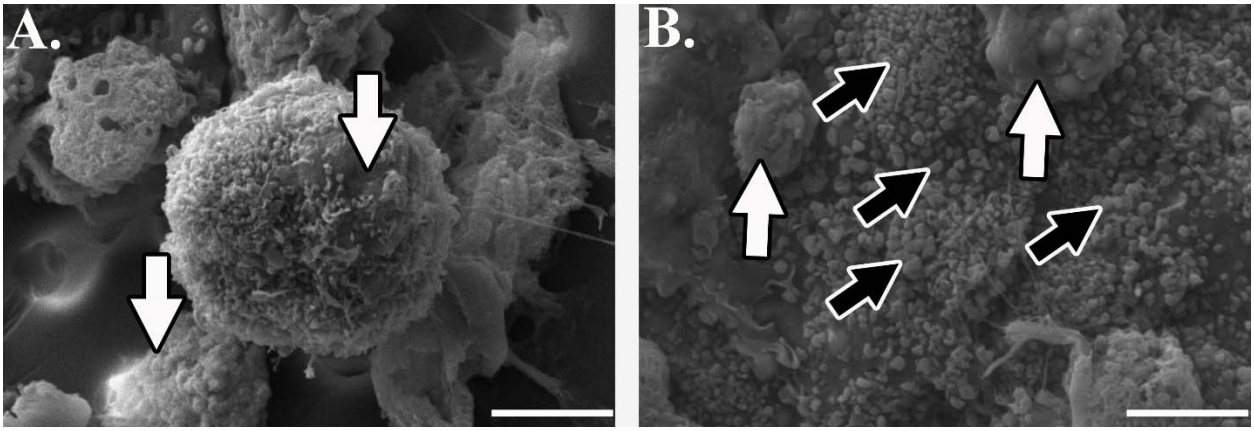

Figure 49. Scanning electron photomicrographs feline ASCs cultured in stromal (A) or β cell induction (B) displaying cell cluster morphology (white arrows) and proteinaceous material on the surface of clusters cultured in induction medium (black arrows). Scale bar = 5 µm.

6.3. Discussion

The overarching conclusions from the present study are that feline ASCs isolated from the reproductive organs have endodermal transdifferentiation capability, but cells from male donors have distinct morphology compared to female donors. Induced cells appear to form functional clusters based on zinc accumulation secretion of insulin in response to glucose stimulation, the presence of intracellular insulin, and the pancreatic β-cell specific gene expression [408]. This promising achievement significantly advances the potential to produce custom feline insulin for

exogenous administrations as well as a cell-based therapy for temporary or long term restoration of feline pancreatic β cell function.

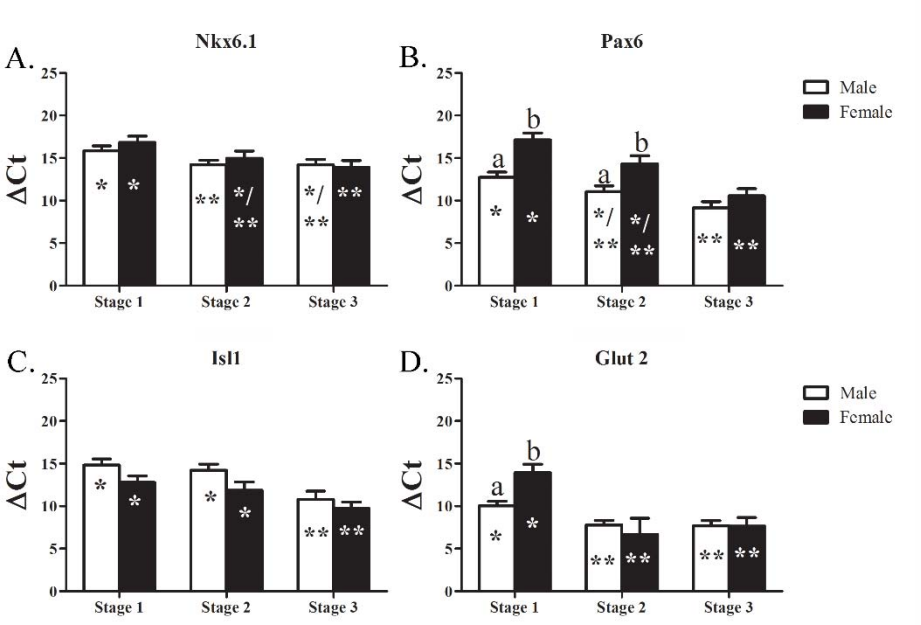

Figure 50. Feline NK6 homeobox 1 (A; NK6.1), paired box 6 (B; Pax6), ISL LIM homeobox 1 (C; Isl1), and glucose transporter 2 (D; Glut2) levels (LS mean ± SEM) in feline ASCs following three induction stages of pancreatic β cell culture induction. Columns with distinct superscripts are significantly different between sex within stages. Different asterisk numbers (*) are significantly different among stages within gender.

The culture protocols used in this study were customized for feline cells and designed to replicate in vivo pancreatic formation and development. Giving species differences, culture methods are most effective when designed for the target species [104, 403, 405, 409]. In the developed three-stage induction system, N-2 and B-27 were intended to enhance proliferation and apoptosis and protect against reactive oxygen species in the absence of FBS [404, 410, 411]. FBS is the common supply in culture medium and it can provide growth factors, nutrients and hormones for cell proliferation and adhesion [47, 315]. Additionally, there are several extrinsic factors used in the system that have beneficial effects on differentiation of MSCs into insulin producing cells [123].

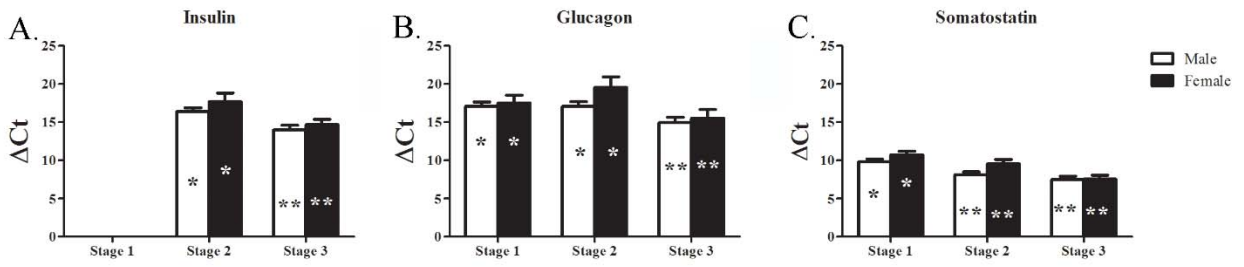

Figure 51. Feline insulin (A), glucagon (B), and somatostatin (C) levels (LS mean ± SEM) in feline ASCs following three stages of pancreatic β cell culture induction. Columns with different asterisk numbers (*) are significantly different among stages within gender.

In detail, at Stage 1 using activin A and sodium butyrate to direct ASCs to undergo endoderm differentiation [409]. ITS, 2-mercaptoethanol, and the supplements can protect ASCs and reduce the risk of apoptosis [409, 412]. The ultra-attachment culture plate used in the present study can enhance cells to form three-dimensional aggregates. The aim of Stage 2 was to induce the endoderm cell clusters formed at Stage 1 into pancreatic endodermal lineage. Taurine was induced into the induction medium and is essential for the development of functional β cells [409]. In the induction process, we found the induced cell clusters performed similar morphology of induced β-cell cluster morphology from other species [411] and lose the capacity to attach to the plastic culture ware which is widely used as one of criteria to define MSC [413]. Cells cultured in stromal medium retain their plastic affinity after culture on ultralow normal culture plates while those in induction medium did not, further confirming differentiation and maturation.

At the final stage, the cell clusters were converted into functional pancreatic hormone-expressing islet-like cell aggregates with the help of GLP-1, nicotinamide, taurine, and β-cellulin. Nicotinamide was reported that it can promote the maturation of precursor cells into insulin-producing cells and increase the rate of proinsulin biosynthesis [414]. Addition of β-cellulin and nicotinamide to the Stage 3 induction medium was to promote β cell maturation and generate cells expressing endocrine hormones including insulin and glucagon [123]. At the final stage, the

induced cell clusters were specifically labeled with the zinc-chelating dye DTZ, which could stain β-cells due to the presence of zinc in insulin-containing secretory granules [408]. Immunofluorescence, DTZ staining, and immune electron microscopy results further confirmed that the induced cells had insulin expression. The RT-PCR studies showed that the induced cells coexpressed insulin, glucagon, and somatostatin. These results are in accordance with normal pancreatic development, in which immature islets are known to coexpress pancreatic hormones [409, 415].

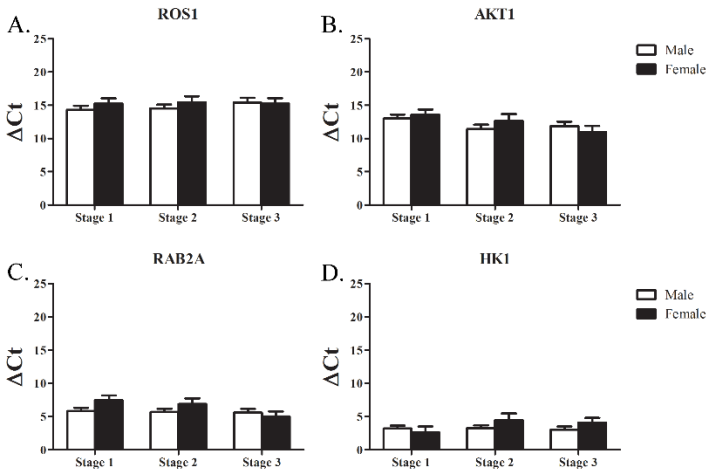

Figure 52. Feline proto-oncogene tyrosine-protein kinase ROS1 (A; ROS1), AKT serine/threonine kinase 1 (B; AKT1), Ras-related protein Rab-2A (C; RAB2A), and hexokinase 1 (D; HK1) levels (LS mean ± SEM) in feline ASCs following three stages of pancreatic β cell culture induction.

Another interesting finding in this study is the mRNA levels of Pax6 and Glut2 differences between male and female ASCs at the early induction stage, suggesting that the cells from male cats may have higher sensitivity than that from female cats. Based on the current reports, human male ASCs have greater osteogenic potential than that female ASCs [416]. Pax6 is the necessary transcription factor that can transactivate the insulin promoters [417]. The higher expression of Pax6 in male ASCs at the early induction stages may indicate that the male ASCs are easier to initiate pancreatic β cell differentiation.

As a whole, from the results obtained, male and female ASCs were proven to have endodermal transdifferentiation capability. The induced cell clusters can secrete insulin under the glucose stimulation. In the clinical context, our present study demonstrated the potential for stem cell-based therapy to treat feline diabetes. Although the mechanisms of the transdifferentiation in feline ASCs are not clear and the pancreatic specific transcription factor expression is still need more evaluation, the current induction can provide a powerful base for future evaluation. The results presented in this study can provide direct evidence supporting the notion that transdifferentiation of feline ASCs to functional insulin-producing cells may represent a viable therapeutic option for feline diabetes.

CHAPTER 7. CONCLUSIONS AND FURTHER STUDIES

This dissertation is focused on the evaluation of the effects of cryopreservation, and physical and chemical environments on adult adipose derived mesenchymal stromal cells (ASCs) from different species. Overall, the therapeutic applications of ASCs in veterinary medicine are in the early stage of development. Even though there are many commercial ASC-based products for dogs, cats, and horses around the world, these applications are not approved by the U.S Food and Drug Administration (FDA). Numerous studies have focused on the characterization of cryopreserved ASCs from several species, while the conflicting results are also reported or the published results are variable. Therefore, more investigations are necessary in the field of ASCs before they are applied in clinical trials. Major contributions of the studies described in this dissertation are the evaluation of cryopreservation effects on ASCs from different species in genetic, protein and ultrastructure levels. Additionally, it is the first time we demonstrated that feline ASCs also have transdifferentiation capability to form functional islet-cell clusters.

The first and third parts in this dissertation, the cryopreservation effects on ASCs isolated from canine and equine adipose tissues were evaluated in ultrastructure, genetic and protein levels. Based on our findings, we found that even though the same cryopreservation technique and cryopreservation medium were employed, cryopreserved ASCs had distinct in vitro properties due to various species different. These findings suggest that the cryopreservation medium designing should be considered the individual characteristics. In the fifth chapter in this dissertation, the cells were selected from the heterogeneous cell population isolated from equine adipose tissue based on the common ASC immunoprofile expression. In this chapter, we found that the selected cell subpopulation was more stable and predictable compared to the unsorted heterogeneous cell population and the embryonic gene expression was enhanced in the selected cell subpopulation

after cryopreservation. Results of the study showed that the heterogeneous cell population isolated from the equine adipose tissue has unpredictable cell properties. Therefore, to purify and select desired cell subpopulation via the immunoprofile expression is necessary for the predictable outcomes. Nevertheless, we also found that the selected cell subpopulation had lower proliferation rate, suggesting the other cell subpopulations in the heterogeneous cell population may make the contribution to the in vitro proliferation. Therefore, the contributions from the other cell subpopulations and environments to the selected cell subpopulation proliferation need to be studied in the future.

Cryopreserved human ASCs were loaded into three commercial bone scaffolds via a spinner flask bioreactor system and then cultured in stromal, osteogenic, or osteogenic for 48 hours followed by stromal culture medium up to 28 days. The results from in vitro human ASC osteogenic study showed that continuous culture in osteogenic medium supports the best human ASC osteogenesis on bone-graft scaffolds. The results from the study demonstrated that the distinct bone graft components may direct human ASCs toward different osteogenic pathways. This work confirms the need to consider individual patient characteristics during the bone graft selection for the greatest treatment outcomes.

In the third part of the dissertation cryopreserved equine ASC and bone marrow mesenchymal stromal cells (BMSCs) were used for equine bone tissue regeneration. It is possible that scaffold component modification can promote bone augment. For the study, custom scaffolds were synthesized, and cryopreserved equine ASCs and BMSCs were loaded onto the scaffolds via the spinner flask bioreactor and then implanted subcutaneously in athymic mice in the absence of osteogenic supplements for up to 9 weeks. De novo bone formation was confirmed and the contributions of exogenous and host MSCs were demonstrated. Also, the mineral containing

scaffolds showed superior osteogenic support versus polymer alone. This work emphasizes the necessity of mineral components in customized osteogenic scaffold designing and further confirms the contribution of exo- and endogenous MSCs for the de novo tissue formation in vivo.

The last part of this dissertation describes using of feline ASCs from reproductive organs to regenerate functional pancreatic β cells. An efficient three-step pancreatic β cell induction system was developed for the feline study. Feline-specific pancreatic induction medium was designed and tested to confirm feline pancreatic differentiation capability. Results of the study showed that feline ASCs have endodermal transdifferentiation capability to form functional islet-like cell clusters in vitro. The system developed in the study can be used for feline ASC-based diabetes mellitus studies to benefit research and clinical applications.

Our research provides critical information to translate ASCs from research to clinical trials in veterinary medicine. These studies investigated the impact of cryopreservation on ASCs isolated from various species and proved for the first time the feline ASCs have endodermal transdifferentiation capability as other species. Further studies may include optimization of cryopreservation medium to minimize the impact on ASC properties based on the species differences, crystallization of secreted feline insulin and three-dimensional structure evaluation, and characterization and functional analysis of induced islet-like cell cluster in vivo.

REFERENCES

1. Marx, C., M.D. Silveira, and N. Beyer Nardi, *Adipose-derived stem cells in veterinary medicine: characterization and therapeutic applications.* Stem cells and development, 2015. **24**(7): p. 803-813.

2. Broeckx, S., et al., *Guidelines to optimize survival and migration capacities of equine mesenchymal stem cells.* J Stem Cell Res Ther, 2013. **3**(147): p. 2.

3. Lalu, M.M., et al., *Safe ty of Cell Therapy with Mesenchymal Stromal Cells (SafeCell): A Systematic Review and Meta-Analysis of Clinical Trials.* 2012.

4. Quimby, J.M., et al., *Safety and efficacy of intravenous infusion of allogeneic cryopreserved mesenchymal stem cells for treatment of chronic kidney disease in cats: results of three sequential pilot studies.* Stem Cell Res Ther, 2013. **4**(2): p. 48.

5. Steinert, A.F., et al., *Concise review: the clinical application of mesenchymal stem cells for musculoskeletal regeneration: current status and perspectives.* Stem cells translational medicine, 2012. **1**(3): p. 237-247.

6. Duan, W., N. Zhang, and M.J. Lopez, *Canine Adipose Tissue Derived Multipotent Stromal Cells Harvested from Infrapatellar and Subcutaneous Adipose Tissue Have Similarin Vitrobehavior.* Veterinary Surgery, 2014. **43**(6): p. E163.

7. McIntosh, K., et al., *The immunogenicity of human adipose ‐derived cells: Temporal changes in vitro.* Stem cells, 2006. **24**(5): p. 1246-1253.

8. Capes-Davis, A., et al., *Check your cultures! A list of cross-contaminated or misidentified cell lines.* International Journal of Cancer, 2010. **127**(1): p. 1-8.

9. Fan, Y., et al., *Oct4 and Sox2 overexpression improves the proliferation and differentiation of bone mesenchymal stem cells in Xiaomeishan porcine.* Genet Mol Res, 2013. **12**(4): p. 6067-79.

10. Wang, L.-N., et al., *Anodic TiO2 nanotubular arrays with pre-synthesized hydroxyapatite—an effective approach to enhance the biocompatibility of titanium.* Journal of nanoscience and nanotechnology, 2013. **13**(8): p. 5316-5326.

11. Wang, Y., et al., *Long-term cultured mesenchymal stem cells frequently develop genomic mutations but do not undergo malignant transformation.* Cell death & disease, 2013. **4**(12): p. e950.

12. Griffin, M.D., T. Ritter, and B.P. Mahon, *Immunological aspects of allogeneic mesenchymal stem cell therapies.* Human gene therapy, 2010. **21**(12): p. 1641-1655.

13. Zaim, M., et al., *Donor age and long-term culture affect differentiation and proliferation of human bone marrow mesenchymal stem cells.* Annals of hematology, 2012. **91**(8): p. 1175-1186.

14. Gao, D. and J. Critser, *Mechanisms of cryoinjury in living cells.* ILAR journal, 2000. **41**(4): p. 187-196.

15. Yong, K.W., et al., *Phenotypic and functional characterization of long-term cryopreserved human adipose-derived stem cells.* Scientific reports, 2015. **5**: p. 9596.

16. Yong, K.W., et al., *Cryopreservation of human mesenchymal stem cells for clinical applications: current methods and challenges.* Biopreservation and biobanking, 2015. **13**(4): p. 231-239.

17. Harel, A., *Cryopreservation and cell banking for autologous mesenchymal stem cell-based therapies.* Cell & Tissue Transplantation & Therapy, 2013. **5**: p. 1.

18. Duan, W. and M.J. Lopez, *Effects of Cryopreservation on Canine Multipotent Stromal Cells from Subcutaneous and Infrapatellar Adipose Tissue.* Stem Cell Reviews and Reports, 2016. **12**(2): p. 257-268.

19. Lawson, A., H. Ahmad, and A. Sambanis, *Cytotoxicity effects of cryoprotectants as single-component and cocktail vitrification solutions.* Cryobiology, 2011. **62**(2): p. 115-122.

20. Levi, B., et al., *Nonintegrating Knockdown and Customized Scaffold Design Enhances Human Adipose‐Derived Stem Cells in Skeletal Repair.* Stem Cells, 2011. **29**(12): p. 2018-2029.

21. Ock, S.-A. and G.-J. Rho, *Effect of dimethyl sulfoxide (DMSO) on cryopreservation of porcine mesenchymal stem cells (pMSCs).* Cell transplantation, 2011. **20**(8): p. 1231-1239.

22. Wang, J., et al., *Effect of phase composition on protein adsorption and osteoinduction of porous calcium phosphate ceramics in mice.* Journal of biomedical materials research Part A, 2014. **102**(12): p. 4234-4243.

23. James, A.W., et al., *Deleterious effects of freezing on osteogenic differentiation of human adipose-derived stromal cells in vitro and in vivo.* Stem cells and development, 2010. **20**(3): p. 427-439.

24. Levi, B., et al., *Regulation of human adipose-derived stromal cell osteogenic differentiation by insulin-like growth factor-1 and platelet-derived growth factor-alpha.* Plastic and reconstructive surgery, 2010. **126**(1): p. 41.

25. Martinello, T., et al., *Cryopreservation does not affect the stem characteristics of multipotent cells isolated from equine peripheral blood.* Tissue Engineering Part C: Methods, 2009. **16**(4): p. 771-781.

26. Martinello, T., et al., *Canine adipose-derived-mesenchymal stem cells do not lose stem features after a long-term cryopreservation.* Research in veterinary science, 2011. **91**(1): p. 18-24.

27. Vidal, M.A., et al., *Evaluation of senescence in mesenchymal stem cells isolated from equine bone marrow, adipose tissue, and umbilical cord tissue.* Stem cells and development, 2011. **21**(2): p. 273-283.

28. Mazur, P., *The role of intracellular freezing in the death of cells cooled at supraoptimal rates.* Cryobiology, 1977. **14**(3): p. 251-272.

29. Mazur, P., *Equilibrium, quasi-equilibrium, and nonequilibrium freezing of mammalian embryos.* Cell biophysics, 1990. **17**(1): p. 53-92.

30. Thirumala, S., et al., *Effect of Various Freezing Parameters on the Immediate Post‐Thaw Membrane Integrity of Adipose Tissue Derived Adult Stem Cells.* Biotechnology progress, 2005. **21**(5): p. 1511-1524.

31. Murphy, S., et al., *Amnion epithelial cell isolation and characterization for clinical use.* Current protocols in stem cell biology, 2010: p. 1E. 6.1-1E. 6.25.

32. Yokoyama, W.M., M.L. Thompson, and R.O. Ehrhardt, *Cryopreservation and thawing of cells.* Current protocols in immunology, 2012: p. A. 3G. 1-A. 3G. 5.

33. Bielanski, A. and G. Vajta, *Risk of contamination of germplasm during cryopreservation and cryobanking in IVF units.* Human reproduction, 2009: p. dep117.

34. Fowler, A. and M. Toner, *Cryo‐injury and biopreservation.* Annals of the new york academy of sciences, 2006. **1066**(1): p. 119-135.

35. Hunt, C.J., *Cryopreservation of human stem cells for clinical application: a review.* Transfusion Medicine and Hemotherapy, 2011. **38**(2): p. 107-123.

36. Degn, K.B., et al., *Effect of intravenous infusion of exenatide (synthetic exendin-4) on glucose-dependent insulin secretion and counterregulation during hypoglycemia.* Diabetes, 2004. **53**(9): p. 2397-2403.

37. Taylor, M., Y. Song, and K. Brockbank, *22 Vitrification in Tissue Preservation: New Developments.* Life in the Frozen State, BJ Fuller, N. Lane, and EE Benson, eds., CRC Press, Boca Raton, FL, 2004: p. 604-641.

38. Berz, D., et al., *Cryopreservation of hematopoietic stem cells.* American journal of hematology, 2007. **82**(6): p. 463-472.

39. Leibo, S., et al., *Effects of freezing on marrow stem cell suspensions: Interactions of cooling and warming rates in the presence of pvp, sucrose, or glycerol.* Cryobiology, 1970. **6**(4): p. 315-332.

40. Katayama, Y., et al., *The effects of a simplified method for cryopreservation and thawing procedures on peripheral blood stem cells.* Bone marrow transplantation, 1997. **19**(3).

41. Thirumala, S., J.M. Gimble, and R.V. Devireddy, *Evaluation of methylcellulose and dimethyl sulfoxide as the cryoprotectants in a serum-free freezing media for cryopreservation of adipose-derived adult stem cells.* Stem cells and development, 2010. **19**(4): p. 513-522.

42. Thirumala, S., J.M. Gimble, and R.V. Devireddy, *Cryopreservation of stromal vascular fraction of adipose tissue in a serum‐free freezing medium.* Journal of tissue engineering and regenerative medicine, 2010. **4**(3): p. 224-232.

43. Fuller, B.J., *Cryoprotectants: the essential antifreezes to protect life in the frozen state.* CryoLetters, 2004. **25**(6): p. 375-388.

44. Scheinkönig, C., et al., *Adoption of long-term cultures to evaluate the cryoprotective potential of trehalose for freezing hematopoietic stem cells.* Bone marrow transplantation, 2004. **34**(6): p. 531-536.

45. Anchordoguy, T.J., et al., *Insights into the cryoprotective mechanism of dimethyl sulfoxide for phospholipid bilayers.* Cryobiology, 1991. **28**(5): p. 467-473.

46. Ding, G., et al., *Allogeneic periodontal ligament stem cell therapy for periodontitis in swine.* Stem Cells, 2010. **28**(10): p. 1829-1838.

47. Liu, Y., et al., *Cryopreservation of human bone marrow‐derived mesenchymal stem cells with reduced dimethylsulfoxide and well‐defined freezing solutions.* Biotechnology progress, 2010. **26**(6): p. 1635-1643.

48. Weng, L., et al., *Molecular dynamics study of effects of temperature and concentration on hydrogen-bond abilities of ethylene glycol and glycerol: implications for cryopreservation.* The Journal of Physical Chemistry A, 2011. **115**(18): p. 4729-4737.

49. Weng, L., et al., *Osmolality and unfrozen water content of aqueous solution of dimethyl sulfoxide.* Journal of Chemical & Engineering Data, 2011. **56**(7): p. 3175-3182.

50. Fahy, G.M., et al., *Cryoprotectant toxicity and cryoprotectant toxicity reduction: in search of molecular mechanisms.* Cryobiology, 1990. **27**(3): p. 247-268.

51. Roddy, G.W., et al., *Action at a Distance: Systemically Administered Adult Stem/Progenitor Cells (MSCs) Reduce Inflammatory Damage to the Cornea Without*

Engraftment and Primarily by Secretion of TNF - α Stimulated Gene/Protein 6. Stem Cells, 2011. **29**(10): p. 1572-1579.

52. Schwarz, C., et al., *Characterization of adipose-derived equine and canine mesenchymal stem cells after incubation in agarose-hydrogel.* Veterinary research communications, 2011. **35**(8): p. 487-499.

53. Zhou, H. and H.H. Xu, *The fast release of stem cells from alginate-fibrin microbeads in injectable scaffolds for bone tissue engineering.* Biomaterials, 2011. **32**(30): p. 7503-7513.

54. Junior, A., et al., *Neurotoxicity associated with dimethylsulfoxide-preserved hematopoietic progenitor cell infusion.* Bone marrow transplantation, 2008. **41**(1): p. 95-97.

55. Fry, L., et al., *Assessing the toxic effects of DMSO on cord blood to determine exposure time limits and the optimum concentration for cryopreservation.* Vox sanguinis, 2015.

56. Thirumala, S., W.S. Goebel, and E.J. Woods, *Clinical grade adult stem cell banking.* Organogenesis, 2009. **5**(3): p. 143-154.

57. Thirumala, S., et al., *Evaluation of polyvinylpyrrolidone as a cryoprotectant for adipose tissue-derived adult stem cells.* Tissue Engineering Part C: Methods, 2009. **16**(4): p. 783-792.

58. Jochems, C.E., et al., *The use of fetal bovine serum: ethical or scientific problem?* ATLA-NOTTINGHAM-, 2002. **30**(2): p. 219-228.

59. Verdanova, M., R. Pytlik, and M.H. Kalbacova, *Evaluation of sericin as a fetal bovine serum-replacing cryoprotectant during freezing of human mesenchymal stromal cells and human osteoblast-like cells.* Biopreservation and biobanking, 2014. **12**(2): p. 99-105.

60. McIntosh, K.R., et al., *Immunogenicity of allogeneic adipose-derived stem cells in a rat spinal fusion model.* Tissue Engineering Part A, 2009. **15**(9): p. 2677-2686.

61. Mitchell, A., et al., *Cryopreservation of equine mesenchymal stem cells in 95% autologous serum and 5% DMSO does not alter post-thaw growth or morphology in vitro compared to fetal bovine serum or allogeneic serum at 20 or 95% and DMSO at 10 or 5%.* Stem cell research & therapy, 2015. **6**(1): p. 1-12.

62. Freimark, D., et al., *Systematic parameter optimization of a Me 2 SO-and serum-free cryopreservation protocol for human mesenchymal stem cells.* Cryobiology, 2011. **63**(2): p. 67-75.

63. Guha, A. and R. Devireddy, *Polyvinylpyrrolidone (PVP) mitigates the damaging effects of intracellular ice formation in adult stem cells.* Annals of biomedical engineering, 2010. **38**(5): p. 1826-1835.

64. McGann, L.E., *Differing actions of penetrating and nonpenetrating cryoprotective agents.* Cryobiology, 1978. **15**(4): p. 382-390.

65. Matsumura, K., J.Y. Bae, and S.H. Hyon, *Polyampholytes as cryoprotective agents for mammalian cell cryopreservation.* Cell transplantation, 2010. **19**(6-1): p. 691-699.

66. Naaldijk, Y., et al., *Effect of different freezing rates during cryopreservation of rat mesenchymal stem cells using combinations of hydroxyethyl starch and dimethylsulfoxide.* BMC biotechnology, 2012. **12**(1): p. 49.

67. Stolzing, A., et al., *Hydroxyethylstarch in cryopreservation–Mechanisms, benefits and problems.* Transfusion and Apheresis Science, 2012. **46**(2): p. 137-147.

68. Bianco, P., P.G. Robey, and P.J. Simmons, *Mesenchymal stem cells: revisiting history, concepts, and assays.* Cell Stem Cell, 2008. **2**(4): p. 313-9.

69. Blitterswijk, C.A.v., *Tissue engineering [electronic resource] / Clemens A. van Blitterswijk*. 2007: London : Academic, 2007.

70. Cho, Y.M., et al., *Betacellulin and nicotinamide sustain PDX1 expression and induce pancreatic β-cell differentiation in human embryonic stem cells.* Biochemical and biophysical research communications, 2008. **366**(1): p. 129-134.

71. da Silva Meirelles, L., A.I. Caplan, and N.B. Nardi, *In search of the in vivo identity of mesenchymal stem cells.* Stem Cells, 2008. **26**.

72. Godara, P., C.D. McFarland, and R.E. Nordon, *Design of bioreactors for mesenchymal stem cell tissue engineering.* Journal of Chemical Technology & Biotechnology, 2008. **83**(4): p. 408-420.

73. Slade, N.P., T. Takeda, and E.L. Squires, *Short Report: Cryopreservation of the equine embryo.* Equine Veterinary Journal, 1985. **17**(S3): p. 40-40.

74. Post, G., et al., *Penetration of zona‐free hamster ova by Siberian tiger sperm.* Zoo biology, 1987. **6**(2): p. 183-187.

75. Bourin, P., et al., *Stromal cells from the adipose tissue-derived stromal vascular fraction and culture expanded adipose tissue-derived stromal/stem cells: a joint statement of the International Federation for Adipose Therapeutics and Science (IFATS) and the International Society for Cellular Therapy (ISCT).* Cytotherapy, 2013. **15**(6): p. 641-648.

76. Screven, R., et al., *Immunophenotype and gene expression profile of mesenchymal stem cells derived from canine adipose tissue and bone marrow.* Veterinary immunology and immunopathology, 2014. **161**(1): p. 21-31.

77. Spencer, N.D., et al., *In vitro expansion and differentiation of fresh and revitalized adult canine bone marrow-derived and adipose tissue-derived stromal cells.* The Veterinary Journal, 2012. **191**(2): p. 231-239.

78. Vieira, N., et al., *Isolation, characterization, and differentiation potential of canine adipose-derived stem cells.* Cell transplantation, 2010. **19**(3): p. 279-289.

79. Guercio, A., et al., *Canine mesenchymal stem cells (MSCs): characterization in relation to donor age and adipose tissue‐harvesting site.* Cell biology international, 2013. **37**(8): p. 789-798.

80. Beaudoin, G.M., et al., *Afadin, a Ras/Rap effector that controls cadherin function, promotes spine and excitatory synapse density in the hippocampus.* The Journal of Neuroscience, 2012. **32**(1): p. 99-110.

81. Reich, C.M., et al., *Isolation, culture and chondrogenic differentiation of canine adipose tissue-and bone marrow-derived mesenchymal stem cells–a comparative study.* Veterinary research communications, 2012. **36**(2): p. 139-148.

82. Edamura, K., et al., *Effects of Cryopreservation on the Cell Viability, Proliferative Capacity and Neuronal Differentiation Potential of Canine Bone Marrow Stromal Cells.* The Journal of Veterinary Medical Science, 2014. **76**(4): p. 573.

83. Bai, S., et al., *NOTCH1 regulates osteoclastogenesis directly in osteoclast precursors and indirectly via osteoblast lineage cells.* Journal of Biological Chemistry, 2008. **283**(10): p. 6509-6518.

84. Arrigoni, E., et al., *Isolation, characterization and osteogenic differentiation of adipose-derived stem cells: from small to large animal models.* Cell and tissue research, 2009. **338**(3): p. 401.

85. Zhang, N., M.A. Dietrich, and M.J. Lopez, *Therapeutic doses of multipotent stromal cells from minimal adipose tissue.* Stem Cell Reviews and Reports, 2014. **10**(4): p. 600-611.

86. Mambelli, L.I., et al., *Characterization of equine adipose tissue–derived progenitor cells before and after cryopreservation.* Tissue Engineering Part C: Methods, 2009. **15**(1): p. 87-94.

87. Eini, F., et al., *The effects of freeze/thawing process on cryopreserved equine umbilical cord blood-derived mesenchymal stem cells.* Comparative Clinical Pathology, 2012. **21**(6): p. 1713-1718.

88. Nguyen, L.H., et al., *Vascularized bone tissue engineering: approaches for potential improvement.* Tissue Engineering Part B: Reviews, 2012. **18**(5): p. 363-382.

89. Ginis, I., B. Grinblat, and M.H. Shirvan, *Evaluation of bone marrow-derived mesenchymal stem cells after cryopreservation and hypothermic storage in clinically safe medium.* Tissue Engineering Part C: Methods, 2012. **18**(6): p. 453-463.

90. Godwin, E.E., et al., *Implantation of bone marrow-derived mesenchymal stem cells demonstrates improved outcome in horses with overstrain injury of the superficial digital flexor tendon.* Equine Vet J, 2012. **44**(1): p. 25-32.

91. Fink, D.W., *FDA regulation of stem cell–based products.* Science, 2009. **324**(5935): p. 1662-1663.

92. Spaas, J., et al., *The effects of equine peripheral blood stem cells on cutaneous wound healing: a clinical evaluation in four horses.* Clinical and experimental dermatology, 2013. **38**(3): p. 280-284.

93. Lian, Q., et al., *Derivation of clinically compliant MSCs from CD105+, CD24- differentiated human ESCs.* Stem Cells, 2007. **25**.

94. Lim, J.-H., et al., *Transplantation of canine umbilical cord blood-derived mesenchymal stem cells in experimentally induced spinal cord injured dogs.* Journal of Veterinary Science, 2007. **8**(3): p. 275-282.

95. Pacini, S., et al., *Suspension of bone marrow-derived undifferentiated mesenchymal stromal cells for repair of superficial digital flexor tendon in race horses.* Tissue Eng, 2007. **13**(12): p. 2949-55.

96. Vidal, M.A., et al., *Characterization of Equine Adipose Tissue-Derived Stromal Cells: Adipogenic and Osteogenic Capacity and Comparison with Bone Marrow-Derived Mesenchymal Stromal Cells.* Veterinary Surgery, 2007. **36**(7): p. 613-622.

97. Caniglia, C., M. Schramme, and R. Smith, *The effect of intralesional injection of bone marrow derived mesenchymal stem cells and bone marrow supernatant on collagen fibril size in a surgical model of equine superficial digital flexor tendonitis.* Equine veterinary journal, 2012. **44**(5): p. 587-593.

98. Mao, L., et al., *Effect of micro-nano-hybrid structured hydroxyapatite bioceramics on osteogenic and cementogenic differentiation of human periodontal ligament stem cell via Wnt signaling pathway.* International journal of nanomedicine, 2015. **10**: p. 7031.

99. Naftanel, M.A. and D.M. Harlan, *Pancreatic islet transplantation.* PLoS Med, 2004. **1**(3): p. e58.

100. Hisanaga, E., et al., *A simple method to induce differentiation of murine bone marrow mesenchymal cells to insulin-producing cells using conophylline and betacellulin-delta4.* Endocrine journal, 2008. **55**(3): p. 535-543.

101. Lin, H.-Y., et al., *Fibronectin and laminin promote differentiation of human mesenchymal stem cells into insulin producing cells through activating Akt and ERK.* Journal of biomedical science, 2010. **17**(1): p. 56.

102. Gao, F., et al., *Extracellular matrix gel is necessary for in vitro cultivation of insulin producing cells from human umbilical cord blood derived mesenchymal stem cells.* Chinese medical journal, 2008. **121**(9): p. 811-818.

103. Timper, K., et al., *Human adipose tissue-derived mesenchymal stem cells differentiate into insulin, somatostatin, and glucagon expressing cells.* Biochemical and biophysical research communications, 2006. **341**(4): p. 1135-1140.

104. Dang, L.T.-T., et al., *Production of islet-like insulin-producing cell clusters in vitro from adipose-derived stem cells.* Biomedical Research and Therapy, 2015. **2**(1): p. 184-192.

105. Marappagounder, D., et al., *Differentiation of mesenchymal stem cells derived from human bone marrow and subcutaneous adipose tissue into pancreatic islet-like clusters in vitro.* Cellular & molecular biology letters, 2013. **18**(1): p. 75-88.

106. Chen, C.-Z., et al., *MicroRNAs modulate hematopoietic lineage differentiation.* science, 2004. **303**(5654): p. 83-86.

107. Chen, D., M. Zhao, and G.R. Mundy, *Bone morphogenetic proteins.* Growth factors, 2004. **22**(4): p. 233-241.

108. Chen, L.-B., X.-B. Jiang, and L. Yang, *Differentiation of rat marrow mesenchymal stem cells into pancreatic islet beta-cells.* World Journal of Gastroenterology, 2004. **10**(20): p. 3016-3020.

109. Chen, S.-l., et al., *Effect on left ventricular function of intracoronary transplantation of autologous bone marrow mesenchymal stem cell in patients with acute myocardial infarction.* The American journal of cardiology, 2004. **94**(1): p. 92-95.

110. Chen, Y.J., et al., *Recruitment of mesenchymal stem cells and expression of TGF‐β1 and VEGF in the early stage of shock wave‐promoted bone regeneration of segmental defect in rats.* Journal of orthopaedic research, 2004. **22**(3): p. 526-534.

111. Hafemann, B., et al., *Cross-linking by 1-ethyl-3- (3-dimethylaminopropyl)-carbodiimide (EDC) of a collagen/elastin membrane meant to be used as a dermal substitute: effects on physical, biochemical and biological features in vitro.* J Mater Sci Mater Med, 2001. **12**(5): p. 437-46.

112. Kuo, C. and C. Lin, *Stem cell therapy: differentiation potential of insulin producing cells from human adipose derived stem cells and umbilical cord MSCs.* International Journal of Clinical Medicine Research, 2014. **1**(1): p. 21-25.

113. Ng, F., et al., *PDGF, TGF-β, and FGF signaling is important for differentiation and growth of mesenchymal stem cells (MSCs): transcriptional profiling can identify markers and signaling pathways important in differentiation of MSCs into adipogenic, chondrogenic, and osteogenic lineages.* Blood, 2008. **112**(2): p. 295-307.

114. Palazuelos, J., et al., *The CB2 cannabinoid receptor controls myeloid progenitor trafficking involvement in the pathogenesis of an animal model of multiple sclerosis.* Journal of Biological Chemistry, 2008. **283**(19): p. 13320-13329.

115. Park, Y.B., et al., *Alterations of proliferative and differentiation potentials of human embryonic stem cells during long-term culture.* Exp Mol Med, 2008. **40**(1): p. 98-108.

116. Reed, S.A. and S.E. Johnson, *Equine umbilical cord blood contains a population of stem cells that express Oct4 and differentiate into mesodermal and endodermal cell types.* Journal of Cellular Physiology, 2008. **215**(2): p. 329-336.

117. Schaefer, S.L., et al., *Effect of rhBMP-2 on tibial plateau fractures in a canine model.* Journal of Orthopaedic Research, 2009. **27**(4): p. 466-471.

118. Teng, S.-H., et al., *Bioactive nanocomposite coatings of collagen/hydroxyapatite on titanium substrates.* Journal of Materials Science: Materials in Medicine, 2008. **19**(6): p. 2453-2461.

119. Vasanjee, S.C., et al., *Characterization of normal canine anterior cruciate ligament-associated synoviocytes.* J Orthop Res, 2008. **26**(6): p. 809-15.

120. Vidal, M.A., et al., *Comparison of chondrogenic potential in equine mesenchymal stromal cells derived from adipose tissue and bone marrow.* Veterinary Surgery, 2008. **37**(8): p. 713-724.

121. Tang, D.-Q., et al., *In vivo and in vitro characterization of insulin-producing cells obtained from murine bone marrow.* Diabetes, 2004. **53**(7): p. 1721-1732.

122. Rooman, I., J. Lardon, and L. Bouwens, *Gastrin stimulates β-cell neogenesis and increases islet mass from transdifferentiated but not from normal exocrine pancreas tissue.* Diabetes, 2002. **51**(3): p. 686-690.

123. Pokrywczynska, M., et al., *Differentiation of stem cells into insulin-producing cells: current status and challenges.* Archivum immunologiae et therapiae experimentalis, 2013. **61**(2): p. 149-158.

124. Martin, I., D. Wendt, and M. Heberer, *The role of bioreactors in tissue engineering.* TRENDS in Biotechnology, 2004. **22**(2): p. 80-86.

125. Yeatts, A.B. and J.P. Fisher, *Bone tissue engineering bioreactors: dynamic culture and the influence of shear stress.* Bone, 2011. **48**(2): p. 171-181.

126. Hutmacher, D.W., *Scaffolds in tissue engineering bone and cartilage.* Biomaterials, 2000. **21**(24): p. 2529-2543.

127. Niklason, L., et al., *Functional arteries grown in vitro.* Science, 1999. **284**(5413): p. 489-493.

128. Radisic, M., et al., *Cardiac tissue engineering using perfusion bioreactor systems.* Nature protocols, 2008. **3**(4): p. 719-738.

129. Schmelzer, E., et al., *Three-dimensional perfusion bioreactor culture supports differentiation of human fetal liver cells.* Tissue Engineering Part A, 2010. **16**(6): p. 2007-2016.

130. Bai, L., G. Meredith, and B. Tuch, *Glucagon-like peptide-1 enhances production of insulin in insulin-producing cells derived from mouse embryonic stem cells.* Journal of Endocrinology, 2005. **186**(2): p. 343-352.

131. Gutniak, M., et al., *Antidiabetogenic effect of glucagon-like peptide-1 (7–36) amide in normal subjects and patients with diabetes mellitus.* New England Journal of Medicine, 1992. **326**(20): p. 1316-1322.

132. Hardikar, A.A., et al., *Functional maturation of fetal porcine β-cells by glucagon-like peptide 1 and cholecystokinin.* Endocrinology, 2002. **143**(9): p. 3505-3514.

133. Abraham, E.J., et al., *Insulinotropic hormone glucagon-like peptide-1 differentiation of human pancreatic islet-derived progenitor cells into insulin-producing cells.* Endocrinology, 2002. **143**(8): p. 3152-3161.

134. Li, L., et al., *Activin A and betacellulin.* Diabetes, 2004. **53**(3): p. 608-615.

135. Suh, M.-R., et al., *Human embryonic stem cells express a unique set of microRNAs.* Developmental biology, 2004. **270**(2): p. 488-498.

136. Wang, R., et al., *Hepatocyte growth factor regulates proliferation and differentiation of epithelial monolayers derived from islets of postnatal rat pancreas.* Journal of endocrinology, 2004. **183**(1): p. 163-171.

137. Schwindt, T.T., et al., *Effects of FGF-2 and EGF removal on the differentiationof mouse neural precursor cells.* Anais da Academia Brasileira de Ciências, 2009. **81**(3): p. 443-452.

138. Sikavitsas, V.I., G.N. Bancroft, and A.G. Mikos, *Formation of three‐dimensional cell/polymer constructs for bone tissue engineering in a spinner flask and a rotating wall vessel bioreactor.* Journal of biomedical materials research, 2002. **62**(1): p. 136-148.

139. Mygind, T., et al., *Mesenchymal stem cell ingrowth and differentiation on coralline hydroxyapatite scaffolds.* Biomaterials, 2007. **28**(6): p. 1036-1047.

140. Stiehler, M., et al., *Effect of dynamic 3‐D culture on proliferation, distribution, and osteogenic differentiation of human mesenchymal stem cells.* Journal of Biomedical Materials Research Part A, 2009. **89**(1): p. 96-107.

141. Wang, X., et al., *Biomimetic modification of porous TiNbZr alloy scaffold for bone tissue engineering.* Tissue Engineering Part A, 2009. **16**(1): p. 309-316.

142. Meinel, L., et al., *Bone tissue engineering using human mesenchymal stem cells: effects of scaffold material and medium flow.* Annals of biomedical engineering, 2004. **32**(1): p. 112-122.

143. Kim, H.J., et al., *Bone Regeneration on Macroporous Aqueous‐Derived Silk 3‐D Scaffolds.* Macromolecular bioscience, 2007. **7**(5): p. 643-655.

144. Rauh, J., et al., *Bioreactor systems for bone tissue engineering.* Tissue Engineering Part B: Reviews, 2011. **17**(4): p. 263-280.

145. Botchwey, E.A., et al., *Tissue engineered bone: Measurement of nutrient transport in three‐dimensional matrices.* Journal of Biomedical Materials Research Part A, 2003. **67**(1): p. 357-367.

146. Yu, X., et al., *Bioreactor-based bone tissue engineering: the influence of dynamic flow on osteoblast phenotypic expression and matrix mineralization.* Proceedings of the National Academy of Sciences of the United States of America, 2004. **101**(31): p. 11203-11208.

147. Goldstein, A.S., et al., *Effect of convection on osteoblastic cell growth and function in biodegradable polymer foam scaffolds.* Biomaterials, 2001. **22**(11): p. 1279-1288.

148. Song, K., et al., *Three‐dimensional fabrication of engineered bone with human bio‐derived bone scaffolds in a rotating wall vessel bioreactor.* Journal of biomedical materials research Part A, 2008. **86**(2): p. 323-332.

149. Diederichs, S., et al., *Dynamic cultivation of human mesenchymal stem cells in a rotating bed bioreactor system based on the Z® RP Platform.* Biotechnology progress, 2009. **25**(6): p. 1762-1771.

150. Anton, F., et al., *Design and characterization of a rotating bed system bioreactor for tissue engineering applications.* Biotechnology progress, 2008. **24**(1): p. 140-147.

151. Suck, K., et al., *Cultivation of MC3T3‐E1 cells on a newly developed material (Sponceram®) using a rotating bed system bioreactor.* Journal of Biomedical Materials Research Part A, 2007. **80**(2): p. 268-275.

152. Bancroft, G.N., V.I. Sikavitsas, and A.G. Mikos, *Technical note: Design of a flow perfusion bioreactor system for bone tissue-engineering applications.* Tissue engineering, 2003. **9**(3): p. 549-554.

153. Wang, Y., et al., *Application of perfusion culture system improves in vitro and in vivo osteogenesis of bone marrow-derived osteoblastic cells in porous ceramic materials.* Tissue engineering, 2003. **9**(6): p. 1205-1214.

154. Bancroft, G.N., et al., *Fluid flow increases mineralized matrix deposition in 3D perfusion culture of marrow stromal osteoblasts in a dose-dependent manner.* Proceedings of the National Academy of Sciences, 2002. **99**(20): p. 12600-12605.

155. Datta, N., et al., *In vitro generated extracellular matrix and fluid shear stress synergistically enhance 3D osteoblastic differentiation.* Proceedings of the National Academy of Sciences of the United States of America, 2006. **103**(8): p. 2488-2493.

156. Holtorf, H.L., J.A. Jansen, and A.G. Mikos, *Flow perfusion culture induces the osteoblastic differentiation of marrow stromal cell‐scaffold constructs in the absence of dexamethasone.* Journal of Biomedical Materials Research Part A, 2005. **72**(3): p. 326-334.

157. Gomes, M.E., et al., *Effect of flow perfusion on the osteogenic differentiation of bone marrow stromal cells cultured on starch‐based three‐dimensional scaffolds.* Journal of Biomedical Materials Research Part A, 2003. **67**(1): p. 87-95.

158. Cartmell, S.H., et al., *Effects of medium perfusion rate on cell-seeded three-dimensional bone constructs in vitro.* Tissue engineering, 2003. **9**(6): p. 1197-1203.

159. Gomes, M.E., et al., *Influence of the porosity of starch-based fiber mesh scaffolds on the proliferation and osteogenic differentiation of bone marrow stromal cells cultured in a flow perfusion bioreactor.* Tissue engineering, 2006. **12**(4): p. 801-809.

160. Holtorf, H.L., et al., *Flow perfusion culture of marrow stromal cells seeded on porous biphasic calcium phosphate ceramics.* Annals of biomedical engineering, 2005. **33**(9): p. 1238-1248.

161. Sailon, A.M., et al., *A novel flow-perfusion bioreactor supports 3D dynamic cell culture.* BioMed Research International, 2009. **2009**.

162. Hofmann, A., et al., *Bioengineered human bone tissue using autogenous osteoblasts cultured on different biomatrices.* Journal of Biomedical Materials Research Part A, 2003. **67**(1): p. 191-199.

163. Sikavitsas, V.I., et al., *Influence of the in vitro culture period on the in vivo performance of cell/titanium bone tissue‐engineered constructs using a rat cranial critical size defect model.* Journal of Biomedical Materials Research Part A, 2003. **67**(3): p. 944-951.

164. Grellier, M., et al., *Responsiveness of human bone marrow stromal cells to shear stress.* Journal of tissue engineering and regenerative medicine, 2009. **3**(4): p. 302-309.

165. Kapur, S., D.J. Baylink, and K.-H.W. Lau, *Fluid flow shear stress stimulates human osteoblast proliferation and differentiation through multiple interacting and competing signal transduction pathways.* Bone, 2003. **32**(3): p. 241-251.

166. Kreke, M.R., W.R. Huckle, and A.S. Goldstein, *Fluid flow stimulates expression of osteopontin and bone sialoprotein by bone marrow stromal cells in a temporally dependent manner.* Bone, 2005. **36**(6): p. 1047-1055.

167. Kreke, M.R., et al., *Effect of intermittent shear stress on mechanotransductive signaling and osteoblastic differentiation of bone marrow stromal cells.* Tissue Engineering Part A, 2008. **14**(4): p. 529-537.

168. Li, D., et al., *Effects of flow shear stress and mass transport on the construction of a large-scale tissue-engineered bone in a perfusion bioreactor.* Tissue Engineering Part A, 2009. **15**(10): p. 2773-2783.

169. Sikavitsas, V.I., et al., *Mineralized matrix deposition by marrow stromal osteoblasts in 3D perfusion culture increases with increasing fluid shear forces.* Proceedings of the National Academy of Sciences, 2003. **100**(25): p. 14683-14688.

170. Grayson, W.L., et al., *Effects of initial seeding density and fluid perfusion rate on formation of tissue-engineered bone.* Tissue Engineering Part A, 2008. **14**(11): p. 1809-1820.

171. Sikavitsas, V.I., et al., *Flow perfusion enhances the calcified matrix deposition of marrow stromal cells in biodegradable nonwoven fiber mesh scaffolds.* Annals of biomedical engineering, 2005. **33**(1): p. 63.

172. Fröhlich, M., et al., *Bone grafts engineered from human adipose-derived stem cells in perfusion bioreactor culture.* Tissue Engineering Part A, 2009. **16**(1): p. 179-189.

173. Fortier, L.A. and A.J. Travis, *Stem cells in veterinary medicine.* Stem Cell Res Ther, 2011. **2**(1): p. 9.

174. Engels, P., et al., *Harvest site influences the growth properties of adipose derived stem cells.* Cytotechnology, 2013. **65**(3): p. 437-445.

175. Buschmann, J., et al., *Yield and proliferation rate of adipose-derived stromal cells as a function of age, body mass index and harvest site—increasing the yield by use of adherent and supernatant fractions?* Cytotherapy, 2013. **15**(9): p. 1098-1105.

176. Avram, A.S., M.M. Avram, and W.D. James, *Subcutaneous fat in normal and diseased states: 2. Anatomy and physiology of white and brown adipose tissue.* Journal of the American Academy of Dermatology, 2005. **53**(4): p. 671-683.

177. Wajchenberg, B.L., *Subcutaneous and Visceral Adipose Tissue: Their Relation to the Metabolic Syndrome.* Endocrine Reviews, 2000. **21**(6): p. 697-738.

178. Klaus, S., *Functional differentiation of white and brown adipocytes.* BioEssays, 1997. **19**(3): p. 215-223.

179. Spivakov, M. and A.G. Fisher, *Epigenetic signatures of stem-cell identity.* Nat Rev Genet, 2007. **8**(4): p. 263-271.

180. Gimble, J.M., A.J. Katz, and B.A. Bunnell, *Adipose-Derived Stem Cells for Regenerative Medicine.* Circulation Research, 2007. **100**(9): p. 1249-1260.

181. Zhang, N., M.A. Dietrich, and M.J. Lopez, *Canine Intra-Articular Multipotent Stromal Cells (MSC) From Adipose Tissue Have the Highest In Vitro Expansion Rates, Multipotentiality, and MSC Immunophenotypes.* Veterinary Surgery, 2013. **42**(2): p. 137-146.

182. Pires de Carvalho, P., et al., *Comparison of infrapatellar and subcutaneous adipose tissue stromal vascular fraction and stromal/stem cells in osteoarthritic subjects.* Journal of Tissue Engineering and Regenerative Medicine, 2012: p. n/a-n/a.

183. Gimble, J.M. and F. Guilak, *Adipose-derived adult stem cells: isolation, characterization, and differentiation potential.* Cytotherapy, 2003. **5**(5): p. 362-369.

184. Vidal, M.A., et al., *Cell growth characteristics and differentiation frequency of adherent equine bone marrow–derived mesenchymal stromal cells: adipogenic and osteogenic capacity.* Veterinary Surgery, 2006. **35**(7): p. 601-610.

185. Zancanaro, C., et al., *An ultrastructural study of brown adipose tissue in pre-term human new-borns.* Tissue and Cell, 1995. **27**(3): p. 339-348.

186. Mirancea, N. and D. Mirancea, *The ultrastructure of the white subcutaneous adipose tissue.* Proc. Rom. Acad., Series B, 2011. **13**(3): p. 206-11.

187. Guo, Y., et al., *Functional genomic screen reveals genes involved in lipid-droplet formation and utilization.* Nature, 2008. **453**(7195): p. 657-661.

188. Cannon, B. and J. Nedergaard, *Brown adipose tissue: function and physiological significance.* Physiol Rev, 2004. **84**(1): p. 277-359.

189. Nicholls, D.G., S.A. Cunningham, and E. Rial, *Bioenergetic mechanisms of brown adipose tissue thermogenesis.* Brown adipose tissue/edited by Paul Trayhurn and David G. Nicholls, 1986.

190. Rodeheffer, M.S., K. Birsoy, and J.M. Friedman, *Identification of White Adipocyte Progenitor Cells In Vivo.* Cell, 2008. **135**(2): p. 240-249.

191. Spiegelman, B.M. and J.S. Flier, *Obesity and the regulation of energy balance.* Cell, 2001. **104**(4): p. 531-543.

192. Seale, P., et al., *PRDM16 controls a brown fat/skeletal muscle switch.* Nature, 2008. **454**(7207): p. 961-967.

193. Timmons, J.A., et al., *Myogenic gene expression signature establishes that brown and white adipocytes originate from distinct cell lineages.* Proceedings of the National Academy of Sciences, 2007. **104**(11): p. 4401-4406.

194. Won Park, K., D.S. Halperin, and P. Tontonoz, *Before They Were Fat: Adipocyte Progenitors.* Cell Metabolism, 2008. **8**(6): p. 454-457.

195. Lonergan, T., C. Brenner, and B. Bavister, *Differentiation‐related changes in mitochondrial properties as indicators of stem cell competence.* Journal of cellular physiology, 2006. **208**(1): p. 149-153.

196. Lonergan, T., B. Bavister, and C. Brenner, *Mitochondria in stem cells.* Mitochondrion, 2007. **7**(5): p. 289-296.

197. Muldrew, K. and L.E. McGann, *Mechanisms of intracellular ice formation.* Biophysical journal, 1990. **57**(3): p. 525.

198. Fahy, G.M., *The relevance of cryoprotectant "toxicity" to cryobiology.* Cryobiology, 1986. **23**(1): p. 1-13.

199. Farrant, J., et al., *Use of two-step cooling procedures to examine factors influencing cell survival following freezing and thawing.* Cryobiology, 1977. **14**(3): p. 273-286.

200. Todorov, P., et al., *Comparative studies of different cryopreservation methods for mesenchymal stem cells derived from human fetal liver.* Cell biology international, 2010. **34**(5): p. 455-462.

201. Gautier, J., et al., *A low membrane lipid phase transition temperature is associated with a high cryotolerance of Lactobacillus delbrueckii subspecies bulgaricus CFL1.* Journal of Dairy Science, 2013. **96**(9): p. 5591-5602.

202. Balci, D. and A. Can, *The assessment of cryopreservation conditions for human umbilical cord stroma-derived mesenchymal stem cells towards a potential use for stem cell banking.* Current stem cell research & therapy, 2013. **8**(1): p. 60-72.

203. Davies, O., et al., *The effects of cryopreservation on cells isolated from adipose, bone marrow and dental pulp tissues.* Cryobiology, 2014. **69**(2): p. 342-347.

204. Goodison, S., V. Urquidi, and D. Tarin, *CD44 cell adhesion molecules.* Molecular pathology : MP, 1999. **52**(4): p. 189-196.

205. Camaioni, A., et al., *Effects of exogenous hyaluronic acid and serum on matrix organization and stability in the mouse cumulus cell-oocyte complex.* The Journal of biological chemistry, 1993. **268**(27): p. 20473-20481.

206. Costantini, A., et al., *Effects of cryopreservation on lymphocyte immunophenotype and function.* Journal of Immunological Methods, 2003. **278**(1–2): p. 145-155.

207. Sallusto, F., et al., *Two subsets of memory T lymphocytes with distinct homing potentials and effector functions.* Nature, 1999. **402**: p. 34-38.

208. Palmer, B.E., et al., *Functional and phenotypic characterization of CD57+ CD4+ T cells and their association with HIV-1-induced T cell dysfunction.* The Journal of Immunology, 2005. **175**(12): p. 8415-8423.

209. Katkov, I.I., et al., *Cryopreservation by slow cooling with DMSO diminished production of Oct-4 pluripotency marker in human embryonic stem cells.* Cryobiology, 2006. **53**(2): p. 194-205.

210. Wang, Z.-X., et al., *Oct4 and Sox2 directly regulate expression of another pluripotency transcription factor, Zfp206, in embryonic stem cells.* Journal of Biological Chemistry, 2007. **282**(17): p. 12822-12830.

211. De Nuccio, C., et al., *Peroxisome proliferator activated receptor-γ agonists protect oligodendrocyte progenitors against tumor necrosis factor-alpha-induced damage: Effects on mitochondrial functions and differentiation.* Experimental Neurology, 2015. **271**: p. 506-514.

212. Spiegelman, B.M., *PPAR-gamma: adipogenic regulator and thiazolidinedione receptor.* Diabetes, 1998. **47**(4): p. 507-514.

213. Bernardo, A., et al., *Peroxisome Proliferator-Activated Receptor-γ Agonists Promote Differentiation and Antioxidant Defenses of Oligodendrocyte Progenitor Cells.* Journal of Neuropathology & Experimental Neurology, 2009. **68**(7): p. 797-808.

214. Hovatta, O., et al., *Cryopreservation of human ovarian tissue using dimethylsulphoxide and propanediol-sucrose as cryoprotectants.* Human Reproduction, 1996. **11**(6): p. 1268-1272.

215. Goh, B.C., et al., *Cryopreservation characteristics of adipose‐derived stem cells: maintenance of differentiation potential and viability.* Journal of tissue engineering and regenerative medicine, 2007. **1**(4): p. 322-324.

216. Epperly, M., et al., *Cell phenotype specific kinetics of expression of intratracheally injected manganese superoxide dismutase–plasmid/liposomes (MnSOD–PL) during lung radioprotective gene therapy.* Gene therapy, 2003. **10**(2): p. 163-171.

217. Darling, E.M. and K.A. Athanasiou, *Rapid phenotypic changes in passaged articular chondrocyte subpopulations.* Journal of Orthopaedic Research, 2005. **23**(2): p. 425-432.

218. Caplan, A.I., *Adult mesenchymal stem cells for tissue engineering versus regenerative medicine.* Journal of cellular physiology, 2007. **213**(2): p. 341-347.

219. García-Gareta, E., M.J. Coathup, and G.W. Blunn, *Osteoinduction of bone grafting materials for bone repair and regeneration.* Bone, 2015. **81**: p. 112-121.

220. Delloye, C., et al., *Bone allografts.* Bone & Joint Journal, 2007. **89**(5): p. 574-580.

221. Laurencin, C., Y. Khan, and S.F. El-Amin, *Bone graft substitutes.* Expert review of medical devices, 2014.

222. Bosetti, M., et al., *Comparative in vitro study of four commercial biomaterials used for bone grafting.* J Appl Biomater Funct Mater, 2013. **11**: p. e80-e88.

223. Grottkau, B.E. and Y. Lin, *Osteogenesis of adipose-derived stem cells.* Bone research, 2013. **1**(2): p. 133-145.

224. Bergman, R., et al., *Age‐related changes in osteogenic stem cells in mice.* Journal of Bone and Mineral Research, 1996. **11**(5): p. 568-577.

225. Uccelli, A., L. Moretta, and V. Pistoia, *Mesenchymal stem cells in health and disease.* Nature Reviews Immunology, 2008. **8**(9): p. 726-736.

226. Silva, I. and J. Branco, *Rank/Rankl/opg: literature review.* Acta reumatológica portuguesa, 2011. **36**(3).

227. Idris, A.I., et al., *Cannabinoid receptor type 1 protects against age-related osteoporosis by regulating osteoblast and adipocyte differentiation in marrow stromal cells.* Cell Metabolism, 2009. **10**(2): p. 139-147.

228. Galve-Roperh, I., et al., *Cannabinoid receptor signaling in progenitor/stem cell proliferation and differentiation.* Progress in lipid research, 2013. **52**(4): p. 633-650.

229. Idris, A.I., et al., *Regulation of bone mass, bone loss and osteoclast activity by cannabinoid receptors.* Nature medicine, 2005. **11**(7): p. 774-779.

230. Ofek, O., et al., *Peripheral cannabinoid receptor, CB2, regulates bone mass.* Proceedings of the National Academy of Sciences of the United States of America, 2006. **103**(3): p. 696-701.

231. Tam, J., et al., *The cannabinoid CB1 receptor regulates bone formation by modulating adrenergic signaling.* The FASEB journal, 2008. **22**(1): p. 285-294.

232. Kondo, H., S. Takeuchi, and A. Togari, *β-Adrenergic signaling stimulates osteoclastogenesis via reactive oxygen species.* American Journal of Physiology-Endocrinology and Metabolism, 2013. **304**(5): p. E507-E515.

233. Ferreira, A.M., et al., *Collagen for bone tissue regeneration.* Acta biomaterialia, 2012. **8**(9): p. 3191-3200.

234. Lee, C.H., A. Singla, and Y. Lee, *Biomedical applications of collagen.* International journal of pharmaceutics, 2001. **221**(1): p. 1-22.

235. Van Hoff, C., et al., *Effectiveness of ultraporous β-tricalcium phosphate (vitoss) as bone graft substitute for cavitary defects in benign and low-grade malignant bone tumors.* American journal of orthopedics (Belle Mead, NJ), 2012. **41**(1): p. 20-23.

236. Wu, S., et al., *Biomimetic porous scaffolds for bone tissue engineering.* Materials Science and Engineering: R: Reports, 2014. **80**: p. 1-36.

237. Chan, B.P., et al., *Mesenchymal stem cell–encapsulated collagen microspheres for bone tissue engineering.* Tissue Engineering Part C: Methods, 2009. **16**(2): p. 225-235.

238. Inzana, J.A., et al., *3D printing of composite calcium phosphate and collagen scaffolds for bone regeneration.* Biomaterials, 2014. **35**(13): p. 4026-4034.

239. Miguel, F.B., et al., *Regeneration of critical bone defects with anionic collagen matrix as scaffolds.* Journal of Materials Science: Materials in Medicine, 2013. **24**(11): p. 2567-2575.

240. Damron, T.A., *Use of 3D β-tricalcium phosphate (Vitoss®) scaffolds in repairing bone defects.* 2007.

241. Dawson, E., et al., *Recombinant human bone morphogenetic protein-2 on an absorbable collagen sponge with an osteoconductive bulking agent in posterolateral arthrodesis with instrumentation.* The Journal of Bone & Joint Surgery, 2009. **91**(7): p. 1604-1613.

242. You, M.-H., et al., *Synergistically enhanced osteogenic differentiation of human mesenchymal stem cells by culture on nanostructured surfaces with induction media.* Biomacromolecules, 2010. **11**(7): p. 1856-1862.

243. Polini, A., et al., *Osteoinduction of human mesenchymal stem cells by bioactive composite scaffolds without supplemental osteogenic growth factors.* PloS one, 2011. **6**(10): p. e26211.

244. Castano-Izquierdo, H., et al., *Pre-culture period of mesenchymal stem cells in osteogenic media influences their in vivo bone forming potential.* Journal of Biomedical Materials Research Part A, 2007. **82A**(1): p. 129-138.

245. Xie, L., et al., *In vitro mesenchymal trilineage differentiation and extracellular matrix production by adipose and bone marrow derived adult equine multipotent stromal cells on a collagen scaffold.* Stem Cell Reviews and Reports, 2013. **9**(6): p. 858-872.

246. Edwards, C. and W. O'brien, *Modified assay for determination of hydroxyproline in a tissue hydrolyzate.* Clinica chimica acta, 1980. **104**(2): p. 161-167.

247. Enobakhare, B.O., D.L. Bader, and D.A. Lee, *Quantification of Sulfated Glycosaminoglycans in Chondrocyte/Alginate Cultures, by Use of 1,9-Dimethylmethylene Blue.* Analytical Biochemistry, 1996. **243**(1): p. 189-191.

248. Ohnishi, S.T. and J.K. Barr, *A simplified method of quantitating protein using the biuret and phenol reagents.* Analytical biochemistry, 1978. **86**(1): p. 193-200.

249. Ilmer, M., et al., *Human Osteoblast–Derived Factors Induce Early Osteogenic Markers in Human Mesenchymal Stem Cells.* Tissue Engineering Part A, 2009. **15**(9): p. 2397-2409.

250. Nakamura, A., et al., *Osteocalcin secretion as an early marker of in vitro osteogenic differentiation of rat mesenchymal stem cells.* Tissue Engineering Part C: Methods, 2009. **15**(2): p. 169-180.

251. Matsushima, A., et al., *In Vivo Osteogenic Capability of Human Mesenchymal Cells Cultured on Hydroxyapatite and on β‐Tricalcium Phosphate.* Artificial organs, 2009. **33**(6): p. 474-481.

252. Osathanon, T., et al., *The responses of human adipose-derived mesenchymal stem cells on polycaprolactone-based scaffolds: an in vitro study.* Tissue Engineering and Regenerative Medicine, 2014. **11**(3): p. 239-246.

253. Zuk, P.A., *Tissue engineering craniofacial defects with adult stem cells? Are we ready yet?* Pediatric research, 2008. **63**(5): p. 478-486.

254. Zanetti, A.S., et al., *Human adipose‐derived stem cells and three‐dimensional scaffold constructs: A review of the biomaterials and models currently used for bone regeneration.* Journal of Biomedical Materials Research Part B: Applied Biomaterials, 2013. **101**(1): p. 187-199.

255. Ngiam, M., et al., *The fabrication of nano-hydroxyapatite on PLGA and PLGA/collagen nanofibrous composite scaffolds and their effects in osteoblastic behavior for bone tissue engineering.* Bone, 2009. **45**(1): p. 4-16.

256. Stein, G.S. and J.B. Lian, *Molecular mechanisms mediating proliferation/differentiation interrelationships during progressive development of the osteoblast phenotype.* Endocrine reviews, 1993. **14**(4): p. 424-442.

257. Valenti, M.T., et al., *Gene expression analysis in osteoblastic differentiation from peripheral blood mesenchymal stem cells.* Bone, 2008. **43**(6): p. 1084-1092.

258. Aubin, J., et al., *Osteoblast and chondroblast differentiation.* Bone, 1995. **17**(2): p. S77-S83.

259. Qi, H., et al., *Identification of genes responsible for osteoblast differentiation from human mesodermal progenitor cells.* Proceedings of the National Academy of Sciences, 2003. **100**(6): p. 3305-3310.

260. Liu, Q., et al., *A comparative study of proliferation and osteogenic differentiation of adipose-derived stem cells on akermanite and β-TCP ceramics.* Biomaterials, 2008. **29**(36): p. 4792-4799.

261. Liu, Y., et al., *Influence of calcium phosphate crystal assemblies on the proliferation and osteogenic gene expression of rat bone marrow stromal cells.* Biomaterials, 2007. **28**(7): p. 1393-1403.

262. Meredith, J., B. Fazeli, and M. Schwartz, *The extracellular matrix as a cell survival factor.* Molecular biology of the cell, 1993. **4**(9): p. 953-961.

263. Datta, N., et al., *Effect of bone extracellular matrix synthesized in vitro on the osteoblastic differentiation of marrow stromal cells.* Biomaterials, 2005. **26**(9): p. 971-977.

264. Zan, X., et al., *Effect of roughness on in situ biomineralized CaP-collagen coating on the osteogenesis of mesenchymal stem cells.* Langmuir, 2016. **32**(7): p. 1808-1817.

265. Deligianni, D.D., et al., *Effect of surface roughness of hydroxyapatite on human bone marrow cell adhesion, proliferation, differentiation and detachment strength.* Biomaterials, 2000. **22**(1): p. 87-96.

266. Faia-Torres, A.B., et al., *Differential regulation of osteogenic differentiation of stem cells on surface roughness gradients.* Biomaterials, 2014. **35**(33): p. 9023-9032.

267. Stevens, M.M., *Biomaterials for bone tissue engineering.* Materials today, 2008. **11**(5): p. 18-25.

268. Cote, A.J., et al., *Single-cell differences in matrix gene expression do not predict matrix deposition.* Nature communications, 2016. **7**.

269. Ortega, N., D.J. Behonick, and Z. Werb, *Matrix remodeling during endochondral ossification.* Trends in cell biology, 2004. **14**(2): p. 86-93.

270. Eyre, D.R. and M.A. Weis, *Bone collagen: new clues to its mineralization mechanism from recessive osteogenesis imperfecta.* Calcified tissue international, 2013. **93**(4): p. 338-347.

271. Salbach‐Hirsch, J., et al., *Sulfated glycosaminoglycans support osteoblast functions and concurrently suppress osteoclasts.* Journal of cellular biochemistry, 2014. **115**(6): p. 1101-1111.

272. Lin, Z., et al., *Gene expression dynamics during bone healing and osseointegration.* Journal of periodontology, 2011. **82**(7): p. 1007-1017.

273. Kundu, A.K. and A.J. Putnam, *Vitronectin and collagen I differentially regulate osteogenesis in mesenchymal stem cells.* Biochemical and biophysical research communications, 2006. **347**(1): p. 347-357.

274. Salasznyk, R.M., et al., *ERK signaling pathways regulate the osteogenic differentiation of human mesenchymal stem cells on collagen I and vitronectin.* Cell communication & adhesion, 2004. **11**(5-6): p. 137-153.

275. Gowran, A., K. McKayed, and V.A. Campbell, *The cannabinoid receptor type 1 is essential for mesenchymal stem cell survival and differentiation: implications for bone health.* Stem cells international, 2013. **2013**.

276. Hendaoui, I., et al., *Inhibition of Wnt/β-catenin signaling by a soluble collagen-derived frizzled domain interacting with Wnt3a and the receptors frizzled 1 and 8.* PloS one, 2012. **7**(1): p. e30601.

277. Boyce, B.F. and L. Xing, *Functions of RANKL/RANK/OPG in bone modeling and remodeling.* Archives of biochemistry and biophysics, 2008. **473**(2): p. 139-146.

278. Kim, K., et al., *Early osteogenic signal expression of rat bone marrow stromal cells is influenced by both hydroxyapatite nanoparticle content and initial cell seeding density in biodegradable nanocomposite scaffolds.* Acta biomaterialia, 2011. **7**(3): p. 1249-1264.

279. Wu, X., et al., *Purmorphamine induces osteogenesis by activation of the hedgehog signaling pathway.* Chemistry & biology, 2004. **11**(9): p. 1229-1238.

280. Thorfve, A., et al., *Hydroxyapatite coating affects the Wnt signaling pathway during peri-implant healing in vivo.* Acta biomaterialia, 2014. **10**(3): p. 1451-1462.

281. Krishnan, V., H.U. Bryant, and O.A. MacDougald, *Regulation of bone mass by Wnt signaling.* The Journal of clinical investigation, 2006. **116**(5): p. 1202-1209.

282. Blair, J.M., et al., *Mechanisms of disease: roles of OPG, RANKL and RANK in the pathophysiology of skeletal metastasis.* Nature Clinical Practice Oncology, 2006. **3**(1): p. 41-49.

283. Hofbauer, L., C. Kuhne, and V. Viereck, *The OPG/RANKL/RANK system in metabolic bone diseases.* Journal of Musculoskeletal and Neuronal Interactions, 2004. **4**(3): p. 268.

284. Liu, D.D., et al., *TGF‐β/BMP signaling pathway is involved in cerium‐promoted osteogenic differentiation of mesenchymal stem cells.* Journal of cellular biochemistry, 2013. **114**(5): p. 1105-1114.

285. Ofek, O., et al., *CB2 cannabinoid receptor targets mitogenic Gi protein–cyclin D1 axis in osteoblasts.* Journal of Bone and Mineral Research, 2011. **26**(2): p. 308-316.

286. Makowiecka, J. and K. Wielgus, *Therapeutic potential of cannabinoids—perspectives for the future.* Journal of Natural Fibers, 2014. **11**(4): p. 283-311.

287. Gregory, C.A., et al., *How Wnt signaling affects bone repair by mesenchymal stem cells from the bone marrow.* Annals of the New York Academy of Sciences, 2005. **1049**(1): p. 97-106.

288. Wada, T., et al., *RANKL–RANK signaling in osteoclastogenesis and bone disease.* Trends in molecular medicine, 2006. **12**(1): p. 17-25.

289. Auer, J.A. and J.A. Stick, *Equine surgery*. 1999: WB Saunders.

290. Burchardt, H., *Biology of cortical bone graft incorporation*, in *Bone Transplantation*. 1989, Springer. p. 23-28.

291. Vidal, M.A., et al., *Characterization of Equine Adipose Tissue‐Derived Stromal Cells: Adipogenic and Osteogenic Capacity and Comparison with Bone Marrow‐Derived Mesenchymal Stromal Cells.* Veterinary Surgery, 2007. **36**(7): p. 613-622.

292. Im, G.-I., Y.-W. Shin, and K.-B. Lee, *Do adipose tissue-derived mesenchymal stem cells have the same osteogenic and chondrogenic potential as bone marrow-derived cells?* Osteoarthritis and cartilage, 2005. **13**(10): p. 845-853.

293. Bose, S., M. Roy, and A. Bandyopadhyay, *Recent advances in bone tissue engineering scaffolds.* Trends in biotechnology, 2012. **30**(10): p. 546-554.

294. Simmons, C.A., et al., *Dual growth factor delivery and controlled scaffold degradation enhance in vivo bone formation by transplanted bone marrow stromal cells.* Bone, 2004. **35**(2): p. 562-569.

295. LeGeros, R.Z., *Calcium phosphate-based osteoinductive materials.* Chemical reviews, 2008. **108**(11): p. 4742-4753.

296. Gan, Y., et al., *The clinical use of enriched bone marrow stem cells combined with porous beta-tricalcium phosphate in posterior spinal fusion.* Biomaterials, 2008. **29**(29): p. 3973-3982.

297. McCullen, S., et al., *Electrospun composite poly (L-lactic acid)/tricalcium phosphate scaffolds induce proliferation and osteogenic differentiation of human adipose-derived stem cells.* Biomedical materials, 2009. **4**(3): p. 035002.

298. Dorozhkin, S.V., *Calcium orthophosphate bioceramics.* Ceramics International, 2015. **41**(10): p. 13913-13966.

299. Hu, Y., et al., *Development of a porous poly (L‐lactic acid)/hydroxyapatite/collagen scaffold as a BMP delivery system and its use in healing canine segmental bone defect.* Journal of Biomedical Materials Research Part A, 2003. **67**(2): p. 591-598.

300. Anderson, J.M. and M.S. Shive, *Biodegradation and biocompatibility of PLA and PLGA microspheres.* Advanced drug delivery reviews, 2012. **64**: p. 72-82.

301. Fitzgerald, R. and D. Vleggaar, *Using poly-L-lactic acid (PLLA) to mimic volume in multiple tissue layers.* Journal of drugs in dermatology: JDD, 2009. **8**(10 Suppl): p. s5-14.

302. Liu, X. and P.X. Ma, *Polymeric scaffolds for bone tissue engineering.* Annals of biomedical engineering, 2004. **32**(3): p. 477-486.

303. Danoux, C.B., et al., *In vitro and in vivo bioactivity assessment of a polylactic acid/hydroxyapatite composite for bone regeneration.* Biomatter, 2014. **4**(1): p. e27664.

304. Barbieri, D., et al., *Influence of polymer molecular weight in osteoinductive composites for bone tissue regeneration.* Acta biomaterialia, 2013. **9**(12): p. 9401-9413.

305. Shah, S., K. Zhu, and C. Pitt, *Poly-DL-lactic acid: polyethylene glycol block copolymers. The influence of polyethylene glycol on the degradation of poly-DL-lactic acid.* Journal of Biomaterials Science, Polymer Edition, 1994. **5**(5): p. 421-431.

306. Ma, P.X., et al., *Engineering new bone tissue in vitro on highly porous poly (α‐hydroxyl acids)/hydroxyapatite composite scaffolds.* Journal of biomedical materials research, 2001. **54**(2): p. 284-293.

307. Milner, P.I., P.D. Clegg, and M.C. Stewart, *Stem cell–based therapies for bone repair.* Veterinary Clinics of North America: Equine Practice, 2011. **27**(2): p. 299-314.

308. Sittinger, M., D.W. Hutmacher, and M.V. Risbud, *Current strategies for cell delivery in cartilage and bone regeneration.* Current opinion in biotechnology, 2004. **15**(5): p. 411-418.

309. Plunkett, N. and F.J. O'Brien, *Bioreactors in tissue engineering.* Technology and Health Care, 2011. **19**(1): p. 55-69.

310. Sladkova, M. and G.M. de Peppo, *Bioreactor systems for human bone tissue engineering.* Processes, 2014. **2**(2): p. 494-525.

311. Arnsdorf, E.J., P. Tummala, and C.R. Jacobs, *Non-canonical Wnt signaling and N-cadherin related β-catenin signaling play a role in mechanically induced osteogenic cell fate.* PloS one, 2009. **4**(4): p. e5388.

312. Arnsdorf, E.J., et al., *Mechanically induced osteogenic differentiation–the role of RhoA, ROCKII and cytoskeletal dynamics.* Journal of cell science, 2009. **122**(4): p. 546-553.

313. Bara, J.J., et al., *Bone marrow-derived mesenchymal stem cells become antiangiogenic when chondrogenically or osteogenically differentiated: implications for bone and cartilage tissue engineering.* Tissue Engineering Part A, 2013. **20**(1-2): p. 147-159.

314. Duan, W. and M.J. Lopez, *Effects of Cryopreservation on Canine Multipotent Stromal Cells from Subcutaneous and Infrapatellar Adipose Tissue.* Stem Cell Reviews and Reports, 2015: p. 1-12.

315. Lopez, M. and J. Jarazo, *State of the art: stem cells in equine regenerative medicine.* Equine veterinary journal, 2015. **47**(2): p. 145-154.

316. Koch, T.G., L.C. Berg, and D.H. Betts, *Current and future regenerative medicine-principles, concepts, and therapeutic use of stem cell therapy and tissue engineering in equine medicine.* Can Vet J, 2009. **50**(2): p. 155-165.

317. Koch, T.G., L.C. Berg, and D.H. Betts, *Current and future regenerative medicine—principles, concepts, and therapeutic use of stem cell therapy and tissue engineering in equine medicine.* The Canadian Veterinary Journal, 2009. **50**(2): p. 155.

318. Taylor, S., R. Smith, and P. Clegg, *Mesenchymal stem cell therapy in equine musculoskeletal disease: scientific fact or clinical fiction?* Equine veterinary journal, 2007. **39**(2): p. 172-180.

319. Lee, J.E., et al., *Effects of the controlled-released TGF-β1 from chitosan microspheres on chondrocytes cultured in a collagen/chitosan/glycosaminoglycan scaffold.* Biomaterials, 2004. **25**(18): p. 4163-4173.

320. Rand, J.S., et al., *Canine and feline diabetes mellitus: nature or nurture?* The Journal of nutrition, 2004. **134**(8): p. 2072S-2080S.

321. Stegemann, H. and K. Stalder, *Determination of hydroxyproline.* Clinica chimica acta, 1967. **18**(2): p. 267-273.

322. Hartree, E.F., *Determination of protein: a modification of the Lowry method that gives a linear photometric response.* Analytical biochemistry, 1972. **48**(2): p. 422-427.

323. Zhang, P., et al., *In vivo mineralization and osteogenesis of nanocomposite scaffold of poly (lactide-co-glycolide) and hydroxyapatite surface-grafted with poly (L-lactide).* Biomaterials, 2009. **30**(1): p. 58-70.

324. Suchanek, W. and M. Yoshimura, *Processing and properties of hydroxyapatite-based biomaterials for use as hard tissue replacement implants.* Journal of Materials Research, 1998. **13**(01): p. 94-117.

325. Progatzky, F., M.J. Dallman, and C.L. Celso, *From seeing to believing: labelling strategies for in vivo cell-tracking experiments.* Interface focus, 2013. **3**(3): p. 20130001.

326. Pizzute, T., K. Lynch, and M. Pei, *Impact of tissue-specific stem cells on lineage-specific differentiation: a focus on the musculoskeletal system.* Stem Cell Reviews and Reports, 2015. **11**(1): p. 119-132.

327. Monaco, E., et al., *Transcriptomics comparison between porcine adipose and bone marrow mesenchymal stem cells during in vitro osteogenic and adipogenic differentiation.* PloS one, 2012. **7**(3): p. e32481.

328. Feng, Y.-F., et al., *Effect of reactive oxygen species overproduction on osteogenesis of porous titanium implant in the present of diabetes mellitus.* Biomaterials, 2013. **34**(9): p. 2234-2243.

329. Zhang, N., M.A. Dietrich, and M.J. Lopez, *Canine Intra‐Articular Multipotent Stromal Cells (MSC) From Adipose Tissue Have the Highest In Vitro Expansion Rates, Multipotentiality, and MSC Immunophenotypes.* Veterinary Surgery, 2013. **42**(2): p. 137-146.

330. Zhang, X., et al., *The roles of bone morphogenetic proteins and their signaling in the osteogenesis of adipose-derived stem cells.* Tissue Engineering Part B: Reviews, 2013. **20**(1): p. 84-92.

331. Seo, J.-p., et al., *Comparison of allogeneic platelet lysate and fetal bovine serum for in vitro expansion of equine bone marrow-derived mesenchymal stem cells.* Research in veterinary science, 2013. **95**(2): p. 693-698.

332. Zuk, P., *Adipose-derived stem cells in tissue regeneration: a review.* ISRN Stem Cells, 2013. **2013**.

333. David Roodman, G., *Role of stromal‐derived cytokines and growth factors in bone metastasis.* Cancer, 2003. **97**(S3): p. 733-738.

334. Festuccia, C., et al., *Osteoblast conditioned media contain TGF‐β1 and modulate the migration of prostate tumor cells and their interactions with extracellular matrix components.* International journal of cancer, 1999. **81**(3): p. 395-403.

335. Kim, K.-I., S. Park, and G.-I. Im, *Osteogenic differentiation and angiogenesis with cocultured adipose-derived stromal cells and bone marrow stromal cells.* Biomaterials, 2014. **35**(17): p. 4792-4804.

336. Yang, C., et al., *Osteoconductivity and biodegradation of synthetic bone substitutes with different tricalcium phosphate contents in rabbits.* Journal of Biomedical Materials Research Part B: Applied Biomaterials, 2014. **102**(1): p. 80-88.

337. Roohani-Esfahani, S.-I., et al., *The influence hydroxyapatite nanoparticle shape and size on the properties of biphasic calcium phosphate scaffolds coated with hydroxyapatite–PCL composites.* Biomaterials, 2010. **31**(21): p. 5498-5509.

338. Samavedi, S., A.R. Whittington, and A.S. Goldstein, *Calcium phosphate ceramics in bone tissue engineering: a review of properties and their influence on cell behavior.* Acta biomaterialia, 2013. **9**(9): p. 8037-8045.

339. Sikavitsas, V.I., G.N. Bancroft, and A.G. Mikos, *Formation of three-dimensional cell/polymer constructs for bone tissue engineering in a spinner flask and a rotating wall vessel bioreactor.* Journal of Biomedical Materials Research, 2002. **62**(1): p. 136-148.

340. Amini, A.R., C.T. Laurencin, and S.P. Nukavarapu, *Bone tissue engineering: recent advances and challenges.* Critical Reviews™ in Biomedical Engineering, 2012. **40**(5).

341. Laschke, M.W., et al., *Angiogenesis in tissue engineering: breathing life into constructed tissue substitutes.* Tissue engineering, 2006. **12**(8): p. 2093-2104.

342. Dawson, E., et al., *Biomaterials for stem cell differentiation.* Advanced drug delivery reviews, 2008. **60**(2): p. 215-228.

343. Bonjour, J.-P., *Calcium and phosphate: a duet of ions playing for bone health.* Journal of the American College of Nutrition, 2011. **30**(sup5): p. 438S-448S.

344. Kruyt, M.C., et al., *Analysis of ectopic and orthotopic bone formation in cell-based tissue-engineered constructs in goats.* Biomaterials, 2007. **28**(10): p. 1798-1805.

345. Scott, M.A., et al., *Brief review of models of ectopic bone formation.* Stem cells and development, 2011. **21**(5): p. 655-667.

346. Nagy, K., et al., *Induced Pluripotent Stem Cell Lines Derived from Equine Fibroblasts.* Stem Cell Reviews and Reports, 2011. **7**(3): p. 693-702.

347. Zhang, Y., et al., *Comparing immunocompetent and immunodeficient mice as animal models for bone tissue engineering.* Oral diseases, 2015. **21**(5): p. 583-592.

348. Higuera, G.A., et al., *In vivo screening of extracellular matrix components produced under multiple experimental conditions implanted in one animal.* Integrative biology, 2013. **5**(6): p. 889-898.

349. Thompson, E.M., et al., *Recapitulating endochondral ossification: a promising route to in vivo bone regeneration.* Journal of tissue engineering and regenerative medicine, 2015. **9**(8): p. 889-902.

350. Cornell, C.N. and J.M. Lane, *Newest factors in fracture healing.* Clinical orthopaedics and related research, 1992. **277**: p. 297-311.

351. Rizzi, S.C., et al., *Biodegradable polymer/hydroxyapatite composites: surface analysis and initial attachment of human osteoblasts.* Journal of Biomedical Materials Research, 2001. **55**(4): p. 475-486.

352. Peng, F., X. Yu, and M. Wei, *In vitro cell performance on hydroxyapatite particles/poly (L-lactic acid) nanofibrous scaffolds with an excellent particle along nanofiber orientation.* Acta Biomaterialia, 2011. **7**(6): p. 2585-2592.

353. Montjovent, M.O., et al., *Repair of critical size defects in the rat cranium using ceramic‐reinforced PLA scaffolds obtained by supercritical gas foaming.* Journal of Biomedical Materials Research Part A, 2007. **83**(1): p. 41-51.

354. Montjovent, M.-O., et al., *Biocompatibility of bioresorbable poly (L-lactic acid) composite scaffolds obtained by supercritical gas foaming with human fetal bone cells.* Tissue engineering, 2005. **11**(11-12): p. 1640-1649.

355. Mitchell, J.B., et al., *Immunophenotype of human adipose‐derived cells: temporal changes in stromal‐associated and stem cell‐associated markers.* Stem cells, 2006. **24**(2): p. 376-385.

356. Oberbauer, E., et al., *Enzymatic and non-enzymatic isolation systems for adipose tissue-derived cells: current state of the art.* Cell Regeneration, 2015. **4**(1): p. 7.

357. de Mattos Carvalho, A., et al., *Isolation and immunophenotypic characterization of mesenchymal stem cells derived from equine species adipose tissue.* Veterinary immunology and immunopathology, 2009. **132**(2): p. 303-306.

358. Millan, A., T. Landerholm, and J. Chapman, *Comparison between collagenase adipose digestion and Stromacell mechanical dissociation for mesenchymal stem cell separation.* McNair Scholars J CSUS, 2014. **15**: p. 86-101.

359. Frisbie, D. and R. Smith, *Clinical update on the use of mesenchymal stem cells in equine orthopaedics.* Equine Veterinary Journal, 2010. **42**(1): p. 86-89.

360. Lee, H.Y., et al., *Adult bone marrow stromal cell-based tissue-engineered aggrecan exhibits ultrastructure and nanomechanical properties superior to native cartilage.* Osteoarthritis and Cartilage, 2010. **18**(11): p. 1477-1486.

361. Nicpoń, J., K. Marycz, and J. Grzesiak, *Therapeutic effect of adipose-derived mesenchymal stem cell injection in horses suffering from bone spavin.* Polish journal of veterinary sciences, 2013. **16**(4): p. 753-754.

362. Zuk, P.A., et al., *Multilineage cells from human adipose tissue: implications for cell-based therapies.* Tissue engineering, 2001. **7**(2): p. 211-228.

363. Li, H., et al., *Adipogenic potential of adipose stem cell subpopulations.* Plastic and reconstructive surgery, 2011. **128**(3): p. 663.

364. Strioga, M., et al., *Same or not the same? Comparison of adipose tissue-derived versus bone marrow-derived mesenchymal stem and stromal cells.* Stem cells and development, 2012. **21**(14): p. 2724-2752.

365. Mattanovich, D. and N. Borth, *Applications of cell sorting in biotechnology.* Microbial cell factories, 2006. **5**(1): p. 12.

366. Garvican, E.R., et al., *Viability of equine mesenchymal stem cells during transport and implantation.* Stem cell research & therapy, 2014. **5**(4): p. 1.

367. Saadeh, P.B., et al., *Human cartilage engineering: chondrocyte extraction, proliferation, and characterization for construct development.* Annals of plastic surgery, 1999. **42**(5): p. 509-513.

368. Kretlow, J.D., et al., *Donor age and cell passage affects differentiation potential of murine bone marrow-derived stem cells.* BMC cell biology, 2008. **9**(1): p. 60.

369. Kershaw, E.E. and J.S. Flier, *Adipose tissue as an endocrine organ.* The Journal of Clinical Endocrinology & Metabolism, 2004. **89**(6): p. 2548-2556.

370. Docheva, D., et al., *Human mesenchymal stem cells in contact with their environment: surface characteristics and the integrin system.* Journal of cellular and molecular medicine, 2007. **11**(1): p. 21-38.

371. Cawthorn, W.P., E.L. Scheller, and O.A. MacDougald, *Adipose tissue stem cells meet preadipocyte commitment: going back to the future.* Journal of lipid research, 2012. **53**(2): p. 227-246.

372. Ahern, B.J., et al., *Evaluation of equine peripheral blood apheresis product, bone marrow, and adipose tissue as sources of mesenchymal stem cells and their differentation potential.* Am J Vet Res, 2011. **72**(1): p. 127-33.

373. Liu, G., et al., *Evaluation of the viability and osteogenic differentiation of cryopreserved human adipose-derived stem cells.* Cryobiology, 2008. **57**(1): p. 18-24.

374. Knabe, C., et al., *Effect of β-tricalcium phosphate particles with varying porosity on osteogenesis after sinus floor augmentation in humans.* Biomaterials, 2008. **29**(14): p. 2249-2258.

375. Pierantozzi, E., et al., *Human pericytes isolated from adipose tissue have better differentiation abilities than their mesenchymal stem cell counterparts.* Cell and tissue research, 2015. **361**(3): p. 769-778.

376. Leis, O., et al., *Sox2 expression in breast tumours and activation in breast cancer stem cells.* Oncogene, 2012. **31**(11): p. 1354-1365.

377. Greco, S.J., K. Liu, and P. Rameshwar, *Functional similarities among genes regulated by OCT4 in human mesenchymal and embryonic stem cells.* Stem cells, 2007. **25**(12): p. 3143-3154.

378. Jeter, C.R., et al., *Functional evidence that the self‐renewal gene NANOG regulates human tumor development.* Stem cells, 2009. **27**(5): p. 993-1005.

379. Ezeh, U.I., et al., *Human embryonic stem cell genes OCT4, NANOG, STELLAR, and GDF3 are expressed in both seminoma and breast carcinoma.* Cancer, 2005. **104**(10): p. 2255-2265.

380. Valenta, T., G. Hausmann, and K. Basler, *The many faces and functions of β‐catenin.* The EMBO journal, 2012. **31**(12): p. 2714-2736.

381. Reya, T., et al., *Stem cells, cancer, and cancer stem cells.* nature, 2001. **414**(6859): p. 105-111.

382. Nagata, S. and P. Golstein, *The Fas death factor.* Science, 1995. **267**(5203): p. 1449.

383. Suda, T., et al., *Expression of the Fas ligand in cells of T cell lineage.* The Journal of Immunology, 1995. **154**(8): p. 3806-3813.

384. Chen, L., et al., *CD95 promotes tumour growth.* Nature, 2010. **465**(7297): p. 492-496.

385. Arinzeh, T.L., et al., *Allogeneic mesenchymal stem cells regenerate bone in a critical-sized canine segmental defect.* J Bone Joint Surg Am, 2003. **85**(10): p. 1927-1935.

386. Peter, M.E. and P. Krammer, *The CD95 (APO-1/Fas) DISC and beyond.* Cell Death & Differentiation, 2003. **10**(1): p. 26-35.

387. Akiyama, K., et al., *Mesenchymal-stem-cell-induced immunoregulation involves FAS-ligand-/FAS-mediated T cell apoptosis.* Cell stem cell, 2012. **10**(5): p. 544-555.

388. Van der Valk, J., et al., *The humane collection of fetal bovine serum and possibilities for serum-free cell and tissue culture.* Toxicology in vitro, 2004. **18**(1): p. 1-12.

389. Goossens, M., et al., *Response to insulin treatment and survival in 104 cats with diabetes mellitus (1985–1995).* Journal of Veterinary Internal Medicine, 1998. **12**(1): p. 1-6.

390. McCann, T.M., et al., *Feline diabetes mellitus in the UK: the prevalence within an insured cat population and a questionnaire-based putative risk factor analysis.* Journal of Feline Medicine & Surgery, 2007. **9**(4): p. 289-299.

391. Panciera, D., et al., *Epizootiologic patterns of diabetes mellitus in cats: 333 cases (1980-1986).* Journal of the American Veterinary Medical Association, 1990. **197**(11): p. 1504-1508.

392. Prahl, A., et al., *Time trends and risk factors for diabetes mellitus in cats presented to veterinary teaching hospitals.* Journal of Feline Medicine & Surgery, 2007. **9**(5): p. 351-358.

393. O'Brien, T., *Pathogenesis of feline diabetes mellitus.* Molecular and cellular endocrinology, 2002. **197**(1): p. 213-219.

394. Schwartz, A., *Diabetes mellitus: does it affect bone?* Calcified Tissue International, 2003. **73**(6): p. 515-519.

395. Shehadeh, A. and T.J. Regan, *Cardiac consequences of diabetes mellitus.* Clinical cardiology, 1995. **18**(6): p. 301-305.

396. Mizisin, A.P., et al., *Neurological complications associated with spontaneously occurring feline diabetes mellitus.* Journal of Neuropathology & Experimental Neurology, 2002. **61**(10): p. 872-884.

397. Fu, Z., E.R. Gilbert, and D. Liu, *Regulation of insulin synthesis and secretion and pancreatic Beta-cell dysfunction in diabetes.* Current diabetes reviews, 2013. **9**(1): p. 25.

398. Betsholtz, C., et al., *Structure of cat islet amyloid polypeptide and identification of amino acid residues of potential significance for islet amyloid formation.* Diabetes, 1990. **39**(1): p. 118-122.

399. Chance, R.E., R.M. Ellis, and W.W. Bromer, *Porcine proinsulin: characterization and amino acid sequence.* Science, 1968. **161**(3837): p. 165-167.

400. Kono, S., et al., *Phenotypic and functional properties of feline dedifferentiated fat cells and adipose-derived stem cells.* The Veterinary Journal, 2014. **199**(1): p. 88-96.

401. Webb, T.L., J.M. Quimby, and S.W. Dow, *In vitro comparison of feline bone marrow-derived and adipose tissue-derived mesenchymal stem cells.* Journal of feline medicine and surgery, 2012. **14**(2): p. 165-168.

402. Moshtagh, P.R., S.H. Emami, and A.M. Sharifi, *Differentiation of human adipose-derived mesenchymal stem cell into insulin-producing cells: an in vitro study.* Journal of physiology and biochemistry, 2013. **69**(3): p. 451-458.

403. Buang, M.L.M., et al., *In vitro generation of functional insulin-producing cells from lipoaspirated human adipose tissue-derived stem cells.* Archives of medical research, 2012. **43**(1): p. 83-88.

404. Dave, S., A. Vanikar, and H. Trivedi, *Extrinsic factors promoting in vitro differentiation of insulin-secreting cells from human adipose tissue-derived mesenchymal stem cells.* Applied biochemistry and biotechnology, 2013. **170**(4): p. 962-971.

405. Dubey, A., et al., *198 isolation, characterization, and in vitro differentiation of goat adipose-tissue-derived mesenchymal stem cells into pancreatic islets-like cells.* Reproduction, Fertility and Development, 2014. **26**(1): p. 213-213.

406. Shapiro, A.J., et al., *Islet transplantation in seven patients with type 1 diabetes mellitus using a glucocorticoid-free immunosuppressive regimen.* New England Journal of Medicine, 2000. **343**(4): p. 230-238.

407. Ryan, E.A., et al., *Five-year follow-up after clinical islet transplantation.* Diabetes, 2005. **54**(7): p. 2060-2069.

408. D'Amour, K.A., et al., *Production of pancreatic hormone-expressing endocrine cells from human embryonic stem cells.* Nature biotechnology, 2006. **24**(11): p. 1392.

409. Chandra, V., et al., *Generation of pancreatic hormone‐expressing islet‐like cell aggregates from murine adipose tissue‐derived stem cells.* Stem Cells, 2009. **27**(8): p. 1941-1953.

410. Evans, J.L., et al., *Are oxidative stress− activated signaling pathways mediators of insulin resistance and β-cell dysfunction?* Diabetes, 2003. **52**(1): p. 1-8.

411. Okura, H., et al., *Transdifferentiation of human adipose tissue-derived stromal cells into insulin-producing clusters.* Journal of Artificial Organs, 2009. **12**(2): p. 123-130.

412. Janjic, D. and C.B. Wollheim, *Effect of 2‐mercaptoethanol on glutathione levels, cystine uptake and insulin secretion in insulin‐secreting cells.* European Journal of Biochemistry, 1992. **210**(1): p. 297-304.

413. Dominici, M., et al., *Minimal criteria for defining multipotent mesenchymal stromal cells. The International Society for Cellular Therapy position statement.* Cytotherapy, 2006. **8**.

414. Vaca, P., et al. *Nicotinamide induces both proliferation and differentiation of embryonic stem cells into insulin-producing cells*. in *Transplantation proceedings*. 2003. Elsevier.

415. Polak, M., et al., *Early pattern of differentiation in the human pancreas.* Diabetes, 2000. **49**(2): p. 225-232.

416. Aksu, A.E., et al., *Role of gender and anatomical region on induction of osteogenic differentiation of human adipose-derived stem cells.* Annals of plastic surgery, 2008. **60**(3): p. 306-322.

417. Sander, M., et al., *Genetic analysis reveals that PAX6 is required for normal transcription of pancreatic hormone genes and islet development.* Genes & development, 1997. **11**(13): p. 1662-1673.

APPENDIX: PERMISSION TO REPRINT

VITA

Wei Duan was born in Wuhan, Hubei Province, China. He was accepted into Huazhong University of Science & Technology in the fall semester of 2005. He received his bachelor's degree in Biomedical Engineering in 2009 and then he came to Shanghai Institute of Ceramics, Chinese Academy of Sciences to pursue his master degree in the fall semester of 2009. After received his master's degree in Material Sciences in 2012, he came to the School of Veterinary Medicine at Louisiana State University in Baton Rouge and joined the Veterinary Clinical Sciences Department to pursue his doctoral degree in the spring semester of 2013.